Annual Report
Jahresbericht

2021

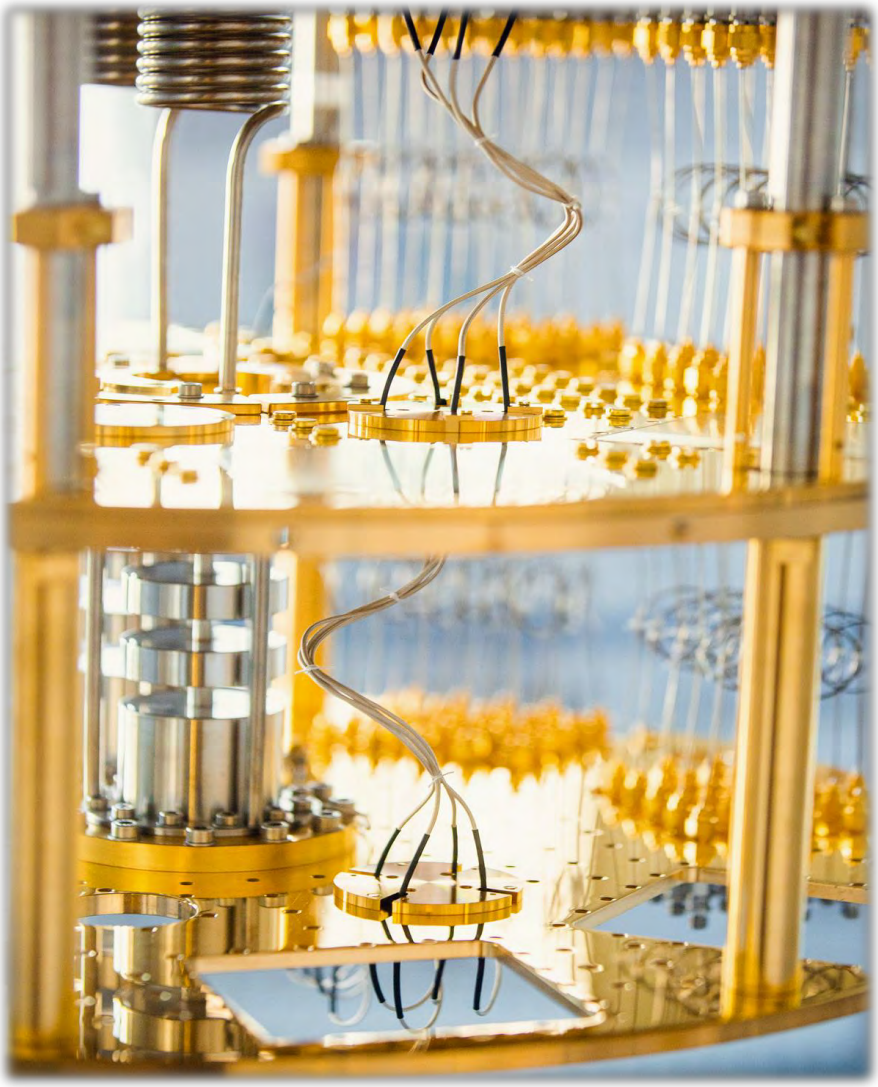

Walther–Meißner–Institut
für Tieftemperaturforschung

Bayerische Akademie der Wissenschaften

Cover photo: interior view of a dry dilution refrigerator

Contact:

Prof. Dr. Rudolf Gross
Walther–Meißner–Institut für Tieftemperaturforschung
Bayerische Akademie der Wissenschaften
and
Lehrstuhl für Technische Physik – E23
Technische Universität München

Address:

Walther–Meißner–Str. 8
D - 85748 Garching
GERMANY

Phone: +49 – (0)89 289 14249
Fax: +49 – (0)89 289 14206
e–mail: Rudolf.Gross@wmi.badw.de
www: http://www.wmi.badw.de

Secretary's Office and Administration:

Emel Dönertas

Phone: +49 – (0)89 289 14202
Fax: +49 – (0)89 289 14206
e–mail: Emel.Doenertas@wmi.badw.de
Sekretariat@wmi.badw.de

Andrea Person

Phone: +49 – (0)89 289 14205
Fax: +49 – (0)89 289 14206
e–mail: Andrea.Person@wmi.badw.de
Verwaltung@wmi.badw.de

Walther-Meißner-Institut
DER BAYERISCHEN AKADEMIE DER WISSENSCHAFTEN

Preface

Dear colleagues, friends, partners, and alumni of the Walther-Meißner-Institute (WMI),

the year 2021 was a very special one and – despite of its challenges related the Covid-19 pandemic – a highly successful and busy one for the WMI. Apart from our big success in research, in acquiring substantial external funding and in pushing ahead strategic developments, a particularly important achievement was the fact that we did not have to suffer from many Covid-19 infections at WMI and that we learnt to live with the virus by adapting our everyday working life. Therefore, in our ***Annual Report 2021*** we can make a very positive look back on the last year. As in previous years our Annual Report provides not only selected highlights of our research activities, but also relevant statistical data, an overview of our teaching and public engagement activities, and information on recent developments in infrastructure and experimental facilities. I hope that our Annual Report 2021 inspires your interest in the WMI.

Research at an international top-level requires – and this is particularly true for times of crisis – commitment, creativity, and sometimes courageous decisions and the willingness to go down new avenues. Therefore, in the first place I would like to thank all members of WMI for their excellent work and personal commitment in 2021. These are the key ingredients for keeping our research activities on a high level. In the same way I would like to thank our partners all over the world for their constructive cooperation and, of course, our sponsors for their trust and support. I particularly would like to emphasize the persistent support of the Bavarian Ministry for Science and Arts, the German Research Foundation, the Federal Ministry of Education and Research, and the European Union. There generous funding is the key to our success.

The WMI is very successful in attracting external funding for its research projects since decades. Nevertheless, the year 2021 was very special in this respect: with a total volume exceeding 25 Mio. € it was the most successful year in the history of WMI regarding the acquisition of third-party funding. Part of this success is related to the ***Munich Quantum Valley (MQV)***, which is supported by the Bavarian State Government with 300 Mio. € over the next five years and will be officially inaugurated by Prime Minister Söder in January 2022. The WMI has been one of the initiators of MQV and one of the key players in setting up the structure and research program of MQV. Today, we are pleased to see that our pioneering work on solid-state based quantum systems over the past two decades is rewarded with trust to lead the coordinated projects aiming at the realization of superconducting quantum computers. Stefan Filipp coordinates the two interlinked projects ***«Munich Quantum Valley – Superconducting Qubit Quantum Computing (SQQC)»***, funded by the Bavarian State Government within MQV, and the BMBF project ***«Munich Quantum Valley Quantum Computer Demonstrators – Superconducting Qubits (MUNIQC-SC)»***. There is an accompanying project ***«Munich Quantum Valley – Quantum Technology Park and Entrepreneurship (QTPE)»***, which is coordinated by Rudolf Gross and takes care about technological infrastructure and entrepreneurial activities.

Despite the great success of our quantum computing related activities I will not forget to mention the similar success of our activities on quantum microwave communication and sensing. Besides the ongoing EU Quantum Technology Flagship project ***QMiCS*** (see 21), we started the new BMBF project ***QuaRaTe*** in February 2021 (see 22) and get granted the BMBF project ***QuaMToMe***, which started only in November 2021. The former aims at studying the foundations of radar systems making use of quantum correlations and the latter focusses on the realization of so-called quantum tokens. Finally, the WMI also is a key partner in the new QuantERA Cofund Project ***«Shortcuts to Adiabaticity for Quantum Computation and Simulation (STAQS)»***, which will start in 2022.

Due to the success of the WMI in applying for third-party funding, we fortunately can significantly invest in future technological infrastructure. In the Annual Report 2020 we could report on the installation of the Plassys UHV deposition system for qubit fabrication and an Bluefors XLD 1000 cryogen-free dilution refrigerator with large cooling power, huge sample space and large number of microwave lines. In 2021, we could install two more Bluefors dilution fridges, one with a rapid sample change option (see page 69). Unfortunately, there have been delays in the delivery of the UHV MBE/PLD deposition cluster for the fabrication of quantum materials and the new helium liquefaction system (see page 13). These systems will go into operation only early in 2022. The same is true for the new scanning electron microscope. I would like to thank all the team members who contributed to writing the successful proposals, carrying out the European-wide tenders, clarifying all the technical details in the purchasing process, and preparing the technical infrastructure for the installation of the new equipment.

Despite the unfavorable circumstances due to the Covid-19 pandemic and the considerable amount of time required to write (fortunately successful) grant proposals, our research activities stayed on a high level and resulted in a number of high level publications (see page 93). Examples are the first realization of quantum teleportation in the microwave regime, the observation of multiple echos in pulsed electron spin resonance of strongly coupled spin ensembles, or the first observation of magnon pseudospin dynamics and the Hanle effect in antiferromagnets. The high impact of our research work is documented by about 2 500 citations of WMI publications in 2021 (ISI Web of Science).

Attracting and educating the best students and young scientists and providing a platform for them to make the next career steps, is a core interest of WMI. Therefore, we are very happy that 7 bachelor, 14 master, 5 Ph.D. students and 1 habilitation candidate completed their theses in 2021, while 14 master and 24 Ph.D. students as well as 2 habilitation candidates are still ongoing (see page 99). Due to the large number of third-party funded research projects the number of Ph.D. students grew to a record values in 2021 and is expected to further increase. This is causing increasing problems with office space. Regarding the hiring of technical and scientific staff, a important problem is the uncompetitive salary scale in the public sector compared to industry. This is a particular drawback for the Munich area with its very high living expenses. Finding qualified technicians and engineers becomes increasingly difficult, not to say impossible.

Finally, I would like to thank the scientific, technical and administrative staff of WMI for its outstanding performance in 2021! I also would like to thank our Scientific Advisory Board for their trust and guidance and, last but not least, all our friends and sponsors for their interest and continuous support. I am looking forward to a successful continuation in 2022.

Garching, December 2021

Rudolf Gross

Contents

The Walther–Meißner–Institute

General Information

The ***Walther-Meißner-Institute for Low Temperature Research (WMI)*** was originally operated by the Commission for Low Temperature Research of the ***Bavarian Academy of Sciences and Humanities (BAdW)***. Between 2013 and 2015, the Bavarian Academy of Sciences and Humanities with its more than 300 employees was reorganized. With the passing of the new statutes in October 2015, the 36 Commissions (Research Groups) of the Academy — they were originally set up in order to carry out long-term projects, which are too ambitious for the lifetime or capacity of any single researcher, or which require the collaboration of specialists in various disciplines — were abolished. The research program of BAdW is now implemented in Academy Institutes (such as the Walther-Meißner-Institute, the Leibniz Supercomputing Center or the Bavarian Research Institute for Digital Transformation) and Academy Projects. The Academy Institutes and Projects are managed by the Institute and Project Committees and supervised by the Institute and Project Advisory Boards, respectively. In this way a clear separation between the managing bodies of the institutes/projects (responsible for the implementation of the research programs) and the corresponding supervisory bodies (responsible for the quality control) was established. To this end, also the Commission for Low Temperature Research was dissolved and replaced by the WMI Committee and the WMI Advisory Board in 2015.

The historical roots of WMI go back to ***Walther Meißner***. He founded the Commission for Low Temperature Research in 1946 when he was president of BAdW (1946 – 1950). The first research activities then were started in 1946 in the Herrsching barracks. After the retirement of Walther Meißner in 1952, Heinz Maier-Leibnitz, who followed Walther Meißner on the Chair for Technical Physics of the Technical University of Munich (TUM), became the new head of the Commission for Low Temperature Research. In 1967, the commission moved to the Garching research campus after the construction of the new «*Zentralinstitut für Tieftemperaturforschung*» (ZTTF) was completed (director: Prof. Heinz Maier-Leibnitz, technical director: Prof. Franz Xaver Eder). Until 1972, the theory group of the Institute Laue Langevin was hosted at the ZTTF with prominent members such as Peter Fulde. In 1980, Prof. Dr. Klaus Andres became the new director of the ZTTF again associated with the Chair for Technical Physics (E23) at TUM. In 1982, the ZTTF was renamed into Walther-Meißner-Institute for Low Temperature Research (WMI) on the occasion of the 100. anniversary of Walther Meißner's birth.

In 2000, Prof. Dr. Rudolf Gross followed Klaus Andreas on the Chair for Technical Physics (E23) at TUM and as the new director of WMI. He significantly reoriented and extended the scientific focus of WMI by starting new activities in the field of quantum science and technology, as well in magnetism, spin dynamics and spin electronics. Even more importantly, he newly established the materials technology for superconducting and magnetic materials (both in form of thin films and single crystals) and a clean room facility, allowing for the fabrication

of solid-state nanostructures. These measures had been very successful and allowed WMI to play a leading role in several coordinated research projects in the field of quantum science and technology [e.g. Collaborative Research Center 631 on Solid-State Quantum Information Processing (2003-2015), Cluster of Excellence ***Munich Center for Quantum Science and Technology*** (since 2019), EU Quantum Technology Flagship Project QMiCS (2018-2022)] as well as in nanosciences [e.g. Cluster of Excellence Nanosystems Initiative Munich (2006-2019)]. The WMI also played a leading role in initiating the ***Munich Quantum Valley*** in 2020 (see strategy paper ***«Munich Quantum Valley Initiative»***). To accommodate the new activities, starting from 2000 the so far unused basement of the WMI building was made available for technical infrastructure (airconditioning, particulate airfilters, pure water system etc. for clean room) and additional laboratory space. Fortunately, in 2008 WMI succeeded in getting extra money from the state government within the so-called *«Konjunkturpaket II»* to establish the new *«WMI Quantum Science Laboratory»* in the basement of the building, providing about 150 m^2 additional laboratory space particularly suited for low temperature facilities and ultra-sensitive studies on solid state quantum systems. The WMI Quantum Science Laboratory was fully operational early in 2011 and meanwhile hosts several mK systems and sophisticated experimental techniques for the study of solid state based quantum systems and circuits. In 2016, the Bavarian Ministry for Science and Arts granted more than 6 Mio. Euro for redevelopment measures regarding the technical infrastructure, safety requirements and energy efficiency. An important part of the building project implemented in 2017/18 was the reconstruction of the entrance area and the main staircase, providing now direct access to the new WMI Quantum Laboratories in the basement of the WMI building as well as additional communication areas and meeting rooms in the ground floor. Moreover, it included the replacement of all windows and doors, the upgrade of the technical infrastructure for cooling water, air conditioning, liquid nitrogen and helium storage, as well as the complete redevelopment of the mechanical workshop and various safety measures.

With the availability of additional laboratory space and the success of the WMI in Germany's Excellence Initiative (2006-2018), Excellence Strategy (starting from 2019), and other third-party funded research projects, the research activities, the number of staff and obviously the related administrative tasks at WMI were strongly growing. Therefore, Rudolf Gross proposed in 2017 to start the appointment procedure for his successor at an early stage to guarantee sufficient temporal overlap. Moreover, due to the strong increase of staff, research projects and administrative tasks he proposed to change the governance structure of WMI from a single director to a board of up to three directors headed by a managing director. This change of governance structure has been supported by the Scientific Advisory Board of WMI and the decision-making bodies of BAdW. Meanwhile, it is implemented in the new rules of order of WMI valid since 18th October 2019. Already in June 2020, Prof. Dr. Stefan Filipp started as the second scientific director of WMI with strong focus on superconducting quantum computing. He coordinates the activities on superconducting quantum computing within the ***Munich Quantum Valley*** and the BMBF project ***German Quantum Computer based on Superconducting Qubits (GeQCoS)***.

As already mentioned, it is a long tradition that WMI hosts the Chair for Technical Physics (E 23) of TUM with the director of the WMI being a full professor at the Faculty of Physics of TUM. However, in general WMI has established tight links to research groups of both Munich universities, joining technological and human resources in the fields of experimental and theoretical solid-state and condensed matter physics, low temperature techniques, materials science as well as thin film and nanotechnology. Noteworthy, the WMI supplies liquid helium to more than 25 research groups at both Munich universities and provides the technological basis for low temperature research.

Important Discoveries

The WMI looks back on a long history of successful research in low temperature physics. In the following we list some important discoveries as well as experimental and technical developments made at WMI:

- **1961: discovery of flux quantization in multiply connected superconductors**
  (R. Doll, M. Näbauer, *Experimental Proof of Magnetic Flux Quantization in a Superconducting Ring*, Phys. Rev. Lett. **7**, 51-52 (1961)).
- **1986: discovery of an anomalous temperature dependence of the penetration depth in UBe_{13}**
  (F. Gross, B.S. Chandrasekhar, D. Einzel, K. Andres, P.J. Hirschfeld, H.R. Ott, J. Beuers, Z. Fisk, J.L. Smith, *Anomalous Temperature Dependence of the Magnetic Field Penetration Depth in Superconducting UBe_{13}*, Z. Physik B - Condensed Matter **64**, 175-188 (1986)).
- **1992: discovery the intrinsic Josephson effect**
  (R. Kleiner, F. Steinmeyer, G. Kunkel, and P. Müller, *Intrinsic Josephson Effects in $Bi_2Sr_2CaCu_2O_8$ Single Crystals*, Phys. Rev. Lett. **68**, 2394-2397 (1992)).
- **2002: development of dilution refrigerators with pulse tube refrigerator precooling**
  (K. Uhlig, *$^3He/^4He$ Dilution Refrigerator with Pulse Tube Precooling*, Cryogenics **42**, 73-77 (2002)).
- **2010: first demonstration of ultrastrong light-matter interaction**
  (T. Niemczyk, F. Deppe, H. Huebl, E. P. Menzel, F. Hocke, M. J. Schwarz, J. J. Garcia-Ripoll, D. Zueco, T. Hümmer, E. Solano, A. Marx, R. Gross, *Circuit Quantum Electrodynamics in the Ultrastrong-Coupling Regime*, Nature Physics **6**, 772-776 (2010)).
- **2010: development of dual path method for state tomography of propagating quantum microwaves**
  (E.P. Menzel, M. Mariantoni, F. Deppe, M.A. Araque Caballero, A. Baust, T. Niemczyk, E. Hoffmann, A. Marx, E. Solano, R. Gross, *Dual-Path State Reconstruction Scheme for Propagating Quantum Microwaves and Detector Noise Tomography* , Phys. Rev. Lett. **105**, 100401 (2010)).
- **2012: first realization of path entanglement of propagating quantum microwaves**
  (E. P. Menzel, R. Di Candia, F. Deppe, P. Eder, L. Zhong, M. Ihmig, M. Haeberlein, A. Baust, E. Hoffmann, D. Ballester, K. Inomata, T. Yamamoto, Y. Nakamura, E. Solano, A. Marx, R. Gross, *Path Entanglement of Continuous-Variable Quantum Microwaves*, Phys. Rev. Lett. **109**, 250502 (2012)).
- **2013: discovery of the spin Hall magnetoresistance** (jointly with partners at Tohoku University and TU Delft)
  (H. Nakayama, M. Althammer, Y.-T. Chen, K. Uchida, Y. Kajiwara, D. Kikuchi, T. Ohtani, S. Geprägs, M. Opel, S. Takahashi, R. Gross, G. E. W. Bauer, S. T. B. Goennenwein, E. Saitoh, *Spin Hall Magnetoresistance Induced by a Non-Equilibrium Proximity Effect*, Phys. Rev. Lett. **110**, 206601 (2013)).
- **2013: first demonstration of strong magnon-photon coupling**
  (H. Huebl, Ch. Zollitsch, J. Lotze, F. Hocke, M. Greifenstein, A. Marx, R. Gross, S.T.B. Goennenwein, *High Cooperativity in Coupled Microwave Resonator Ferrimagnetic Insulator Hybrids*, Phys. Rev. Lett. **111**, 127003 (2013)).
- **2017: first experimental observation of the spin Nernst effect**
  (S. Meyer, Yan-Ting Chen, S. Wimmer, M. Althammer, S. Geprägs, H. Huebl, D. Ködderitzsch, H. Ebert, G.E.W. Bauer, R. Gross, S.T.B. Goennenwein, *Observation of the spin Nernst effect*, Nature Materials **16**, 977-981 (2017)).
- **2019: first demonstration of remote state preparation in the microwave regime**
  (S. Pogorzalek, K. G. Fedorov, M. Xu, A. Parra-Rodriguez, M. Sanz, M. Fischer, E. Xie, K. Inomata, Y. Nakamura, E. Solano, A. Marx, F. Deppe, R. Gross, *Secure Quantum Remote State Preparation of Squeezed Microwave States*, Nature Communications **10**, 2604 (2019)).

- **2021: first demonstration of quantum teleportation in the microwave regime**
  (K. G. Fedorov, M. Renger, S. Pogorzalek, R. Di Candia, Q. Chen, Y. Nojiri, K. Inomata, Y. Nakamura, M. Partanen, A. Marx, R. Gross, F. Deppe, *Experimental quantum teleportation of propagating microwaves*, Science Advances **7**, eabk0891 (2021)).

Present Research Activities

The research activities of the Walther-Meißner-Institute are focused on low temperature condensed matter and quantum physics (see reports below). The research program is devoted to both **fundamental** and **applied research** and also addresses **materials science, thin film and nanotechnology** aspects. With respect to **basic research** the main focus of the WMI is on

- quantum phenomena and quantum coherence in solid state systems,
- superconductivity and superfluidity,
- magnetism, including spin transport, spin dynamics, spin mechanics and spin caloritronics,
- circuit quantum electrodynamics and circuit electro-nanomechanics,
- ordering and emergent phenomena in correlated quantum matter,
- and the general properties of metallic systems at low and very low temperatures.

The WMI also conducts **applied research** in the fields of

- superconducting quantum circuits for quantum computing,
- solid-state quantum information processing and quantum communication systems,
- superconducting and spin-based devices,
- multi-functional and multiferroic materials,
- and the development of low and ultra-low temperature systems and techniques.

With respect to **materials science, thin film and nanotechnology** the research program is focused on

- the synthesis of superconducting and magnetic materials,
- the single crystal growth of oxide materials,
- the thin film technology of complex superconducting and magnetic heterostructures, including multi-functional and multi-ferroic material systems,
- and the fabrication of superconducting, magnetic and hybrid nanostructures.

The WMI also develops and operates systems and techniques for low and ultra–low temperature experiments. A successful development have been dry mK-systems that can be operated without liquid helium by using a pulse-tube refrigerator for precooling. In the early 2000s, these systems have been successfully commercialized by the company VeriCold Technologies GmbH at Ismaning, Germany, which was taken over by Oxford Instruments in 2007. Currently, in a collaboration with Oxford Instruments such dry dilution refrigerators are used to establish a so-called cryolink, allowing for quantum communication in the microwave regime between two superconducting quantum processors over an about 10 m distance. WMI also operates a helium liquifier with an annual capacity of above 180.000 liters and supplies both Munich universities with liquid helium. To optimize the transfer of liquid helium into transport containers, WMI has developed a pumping system for liquid helium which has been commercialized in collaboration with a company.

To a large extent the research activities of WMI are integrated into national and international research projects such as Clusters of Excellence, Collaborative Research Centers, Research Units, or BMBF and EU projects. The individual research groups of WMI offer a wide range of attractive research opportunities for bachelor and master students, Ph.D. students and postdoctoral fellows.

Experimental Facilities and Resources

The WMI is equipped with state of the art facilities for the preparation and characterization of superconducting and magnetic materials as well as for various low and ultra–low temperature experiments. The main experimental and technological resources of WMI are listed in the following.

Materials Preparation and Fabrication of Nanostructures

- Laser Molecular Beam Epitaxy (L-MBE) system for oxide heterostructures (equipped with in–situ RHEED, Omicron AFM/STM system, atomic oxygen/nitrogen source, infrared-laser heating system, metallization). The L-MBE systems is connected to a UHV magnetron sputtering systems for metals (e.g. Nb, Al, NiPd, ...) and an electron beam deposition system via a UHV transfer chamber
- Plassys MEB550 S4-I UHV electron beam evaporation and sputtering system for qubit fabrication
- molecular beam epitaxy (MBE) system for metals
- UHV cluster tool (Bestec GmbH) consisting of two magnetron sputter deposition systems for superconducting and magnetic heterostructures, respectively, and a load lock
- UHV magnetron sputtering system (Mantis Deposition GmbH) for large-area deposition of superconducting thin films and heterostructures
- Oxford Instruments Plasmalab 80 Plus reactive ion etching (RIE) system with ICP plasma source
- ion beam etching (IBE) system equipped with a LN_2 cooled sample holder
- automated critical point dryer Leica EM CPD 300
- polishing machine for substrate preparation
- ultrasonic bonding machine
- 50 m^2 class 1000 clean room facility
- maskless lithography UV Direct Laser Writer, PicoMaster 200 UV of the company 4PICO, The Netherlands
- 100 kV nB5 Electron Beam Lithography System by NanoBeam Limited, UK, with 6 inch laser stage
- optical lithography (Süss maskaligner MJB 3 and projection lithography)
- four-mirror image furnace for crystal growth

Characterization

- 2–circle x–ray diffractometer (Bruker D8 Advance, sample temperature up to 1 600°C)
- high resolution 4–circle x–ray diffractometer with Göbel mirror and Ge monochromator (Bruker D8 Discover)
- Philips XL 30 SFEG scanning electron microscope with EDX analysis
- UHV room temperature AFM/STM system
- two Raman spectroscopy systems (1.5 to 300 K, in-situ sample preparation)
- tip-enhanced Raman spectroscopy (TERS) system
- SQUID magnetometer (Quantum Design, 1.5 to 700 K, up to 7 T)
- several high field magnet systems (up to 17 T Tesla) with variable temperature inserts
- 7 T split coil magnet systems with optical access and variable temperature insert
- 3D vector magnet (2/2/6 Tesla) with variable temperature inserts
- experimental set–ups for the measurement of noise including low noise SQUID amplifiers and signal analyzers

- high-frequency network analyzers (up to 40 GHz) and various microwave components (sources, mixers, circulators, attenuators) for the determination of high frequency parameters
- ultra-sensitive microwave receiver for state tomography of quantum microwaves (dual path method with FPGA signal processing)
- high-frequency cryogenic probing station (up to 20 GHz, $T > 4$ K)
- magnetooptical Kerr effect (MOKE) system
- broadband ferromagnetic resonance (FMR) system

Low temperature systems and techniques

- several ^{3}He/^{4}He dilution refrigerator inserts for temperatures down to 10 mK
- WMI cryogen-free mK-cooler based on a dilution refrigerator with pulse-tube precooling and equipped with a large number of microwave lines and cold electronics (e.g. amplifiers, circulators, attenuators, directional couplers) for ultra-sensitive experiments on solid state quantum systems
- Oxfod Instruments cryogen-free dilution refrigerator (model VDR 400-10) with a base temperature of about 10 mK equipped with a 3D vector magnet (1/1/6 Tesla)
- Oxfod Instruments cryogen-free dilution refrigerator (model TRITON-15-300) with a base temperature of about 10 mK equipped with a standard bucket tailset
- Oxford Instruments cryogenic link with supporting structure and superconducting microwave link
- Bluefors cryogen-free dilution refrigerator system (model BF-XLD 1000) with a base temperature below 10 mK and, in particular, with large cooling power (about 1 mW at 100 mK) and sample space
- "wet" dilution refrigerators based on liquid helium precooling and equipped with a large number of microwave lines and cold electronics (e.g. amplifiers, circulators, attenuators, beam splitters) for time-domain microwave experiments on solid state quantum systems
- experimental set–ups for the measurement of specific heat, magnetization, thermal expansion as well as electrical and thermal transport properties as a function of temperature, magnetic field and pressure

Building and Reconstruction Measures

Infrastructure and Reconstruction Measures

Rudolf Gross, Achim Marx

Also in 2021, there have been a large number of reconstruction measures required for accommodating new equipment and technical infrastructure. Moreover, several laboratories and office space had to be renovated and reorganized. The most relevant measures have been

- the movement of the high magnetic field laboratory from the basement to the first floor to increase the distance to the experiment on superconducting quantum circuits which suffer from magnetic field noise,
- the preparation of the WMI annexe building for the installation of the new helium liquifier, including the replacement of the old helium gasometers and ventilation system,
- the complete replacement of the compressed air system,
- the installation of the closed-cycle cooling systems for two further dry dilution refrigerators,
- the dismantling of the old UHV cluster deposition system and the preparation of the laboratory for the installation of the new UHV PLD-MBE deposition system for quantum materials, and
- the renovation of the former Raman laboratories.

Experiments with superconducting qubits are quite sensitive to stray magnetic fields. Although such fields can be shielded, this is increasingly demanding with the rapidly growing complexity of superconducting quantum circuits. Therefore, it is optimum to disentangle laboratories for qubit experiments from those employing high magnetic fields. To this end, in 2021 we moved three high magnetic field systems to a new laboratory. This was accompanied with a renovation of the respective laboratories and an upgrade of the high magnetic field setups.

The delivery of the new helium liquefier was announced for October 2021 but had to be postponed until February 2022 due to delays related both to the Covid-19 pandemic and considerable delays in the supply of systems components. Fortunately, parts of the system such as the helium compressor or the balloons for the recovery system arrived in time and already have been installed. The final step – the installation of the coldbox of the liquefier in the main building – hopefully will be completed until March 2022. Without any doubt, the new liquefaction system will guarantee the save and cost efficient supply of liquid helium to the more than 30 research groups at TUM, LMU and MPG for the next two decades.

Considerable delays in the delivery of new technical infrastructure and scientific instrumentation occurred also for the scanning electron microscope (JEOL JSM-IT800) and the new UHV

PLD-MBE cluster deposition system of DCA Instruments Oy. Both will arrive hopefully until March 2022. The latter is designed for the fabrication of complex heterostructures and novel quantum materials. It replaces the meanwhile about 25 years old UHV Laser-MBE system and will be of key importance for the materials oriented research at WMI. In this context it is important to note that samples fabricated with the old UHV Laser-MBE system were the key ingredient for more than 150 publications. This clearly demonstrates the fact that state-of-the-art solid-state physics is hardly possible without modern materials preparation system. We are convinced that the new UHV system consisting of an MBE part, a pulsed laser deposition system and a sputtering system connected via a UHV tunnel (see Fig. 1) will also be the nucleus and enabling technology for many future research projects.

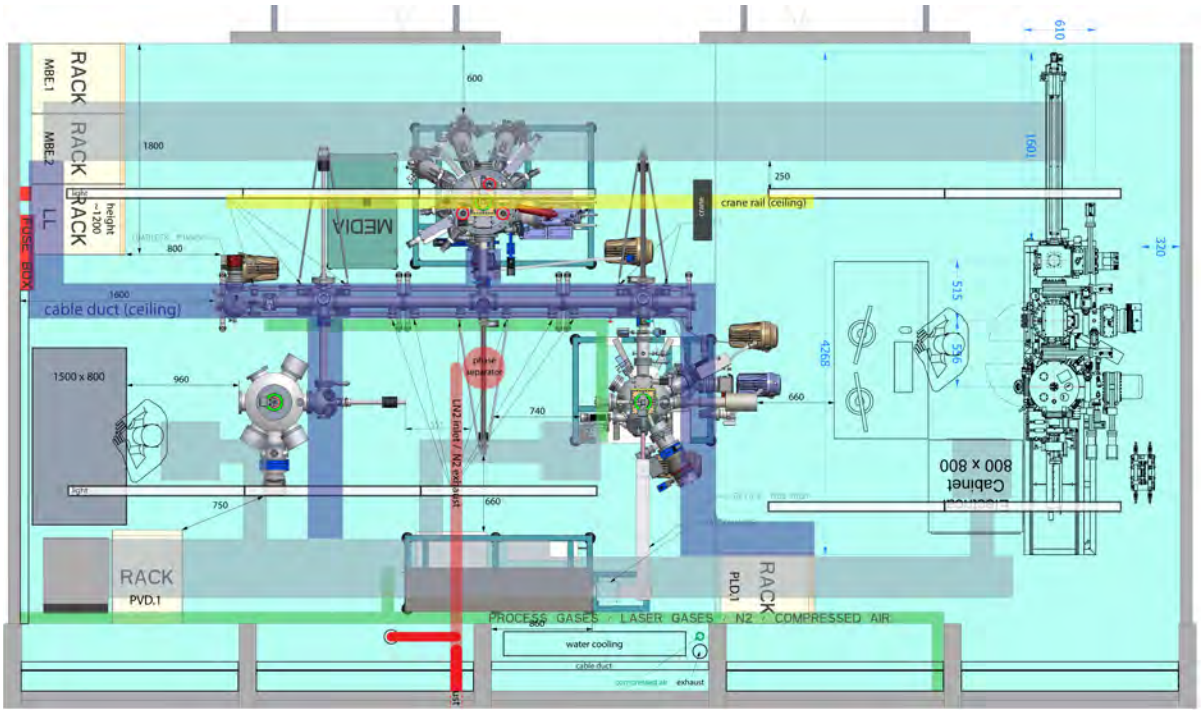

Figure 1: The layout of the thin film laboratory ready for the installation of the new UHV PLD-MBE cluster deposition system of DCA Instruments Oy. On the right, the PLASSYS MEB 550 S4-I UHV deposition system for qubit fabrication is shown, which has been installed already in 2020 and already is a central component for qubit fabrication.

Fortunately, the delivery of dry dilution refrigerators of the company Bluefors Oy came without significant delays. These systems were required for the rapidly growing research activities aiming at the realization of superconducting quantum computers. In 2021, three new systems arrived and two of them, a standard dry dilution refrigerator (Model BF-LD 400) and a so-called bottom loader (Model BF-LD 250/400) allowing for fast sample change, have already been installed and taken into operation. The third system (Model BF-XLD 400/1000) providing large cooling power and very large sample space was delivered late in 2021 and presently is absolving final performance tests.

Joint Research Projects

New Research Projects in Quantum Science and Technology

Rudolf Gross

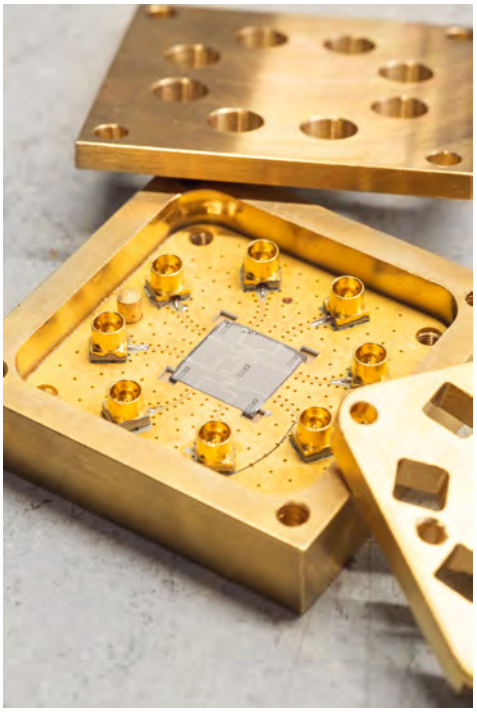

Since more than 20 years, the Walther-Meißner-Institute (WMI) plays a key role in coordinated research programs, excellence centers, graduate schools and initiatives in the field of Quantum Science and Technology (QST). Initially, these research programs (e.g. CRC 631 on «Solid-state Based Quantum Information Processing» (2003 – 2015) or Cluster of Excellence «Nanosystems Initiative Munich» (2006 – 2019)) were fundamental science oriented, aiming at clarifying the physical and technological foundations of solid-state based quantum systems and their applicability for quantum information processing. This basic science oriented research efforts are continued within the Excellence Cluster ***«Munich Center for Quantum Science and Technology»*** (MCQST, since 2019) and the ***«International Max Planck Research School for Quantum Science and Technology»*** (IMPRS-QST, since 2016) or the new QuantERA II ERA-NET Cofund project on ***Shortcuts to Adiabicity for Quantum Computing and Simulation***, which has been granted in December 2021.

The Munich Quantum Valley – Pushing Quantum Applications

With the great success and rapid progress in quantum-oriented fundamental research over the past two decades, it was evident that the focus will move more and more towards applications and the industrial use of quantum technologies. The simple reason is that all leading hightech nations have strong interest in making quantum technologies also an economical success. In Germany, last year the key industrial players founded the ***«Quantum Technology & Application Consortium (QUTAC)*** to bring quantum computing to the level of large-scale industrial application, develop quantum applications to market maturity, and, in general, to strengthen Germany's digital sovereignty. The need for pushing applications of quantum technologies was recognized quite early also by Munich researchers. Already in January 2017 it was proposed to establish a ***Center for Quantum Engineering*** at TUM to better involve the engineering departments in the R&D work required to bring quantum technologies to the market place. Meanwhile this center is in the construction phase and will be ready hopefully until the end of 2024. Another important ingredient in the competition among leading nations is the development of successful industrialization strategies. This does not only include world-class research but also requires to create a productive ecosystems for the interaction between academia and industry, to establish efficient supply chains, to foster start-ups, or to attract venture capital. To this end, the spokespersons of the excellence cluster MCQST supported by Klaus Blaum (MPG) and Raoul Klingner (FhG) proposed to establish the ***«Munich Quantum Valley» (MQV)*** in a **strategy paper** submitted to the Bavarian state

Government in 2020. The key vision of MQV is to build quantum computers based on different technology platforms and to make them accessible to users as well as to develop the required hardware and software technologies.

Meanwhile the Bavarian State Government agreed on supporting the Munich Quantum Valley with about 300 Mio. € over the next five years, starting from October 2021. The Munich Quantum Valley with its seven founding members MPG, LMU, TUM, BAdW, FhG, DLR and FAU Erlangen will be officially inaugurated in January 2022 by Prime Minister Söder. This powerful Bavarian initiative is accompanied by several programs of the Federal Ministries of Education and Research as well as of Economic Affairs and Energy. WMI has been quite active in shaping these programs. For example, Stefan Filipp together with Peter Leibinger was chairman of the ***«Expert Panel for the Development of a National Roadmap in Quantum Computing»***, which has been established in response to the demand of Federal Minister Helge Braun. They developed the ***«Roadmap Quantum Computing»*** as a guideline for future R&D efforts.

WMI Acquires Large Research Projects in QST

The WMI has developed into a key player in the development of superconducting quantum computers in Germany and the new director, Stefan Filipp, coordinates several large projects in this direction. The new projects, which already started in 2021 or will start early in 2022 are (for more details, see page 107):

- Bavarian State Government Project: ***Munich Quantum Valley – Superconducting Qubit Quantum Computing (SQQC)***
  project coordinator: S. Filipp (WMI)
  project partners: TUM, LMU, FAU Erlangen, MPG, FhG.
- Bavarian State Government Project: ***Munich Quantum Valley – Quantum Technology Park and Entrepreneurship (QTPE)***
  project coordinator: R. Gross (WMI)
  project partners: TUM, LMU, FAU Erlangen, MPG, FhG.
- BMBF Coordinated Project: ***Munich Quantum Valley Quantum Computer Demonstrators – Superconducting Qubits (MUNIQC-SC)***, project number: 13N16188
  project coordinator: S. Filipp (WMI)
  project partners: TUM, FhG, FAU Erlangen-Nürnberg, Infineon Technologies AG, IHP GmbH, IQM Germany GmbH, kiutra GmbH, Parity Quantum Computing Germany GmbH, Forschungszentrum Jülich GmbH, Zurich Instruments Germany GmbH.
- BMBF Coordinated Project: ***German Quantum Computer based on Superconducting Qubits (GeQCoS) – Scaling and Demonstrator***, project number: 13N15680
  project coordinator: S. Filipp (WMI)
  project partners: Forschungszentrum Jülich GmbH, KIT, FAU Erlangen-Nürnberg, FhG, Infineon Technologies AG.

The WMI is also very successful in the development and application of microwave-based quantum technologies. For example, within the EU Quantum Technology Flagship Project QMiCS we succeeded in setting up a 6.6 meter long quantum local area network (QLAN) cable connecting two dilution refrigerators at millikelvin temperatures and could perform first state transfer measurements over this QLAN cable (see page 21), which may find useful

applications in distributed quantum computing. In 2021, we could acquired three new projects related to microwave quantum technology:

- BMBF Coordinated Project: ***QUAntenRAdarTEam (QUARATE) – Superconducting Circuits and Quantum Microwaves for Quantum Radar***, project number: 13N15380
  project coordinator: Rohde & Schwarz GmbH & Co. KG, principal investigators of WMI: F. Deppe, K. Fedorov, R. Gross, A. Marx
  project partners: German Aerospace Center (DLR), Technical University of Munich
- BMBF Coordinated Project: ***Storage of Microwave Quantum Tokens in Electron and Nuclear Spin Ensembles (QuaMToMe)***, project number: 16KISQ036
  project coordinator: N. Kukharchyk (WMI)
  project partners: K. Fedorov and H. Huebl (WMI), all three subproject are led by WMI
- QuantERA II ERA-NET Cofund Project: ***Shortcuts to Adiabaticity for Quantum Computation and Simulation (STAQS)***, project number: DE 3444/1-1
  project coordinator: Wolfgang Lechner, University of Innsbruck
  project partners: WMI (F. Deppe, K. Fedorov, R. Gross, A. Marx), University of Napoli, National Research Council (CNR), University of Luxembourg.

The key goals of the QuaRaTe project (see page 22), which started in February 2021, are the laboratory demonstration of a frequency-degenerate quantum radar system, the evaluation of useful application and exploitation scenarios, and the transfer of quantum microwave knowhow to the engineering partners and to the industry.

The QuaMToMe project started in November 2021. The key objectives of this collaborative project is the realization, investigation and demonstration of quantum tokens (Q-tokens) in the microwave regime. The quantum tokens will be implemented in the form of quantum keys stored in quantum memories based on spin ensembles. In general, scalable and long-lived quantum memories represent one of the missing elements needed to build local microwave-based quantum networks. Quantum tokens in the form of propagating squeezed states represent a particularly important use case for such quantum networks. Due to the broad expertise of WMI in this field, all three project partners are located at WMI.

The QuantERA Cofund Project has been granted only in December 2021 and will start early in 2022. The project is fundamental science-oriented but explores a novel concept as a seed for future technological implementations in adiabatic quantum simulation and computing. Its specific goal is to develop a comprehensive set of non-adiabatic building blocks that replace the adiabatic state preparation by non-adiabatic processes using shortcuts to adiabaticity (STA). This fundamentally new paradigm allows one to detach from the adiabatic limit, which currently hinders practical applications, by introducing additional unitary quantum operations to the system. In this promising approach, only early theory work and simplistic experiments exist so far. In the joint effort with leading experimental and theory groups, the project aims at demonstrating the first two-body STA experiment with a scalable architecture, the first STA experiment with a non-scale-invariant system, a novel theoretical framework for STA of statistical ensembles and a novel tensor network framework for STA.

The Fate of the Successful

The WMI is very satisfied about the funding for the new research projects in quantum science and technology and is very happy to play a leading role in the development of supercon-

ducting quantum computers. However, as usual there is also the other side of the coin. It is evident already today that the large application-oriented projects in quantum computing will tie up considerable resources, which will be missing for other more fundamental research oriented activities. Already today there is a shortage in office and laboratory space and the new projects only can be implemented by setting up additional modular buildings. This is the fate of the successful. The success unfortunately also causes problems and significant challenges. Therefore, the coming years will be quite demanding the WMI regarding solving these problems and beating these challenges. However, as research always is subjected to rapid changes and disruptive developments this is unavoidable.

The success of the WMI in the research programs aiming at the development of quantum computers also comes with a change in funding schemes. Whereas in the past the WMI was relying on funding of fundamental research via long-term projects such as DFG Collaborative Research Centers, Priority Programs or Excellence Clusters, there is now a change to development-oriented projects funded via BMBF, EU or MQV, which often require the fulfillment of short-term milestones and quarterly reporting. Therefore, attention has to be drawn to the related effects on the long-term research strategy of the WMI in fundamental science.

The EU Quantum Flagship Project QMiCS

F. Deppe, K. G. Fedorov, A. Marx, M. Renger, O.Ġargiulo, R. Gross [1]

Since 2018, the European Union (EU) fosters the development of quantum technologies via the Quantum Flagship program (www.qt.eu). One of the 20 projects funded in the first call, ***Quantum microwave communication and sensing (QMiCS)*** is coordinated by Frank Deppe from the Walther-Meißner-Institut (WMI). The project logo is shown in Fig. 1. Scientific project partners are Aalto University (AALTO, Finland), École Normale Superieure der Lyon (ENSL, France), Instituto de Telecomunicações (Portugal), Universidad del País Vasco / Euskal Herriko Unibertsitatea (UPV/EHU, Spain), and VTT (Finland). Active industry partners are Oxford Instruments Nanotechnology Ltd. (OINT, United Kingdom) and TTI Norte S.L. (Spain). QMiCS explores continuous-variable quantum microwaves. Its three main goals are a 6.6 meter long quantum local area network (QLAN) cable connecting two dilution refrigerators at millikelvin temperatures, a proof-of-principle quantum illumination experiment, and a the development of a roadmap towards real-life applications of quantum microwaves.

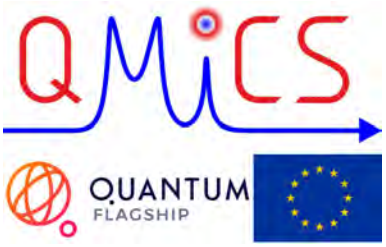

Figure 1: Logos of QMiCS (top), the Quantum Flagship (bottom left), and the EU (bottom right).

In order to mitigate delays due to the recurring restrictions related to the Corona pandemic, QMiCS has been extended by 6 months until March 31, 2022. Although slightly delayed, we have witnessed important progress in 2021. At WMI, we have measured quantum teleportation of truly propagating microwave states for the first time [1]. Using two-mode squeezed states as entanglement resource, we have exceeded a no-cloning threshold for coherent states. Furthermore, we have presented our visions for microwave quantum networks in an article for the general public [2]. Supported by our industrial cryotechnology partner OINT, we have successfully assembled and cooled down the QLAN cable between two dilution refrigerators. Here, the difficulty has been to properly integrate the WMI homebuilt cryostat into the system. Aalto University and WMI are currently testing the HEMT amplifiers provided by partner TTI. Both WMI and ENSL have successfully been testing parametric devices fabricated by partner VTT. In another exciting experiment, ENSL has demonstrated squeezing beyond the usual 3 dB-threshold inside a resonant microwave mode [3].

At WMI, first state transfer measurements over the QLAN cable have shown very encouraging results. Hence, the stage is now prepared to measure quantum teleportation between two dilution refrigerators placed in different labs, one of the key milestones of QMiCS. The second key experiment, namely quantum-radar-type illumination based on frequency-nondegenerate microwave entanglement, has been assembled and is currently ongoing at ENSL.

References

[1] K. G. Fedorov, M. Renger, S. Pogorzalek, R. Di Candia, Q. Chen, Y. Nojiri, K. Inomata, Y. Nakamura, M. Partanen, A. Marx, R. Gross, and F. Deppe, Science Advances **7**, eabk0891 (2021).
[2] F. Deppe, K. G. Fedorov, and A. Marx, Akademie Aktuell **Heft 2**, 36–38 (2021).
[3] R. Dassonneville, R. Assouly, T. Peronnin, A. Clerk, A. Bienfait, and B. Huard, Phys. Rev. X Quantum **2**, 020323 (2021).

[1]We acknowledge support by the German Research Foundation via Germany's Excellence Strategy (EXC-2111-390814868), Elite Network of Bavaria through the program ExQM, EU Flagship project QMiCS (Grant No. 820505), and the German Federal Ministry of Education and Research via the project QUARATE (Grant No. 13N15380).

The BMBF Project QUARATE

F. Deppe, K. G. Fedorov, A. Marx, K. Honasoge, F. Kronowetter, R. Gross [1]

Figure 1: Logos of QUARATE (top) and the German Federal Ministry of Education and Research (bottom).

In February 2021, the project *"QUAnten RAdarTEam (QUARATE)"* funded by the German Federal Ministry of Education and Research via the call *Anwendungsbezogene Forschung in der Quantensensorik, -metrologie sowie -bildgebung* has successfully started at WMI. Additional partners are engineers from *Rohde & Schwarz GmbH & Co. KG* (R&S, coordinator), the German Aerospace Agency (*Deutsches Zentrum für Luft- und Raumfahrt e.V.*, DLR), and *Technische Universität München* (TUM). A brief description can be found at https://www.rohde-schwarz.com/de/knowledge-center/research-projects/quarate/quarate_254591.html. The grand goals of the three-year project are: (1) A laboratory demonstration of a frequency-degenerate quantum radar at millikelvin temperatures; (2) The evaluation of application and exploitation scenarios in terms of a roadmap; (3) A transfer of quantum microwave knowhow to the engineering partners and to the industry partner.

In very simple words, quantum radar exploits quantum correlations to achieve a fundamental sensitivity advantage over the optimal classical radar. While no fundamental roadblocks are expected at this point, the greatest practical challenges will be the cryogenics-room-temperature interfaces and the current limitation of the quantum advantage to single-photon powers. We have outlined the basic principles and visions for microwave quantum radar in Ref. [1] (in German language). In QUARATE, the first tasks for the academic engineering partners are to translate the physics-dominated formalism into an engineering language and to identify suitable terms for a fair comparison to classical radar implementations. At WMI, we are meanwhile making good progress towards the fabrication of qubit-based single microwave photon detectors similar to the ones discussed in Ref. [2]. In a combined effort between WMI and R&S, we are also setting up the remaining parts of the quantum radar receiver.

Currently, the QUARATE project is still in its start-up phase. In addition to implementing a minimal lab demonstration, we investigate paths towards technological scalability. Notably, the field is quite active. Therefore, novel – potentially game-changing – theoretical findings are not at all unlikely. For this reason, we are collaborating actively with Dr. Roberto Di Candia, a renowned theory expert in the field of quantum illumination.

References

[1] F. Deppe, K. G. Fedorov, A. Marx, K. Honasoge, M. Peichl, F. Bischeltsrieder, W. Utschick, J. Russer, M. Würth, B. Güzelarslan, and F. Kronowetter, Technik in Bayern **05/2021**, 18–19 (2021).
[2] R. Dassonneville, R. Assouly, T. Peronnin, P. Rouchon, and B. Huard, Phys. Rev. Applied **14**, 044022 (2021).

[1] We acknowledge support by the German Research Foundation via Germany's 2 Excellence Strategy (EXC-2111-390814868), Elite Network of Bavaria through the program ExQM, EU Flagship project QMiCS (Grant No. 820505), and the German Federal Ministry of Education and Research via the project QUARATE (Grant No. 13N15380). FK is also affiliated to *Rohde & Schwarz GmbH & Co. KG, Mühldorfstraße 15, 81671 München*.

Basic Research

Magnon Hanle Effect in Antiferromagnetic Insulators

T. Wimmer, J. Gückelhorn, M. Opel, S. Geprägs, H. Huebl, R. Gross, M. Althammer [1]
A. Kamra [2,3]

Over the recent decade we have intensively studied the transport of (spin) angular momentum in magnetically ordered insulators. In such systems the quantized excitations of the spin system, i.e. magnons, carry finite spin and enable transport of spin information over distances of several µm [1]. A special case are antiferromagnetic insulators (AFIs), which exhibit in the most simple case two energetically degenerate magnon modes carrying opposite chirality/spin. Both magnon modes then contribute to the spin transport. Thus it is possible to realize superposition states of these two different magnon modes leading to linearly polarized magnon modes carrying zero spin. In our recent publications with theory support from A. Kamra, we describe this pair of magnons with opposite spin and their superpositions via a pseudospin [2, 3] resembling the spin of an electron (see Fig. 1). The experimentally accessible quantity corresponds to the z-component of the pseudospin. In addition, we show that AFIs with specific magnetic anisotropy give rise to coherent dynamics of the pseudospin leading to the observation of the magnon Hanle effect [2, 3].

In more detail, we employ a heavy metal (HM) Pt-strip (injector) to inject a spin current into the AFI via the spin Hall effect, which generates a magnon pseudospin density $\mathcal{S}$ oriented along z underneath the injector (see Fig. 2 (a)-(c)). With a second HM strip (detector), we can then electrically detect the magnon pseudospin density arriving at the detector via the inverse process. In the AFI α-Fe_2O_3, the magnetic easy-plane anisotropy and the Dzyaloshinskii-Moriya interaction (DMI) cause a coherent coupling between the spin-up and spin-down magnons, which leads to a precession of the pseudospin in the x-z plane. This precession can be mapped on a pseudo-field Ω (oriented along $\hat{y}$), which depends on the magnetic anisotropy and the combination of DMI field and canting-induced net magnetization. The latter depends on the external magnetic field, such that we can tune the precession frequency via the application of an external magnetic field. This situation is very similar to the electronic Hanle effect. Three distinct situations are illustrated in Fig. 2(a)-(c). At the compensation field H_c the contributions from anisotropy and DMI cancel each other, such that no precession occurs ($\Omega = 0$) and the pseudospin diffuses through the AFI. In this situation the same injected spin orientation is detected at the HM Pt detector strip, resulting in a positive spin signal. For H_0, the finite pseudospin precession causes the pseudospin of the

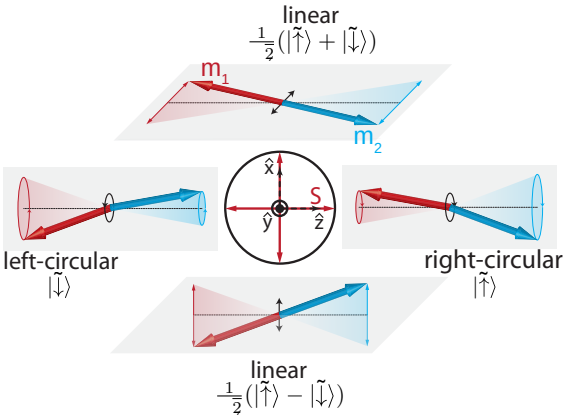

Figure 1: Concept of pseudospin in antiferromagnetic insulators. Within the concept of pseudospin, the left- and right-circular polarized magnon modes represent the spin-down and spin-up states of the pseudospin,i.e. the pseudospin is collinear with the z-axis. The linear polarized magnon modes are superpositions of the left- and right-circular magnon modes, representing zero-spin excitations. The dynamical coupling between these different magnon modes can be described via a rotation of the pseudospin $\mathcal{S}$ around the y-axis caused by a pseudo-field Ω.

[1] We acknowledge financial support from the German Research Foundation under Germany's Excellence Strategy (EXC-2111 - 390814868) and project AL 2110/2-1.

[2] IFIMAC - Condensed Matter Physics Center and Department of Theoretical Condensed Matter Physics,Universidad Autónoma de Madrid, Madrid, Spain.

[3] Financial support via the Research Council of Norway through its Centers of Excellence funding scheme (project 262633, "QuSpin") is gratefully acknowledged.

magnons arriving at the detector strip to be oriented along the x-direction, corresponding to a spin zero state. Thus, no spin signal is detected. At H_{inv}, the magnon pseudospin direction is inverted while propagating from injector to detector, which results in a negative spin signal at the detector.

In our first experiments we used a 15 nm thin α-Fe_2O_3 layer and 5 nm thin Pt strips fabricated at the WMI for the spin injection and detection. The results of these measurements for two different distances between injector and detector (750 nm (blue circles) and 950 nm (black circles)) are shown in Fig. 2(d). Most strikingly, at $\mu_0 H \approx 8$ T we find a maximum positive signal at the detector for both distances. This corresponds to the compensation field H_{c}, at which $\Omega = 0$ and no pseudospin precession occurs. H_{c} only depends on the intrinsic properties of the AFI. Upon further increasing the field above H_{c}, the signal at the detector first decreases to 0 (corresponding to H_0), then becomes negative with a minimum at H_{inv}. At even higher fields, the signal at the detector becomes again positive. Our pseudospin model nicely explains the data as indicated by the white lines, which are a fit to each data set. From these measurements we can extract the magnon diffusion length and obtain values of ≈ 300 nm.

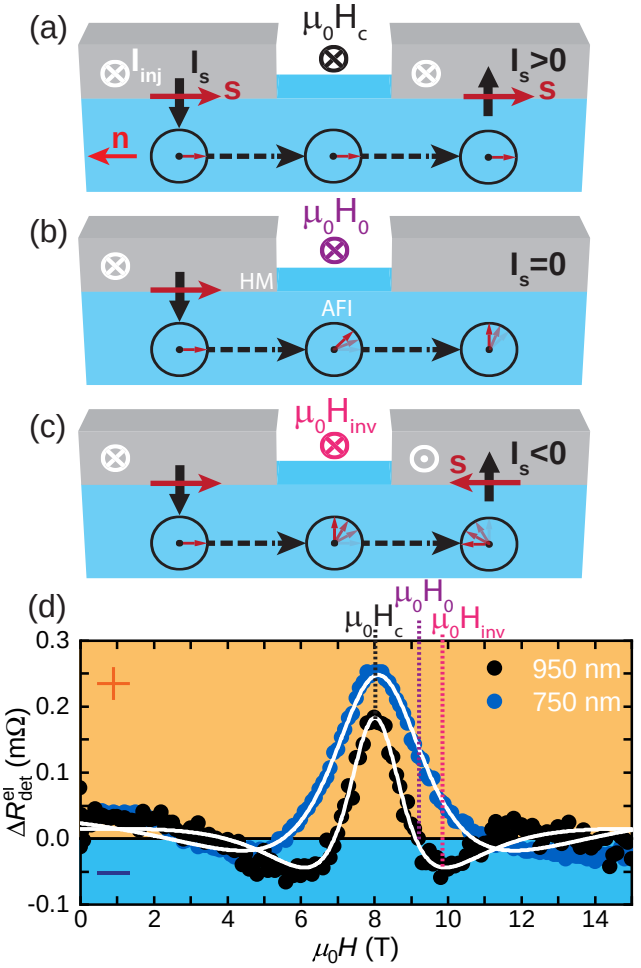

Figure 2: Illustration of the magnon Hanle effect. A pseudospin density polarized in z-direction is injected via the HM strip and propagates in the AFI to the HM detector strip. The external magnetic field allows to control the precession frequency of the pseudospin in the x-z-plane. This results in positive (a), zero (b) and negative (c) spin signals at the detector. (d) Measured spin signal for two injector-detector distances (black and blue circles) as a function of the external magnetic field at $T = 200$ K. White lines represent fits to the obtained data from our one dimensional pseudospin diffusion theory [2].

We are still at the early stages of obtaining a deeper understanding of the pseudospin and its dynamics in AFIs. Our pseudospin model [2] provides an elegant way to describe the complex coupling of the magnon eigenstates in an easy-plane antiferromagnet and the transport of spin information within such a system. Our results show that indeed aspects of electronic spin transport can be mapped onto magnon spin transport in antiferromagnets and results in experimentally accessible effects. Thus, magnon transport in antiferromagnetic insulators is a promising playground to realize magnonic analogues of electron spin transport [2].

References

[1] M. Althammer, physica status solidi (RRL) – Rapid Research Letters **15**, 2100130 (2021).
[2] A. Kamra, T. Wimmer, H. Huebl, and M. Althammer, Physical Review B **102**, 174445 (2020).
[3] T. Wimmer, A. Kamra, J. Gückelhorn, M. Opel, S. Geprägs, R. Gross, H. Huebl, and M. Althammer, Physical Review Letters **125**, 247204 (2020).

Microwave Quantum Teleportation

K. G. Fedorov, M. Renger, F. Fesquet, F. Kronowetter, K. Honasoge, Y. Nojiri, Q. Chen, A. Marx, R. Gross, F. Deppe [1]

The modern field of quantum communication thrives on the promise to deliver efficient and unconditionally secure ways to exchange information by exploiting quantum laws of physics. Here, quantum teleportation stands out as an exemplary protocol, allowing for the disembodied and safe transfer of unknown quantum states using quantum entanglement and classical communication as resources [2]. The recent progress in quantum computation with superconducting circuits led to the requirement of quantum communication between spatially separated superconducting processors operating at microwave frequencies. In pursuit of this goal, we demonstrate the unconditional quantum teleportation of propagating coherent microwave states by exploiting two-mode squeezing and analog feedforward over a macroscopic distance of $d = 0.42\,\mathrm{m}$. We achieve a teleportation fidelity of $F = 0.689 \pm 0.004$, exceeding the asymptotic no-cloning threshold. Thus, the quantum nature of the teleported states is preserved, opening the avenue towards unconditional security in microwave quantum communication, quantum local area networks, and modular quantum computing.

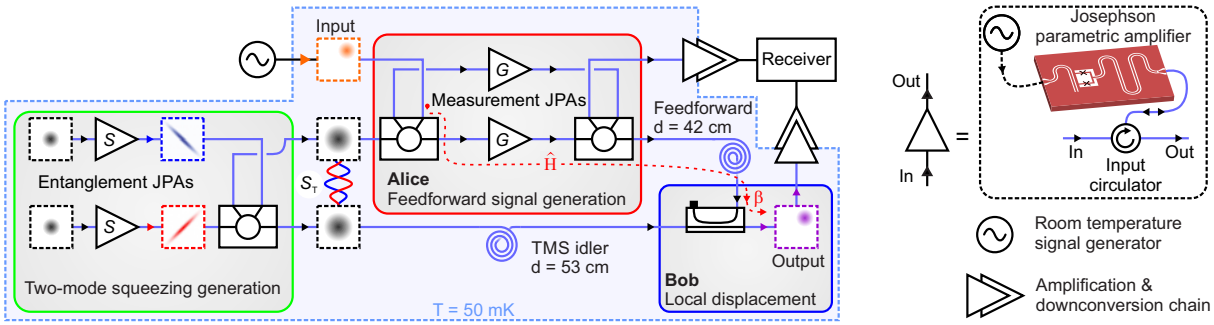

Figure 1: a Experimental implementation of QT with propagating quantum microwaves and analog feedforward. Here, an unknown input coherent state is teleported from Alice to Bob by exploiting quantum entanglement characterized by the two-mode squeezing level $S_T \lesssim S$. The feedforward signal is generated by the measurement JPAs with the degenerate gain G, in combination with two symmetric hybrid rings and a local displacement operation on Bob's side. Plots in dashed boxes represent quantum states in the quasi-probability Wigner phase space spanned by field quadratures p and q. More experimental details can be found in [1].

Quantum teleportation (QT) allows one to achieve the classically impossible goal of transferring an unknown quantum state from one place to another without directly sending it. This task is usually quantified with a teleportation fidelity F, which expresses the overlap in phase space between an unknown input state and a teleported output state. A transition to the quantum realm occurs when exceeding the classical fidelity threshold F_{ct}. Furthermore, exceeding the asymptotic no-cloning threshold $F_{\mathrm{nc}} = 2/3$ ensures unconditional security of teleported coherent states.

Our experimental implementation (see Fig. 1) of QT with propagating microwaves relies on superconducting flux-driven Josephson parametric amplifiers (JPAs) for generation and manipulation of entangled two-mode squeezed microwave states [3, 4]. We use two entanglement JPAs in combination with a hybrid ring for generation of path-entangled TMS states at the outputs of the hybrid ring [5]. Owing to the propagating nature of our TMS states, we can

[1] We acknowledge support by the German Research Foundation via Germany's Excellence Strategy (EXC-2111-390814868), Elite Network of Bavaria through the program ExQM, EU Flagship project QMiCS (Grant No. 820505), and the German Federal Ministry of Education and Research via the project QUARATE (Grant No. 13N15380).

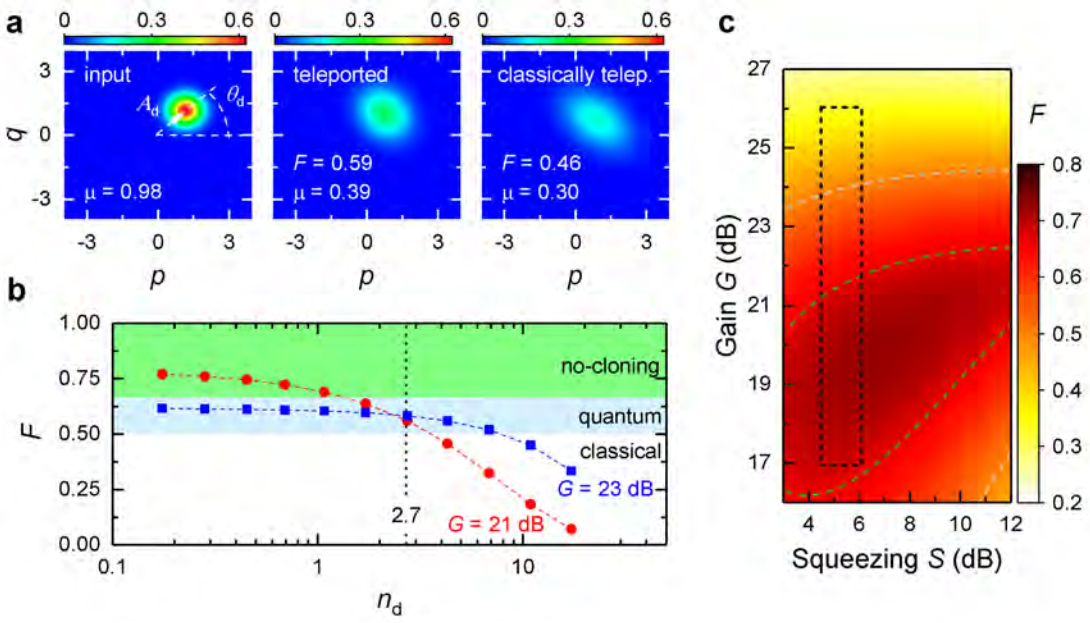

Figure 2: **a** Reconstructed Wigner functions of an input state, teleported state, and classically teleported state for the squeezing level $S = 4.5\,\mathrm{dB}$, the displacement photon number of the input state $n_\mathrm{d} = 2.7$, and the measurement gain $G = 23\,\mathrm{dB}$. Inset values represent the quantum teleportation fidelity F and purity μ. **b** Fidelity F as a function of n_d for two characteristic values of G. Dashed black line marks the operating point illustrated in panel **a**. **c** Extended view over the expected QT performance for the respective theory model, where black dashed box outlines the area studied in the experiment. This theory plot demonstrates that further improvement of teleportation fidelities requires an increase of both the measurement gain G and squeezing level S.

straightforwardly distribute the entangled states between Alice and Bob via superconducting niobium-titanium coaxial cables. Figure 2 shows experimental results of the microwave QT protocol. They include Wigner state tomography over a broad range of input coherent states, corresponding quantum-teleported output states, and classically teleported output states (transferred using the same protocol but in the absence of entanglement resource).

In conclusion, we have successfully implemented the quantum teleportation protocol with propagating microwaves over a distance of 0.42 m in the cryogenic environment. Our teleportation protocol allows us to violate the no-cloning limit over a wide range of input state parameters, corresponding to teleportation fidelities of $F \geq 0.69$ for coherent states with the displacement photon number of $n_\mathrm{d} \leq 1.1$ and the measurement gain $G = 21\,\mathrm{dB}$. The demonstrated microwave quantum teleportation results, in combination with the aforementioned technological advances, bring quantum local area networks between superconducting quantum computers within reach.

References

[1] K. G. Fedorov, M. Renger, S. Pogorzalek, R. D. Candia, Q. Chen, Y. Nojiri, K. Inomata, Y. Nakamura, M. Partanen, A. Marx, R. Gross, and F. Deppe (2021). arXiv:2103.04155 [quant-ph].

[2] C. H. Bennett, G. Brassard, C. Crépeau, R. Jozsa, A. Peres, and W. K. Wootters, Phys. Rev. Lett. **70**, 1895–1899 (1993).

[3] T. Yamamoto, K. Inomata, M. Watanabe, K. Matsuba, T. Miyazaki, W. D. Oliver, Y. Nakamura, and J. S. Tsai, Appl. Phys. Lett. **93**, 042510 (2008).

[4] K. G. Fedorov, S. Pogorzalek, U. Las Heras, M. Sanz, P. Yard, P. Eder, M. Fischer, J. Goetz, E. Xie, K. Inomata, Y. Nakamura, R. Di Candia, E. Solano, A. Marx, F. Deppe, and R. Gross, Sci. Rep. **8**, 6416 (2018).

[5] E. P. Menzel, R. Di Candia, F. Deppe, P. Eder, L. Zhong, M. Ihmig, M. Haeberlein, A. Baust, E. Hoffmann, D. Ballester, K. Inomata, T. Yamamoto, Y. Nakamura, E. Solano, A. Marx, and R. Gross, Phys. Rev. Lett. **109**, 250502 (2012).

Robust Formation of Nanoscale Magnetic Skyrmions in Easy-Plane Anisotropy Thin Film Multilayers with Low Damping

L. Flacke, E. Meidinger, M. Yaqoob, M. Müller, L. Liensberger, M. Althammer, S. Geprägs, H. Huebl, R. Gross, M. Weiler [1,2]
V. Ahrens, S. Mendisch, M. Becherer, [3,4] *L. Körber, A. Kákay,* [5] *T. Böttcher, P. Pirro* [6,7]

Neuromorphic computing is an increasingly desired computing paradigm that allows to merge memory and processing in one device. By overcoming the von Neumann bottleneck it thus increases energy and operation efficiencies. In particular, magnetic textures might come at hand for so-called reservoir computing. To this end, a matrix of pinned magnetic skyrmions within a thin film can be employed to represent a reservoir of individual non-linear units that can additionally store information. By harnessing complex resistance and magnetodynamic responses to AC and DC currents through a skyrmion bath a neuromorphic computing unit can be built [1].

Magnetic skyrmions in thin films usually show a strong size dependence together with a narrow field range for their stabilization which, to some extend, complicates their applicability. Banerjee *et al.* predicted that these difficulties could be overcome by using an easy-plane effective anisotropy energy density [2]. In our recent experiments [3] we investigated this unexplored regime using sputter-deposited $[\mathrm{Pt}(0.6\,\mathrm{nm})/\mathrm{Co_{25}Fe_{75}}(1.1\,\mathrm{nm})/\mathrm{Ir}(0.7\,\mathrm{nm})]_6$ multilayers.

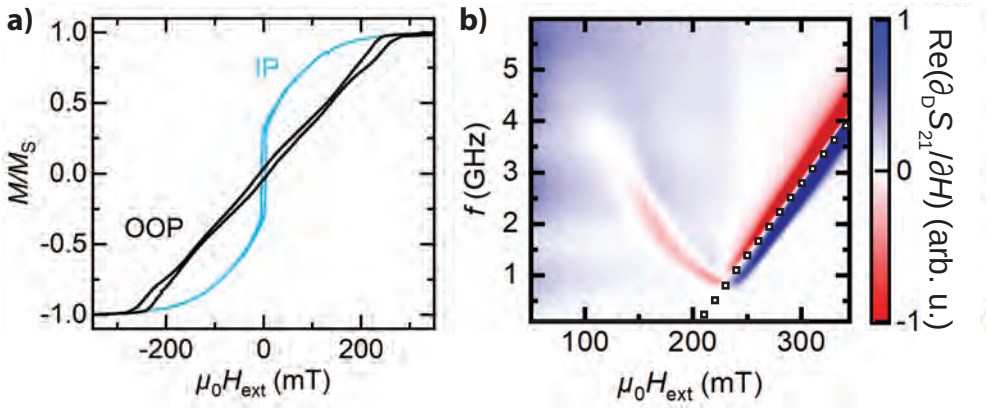

Figure 1: (a) SQUID magnetometry loops with field applied out of the plane (OOP) and in the plane (IP) of the sample. (b) Ferromagnetic resonance (FMR) spectrum depicted by the background corrected real part of the magnetic susceptibility when sweeping from higher magnetic fields to lower fields. The strong signal (FMR) above the saturation field is described by the Kittel equation. Below saturation the fainting signal corresponds to the uniform precession of the skyrmion background which is not aligned with the external field direction.

Figure 1 (a) shows superconducting quantum interference device (SQUID) magnetometry loops for magnetic fields applied in in-plane (IP) and out-of-plane (OOP) direction. A hard axis behavior is observed in OOP, whereas an easy-plane switching loop with a low coercivity is recorded for IP. The decrease of magnetic moment aligned with the IP field can be attributed to domain formation. The anisotropy is additionally confirmed by broadband ferromagnetic

[1]Financial support of the German Research Foundation via projects WE5386/4, WE5386/5 and Germany's Excellence Strategy No. EXC-2111-390814868 is gratefully acknowledged.
[2]new address: Technische Universität Kaiserslautern, 67663 Kaiserslautern, Germany
[3]Technical University of Munich, 80333 Munich, Germany
[4]Financial support of the German Research Foundation via project BE4641/2-1 is gratefully acknowledged.
[5]Helmholtz-Zentrum Dresden-Rossendorf, 01328 Dresden, Germany
[6]Technische Universität Kaiserslautern, 67663 Kaiserslautern, Germany
[7]Financial support of the German Research Foundation via SPP 2137 is gratefully acknowledged.

resonance (FMR) spectroscopy. Figure 1 (b) depicts the real part of the background corrected dynamic magnetic susceptibility for fields applied in OOP. Above saturation the FMR is clearly visible following the Kittel-like, linear behavior. The positive effective magnetization obtained by extrapolating to zero frequency verifies the easy-plane anisotropy of the multilayer.

As both, static (SQUID magnetometry) and dynamic (FMR spectroscopy) measurements reveal the underlying effective anisotropy energy density we examine the domain formation by magnetic force microscopy (MFM). Figure 2 (a) - (g) show the magnetic contrast of the sample by applying various OOP external magnetic fields. We can identify magnetic skyrmions, which appear below saturation, that follow the typical magnetic field evolution: from a magnetically homogeneous state to individual skyrmions (a) - (c), to a dense arrangement (d) - (e) and eventually (g) a spin spiral state at remanence with individual skyrmions trapped in between the spirals. Remarkably, their average apparent radius maintains a constant value of roughly 25 nm for a field range of roughly 150 mT. This is qualitatively different from usual multilayer systems with an easy axis along the surface normal, where Zeeman contributions impose a reduction of size for any non-aligned texture.

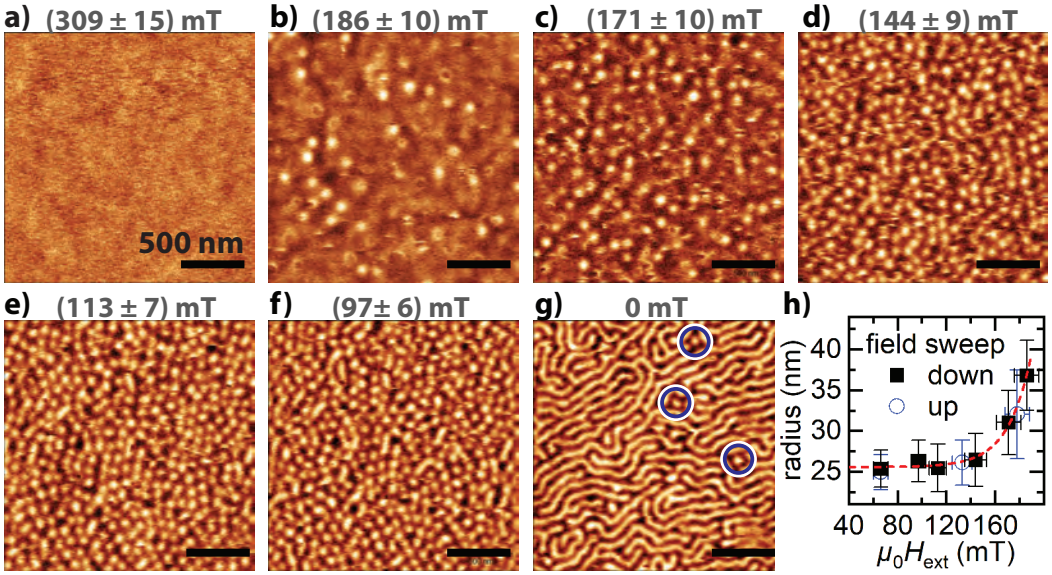

Figure 2: (a) - (g) MFM images recorded at different external magnetic fields applied in OOP. Above saturation no magnetic contrast is observed due to the homogeneous magnetization parallel to the external field. By reducing the field individual skyrmions appear ((b), (c)) which eventually assemble in a dense arrangement ((d) - (f)). At remanence (g) a spin spiral state with individual skyrmions is obtained. (h) The apparent radii of the skyrmions maintain a robust average size for fields up to roughly 150 mT. This property differentiates the skyrmion size response to external magnetic fields qualitatively from multilayers that exhibit a perpendicular magnetic anisotropy.

Skyrmion hosting multilayers with an easy-plane effective anisotropy energy density thus provide a promising platform for a robust skyrmion formation and stabilization. The arrangements observed by MFM can be exploited as a skyrmion reservoir with complex current density distributions and thus endorse first steps closer to applicability for neuromorphic computing.

References

[1] D. Pinna, G. Bourianoff, and K. Everschor-Sitte, Phys. Rev. Appl. **14**, 054020 (2020).
[2] S. Banerjee, J. Rowland, O. Erten, and M. Randeria, Phys. Rev. X **4**, 031045 (2014).
[3] L. Flacke, V. Ahrens, S. Mendisch, L. Körber, T. Böttcher, E. Meidinger, M. Yaqoob, M. Müller, L. Liensberger, A. Kákay, M. Becherer, P. Pirro, M. Althammer, S. Geprägs, H. Huebl, R. Gross, and M. Weiler, Phys. Rev. B **104**, L100417 (2021).

Temperature-Dependent Spin Transport and Current-Induced Torques in Superconductor-Ferromagnet Heterostructures

M. Müller, L. Liensberger, L. Flacke, H. Huebl, R. Gross, M. Weiler, M. Althammer [1]
A. Kamra, [2,3] *W. Belzig* [4,5]

Over the last decade, the field of superconducting spintronics [1, 2] has attracted increasing attention due to the novel and beneficial spin transport properties related to quasiparticles and spin-triplet Cooper pairs in superconductors (SCs). Among those, charge-to-spin current interconversion and the associated spin-orbit torque effects allow for the control of magnetization and its dynamics. Recent experiments [3, 4] focused on the nonequilibrium magnetization dynamics of a ferromagnetic metal (FM) layer adjacent to a SC film. Here, changes of the parameters describing magnetization dynamics below the superconducting transition temperature T_c provide insight into the spin injection in SCs via spin pumping [3, 4] by analyzing the magnetization damping using ferromagnetic resonance (FMR) techniques in SC/FM hybrid systems close to T_c.

In our recent work, we systematically study the magnetization dynamics of SC/FM-heterostructures as a function of temperature at and below T_c including the investigation of linear spin-orbit-torques present in these multilayers. To this end broadband ferromagnetic resonance (bbFMR) experiments in combination with the phase sensitive detection of the microwave transmission signal have been carried out [5]. This approach allows us to simultaneously detect the electrical ac currents due to magnetization dynamics, which arise due to inverse spin-orbit torques (iSOT). We quantify them in terms of the spin-orbit conductivity σ^{SOT} following Ref. [6].

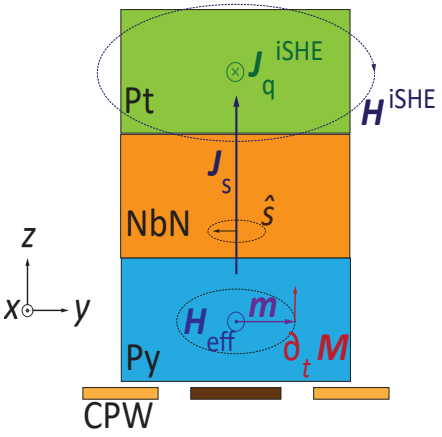

Figure 1: Schematic illustration of in plane bbFMR experiments as well as for the generation of the charge current density $\mathbf{J}_q^{iSHE}$ by ac iSHE. The ac flux $\mathbf{H}^{iSHE}$ generated by $\mathbf{J}_q^{iSHE}$ is coupled into the CPW.

In our experiments, we use NbN and $Ni_{80}Fe_{20}$ (Permalloy, Py) as the SC and FM material, respectively. In more detail, we have in-situ fabricated Pt/NbN/Py heterostructures capped with TaO_x to avoid oxidation of the Py layer on thermally oxidized Si (100) substrates by dc magnetron sputtering taking advantage of the Superbowl UHV-system. BbFMR experiments are performed in a cryogenic environment over a broad frequency and temperature range. The samples are mounted face-down onto a coplanar waveguide (CPW) (see Fig. 1), of which we record the complex microwave transmission S_{21} using a vector network analyzer (VNA) for fixed microwave frequencies as a function of the external magnetic field H_{ext}. From these measurements we obtain the frequency dependence of the FMR field and linewidth, which allows to determine the Gilbert damping parameter α.

[1]Financial support by the German Research Foundation via Germany's Excellence Strategy (EXC-2111-390814868) is gratefully acknowledged.

[2]Center for Quantum Spintronics, Department of Physics, Norwegian University of Science and Technology, Trondheim, Norway.

[3]Financial support by the Research Council of Norway through its Centers of Excellence funding scheme, Project No. 262633 "QuSpin", is gratefully acknowledged.

[4]Department of Physics, University of Konstanz, Germany.

[5]Financial support by the German Research Foundation via Project 425217212 – SFB 1432 is gratefully acknowledged.

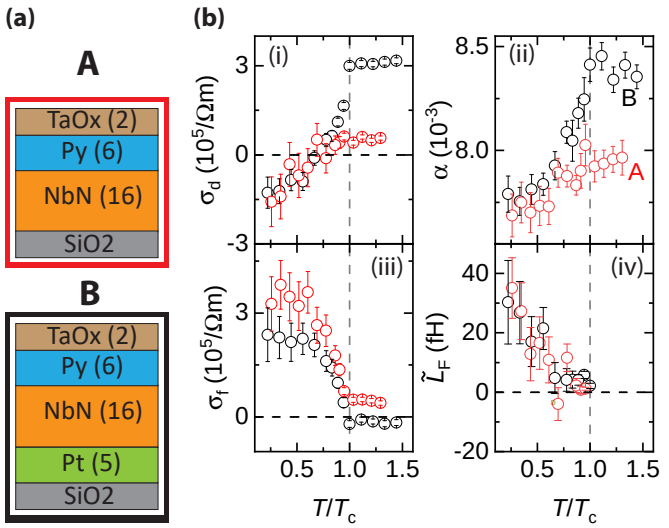

Figure 2: (a) Layer stack of samples investigated in this publication. Numbers show the layer thicknesses in nm. (b) Magnetization dynamics parameters and spin-orbit torque conductivities as function of T/T_c for sample A (red symbols) and sample B (black symbols). (i) Damping-like current-induced torque conductivity σ_d and (ii) Temperature dependence of the Gilbert damping α, which are measurands for the dynamic injection of spin currents. (iii) Extracted field-like current-induced torque σ_f plotted as a function of T/T_c. Due to a complex surface impedance $Z_{eff}(\omega)$ in the SC, the Faraday contribution σ_f^F creates an offset in $\mathrm{Im}(\tilde{L})$ plotted in (iv).

resulting α and σ^{SOT} are plotted in Fig. 2(b) (i)-(iv).

In addition, the magnetization dynamics excited in the Py layer at the FMR pump a spin current density $\mathbf{J}_s$ across the Py/NbN interface, through the NbN layer into the adjacent Pt layer as illustrated in Fig 1. In the Pt and NbN layer, $\mathbf{J}_s$ is converted into a charge current $\mathbf{J}_q$ via the inverse spin Hall effect (iSHE). This spin pumping effect manifests itself as an additional contribution to α as it represents a relaxation channel for angular momentum. Additionally, the ac magnetic field H^{iSHE} generated via the iSHE induced charge current $\mathbf{J}_q^{iSHE}$ is inductively coupled into the CPW and thus can be detected by the VNA and quantified as the damping-like current-induced torque conductivity σ_d following Ref. [6]. Similarly, a 90°-phase shifted signal in the CPW can be attributed to field-like SOT such as the inverse Rashba-Edelstein effect, but also to Faraday currents. These effects are quantified as σ_f. The

To summarize our key results, we detect a substantial field-like and a sign-change of damping-like current-induced torques in FM/SC hybrids, with stack sequences as shown in Fig. 2 (a), below T_c. Our observations on σ_d in Fig. 2(b) (i) are consistent with a shunting effect of the SC and quasiparticle-mediated inverse spin Hall effect (QMiSHE) in NbN. In particular, we establish a complementary detection technique for the QMiSHE. The Gilbert damping $\alpha(T)$ Fig. 2(b) (ii) demonstrates that spin-current transport through NbN into Pt is blocked below T_c. The sizable field-like current-induced torque in Fig. 2(b) (iii) below T_c does not originate from Faraday currents or interfacial iSOTs. This unexplained observation raises questions regarding the theoretical understanding of spin current transport in SC/FM-hybrids. In a follow-up work, we compared our initial results on NbN to those of SC/FM-heterostructures using the strong spin-orbit SC TaN [7]. For TaN, we find a larger contribution from the QMiSHE.

References

[1] G. Yang, C. Ciccarelli, and J. W. A. Robinson, APL Mater. **9**, 050703 (2021).
[2] J. Linder, and J. W. A. Robinson, Nat. Phys. **11**, 307–315 (2015).
[3] C. Bell, S. Milikisyants, M. Huber, and J. Aarts, Phys. Rev. Lett. **100**, 047002 (2008).
[4] K.-R. Jeon, C. Ciccarelli, A. J. Ferguson, H. Kurebayashi, L. F. Cohen, X. Montiel, M. Eschrig, J. W. A. Robinson, and M. G. Blamire, Nat. Mater. **17**, 499–503 (2018).
[5] M. Müller, L. Liensberger, L. Flacke, H. Huebl, A. Kamra, W. Belzig, R. Gross, M. Weiler, and M. Althammer, Phys. Rev. Lett. **126**, 087201 (2021).
[6] A. J. Berger, E. R. Edwards, H. T. Nembach, A. D. Karenowska, M. Weiler, and T. J. Silva, Phys. Rev. B **97**, 94407 (2018).
[7] M. Müller, R. Hoepfl, L. Liensberger, S. Geprägs, H. Huebl, M. Weiler, R. Gross, and M. Althammer, Mater. Quantum. Technol. **1**, 045001 (2021).

Spin Mixing Conductance in EuO/W Heterostructures

M. Opel, S. Geprägs, H. Huebl, R. Gross, M. Althammer [1]
P. Rosenberger, M. Müller [2,3]

The spin Hall magnetoresistance (SMR) allows to investigate the magnetic textures of magnetically ordered insulators in heterostructures with normal metals by magnetotransport experiments. Since its discovery nine years ago, the SMR has received significant attention, and our seminal publication [1] was cited more than 600 times in the Web of Science. The SMR has successfully been employed to probe the magnetic moment configuration in ferrimagnetic, antiferromagnetic, and complex (e.g. canted or chiral) magnetic phases [1–3]. Interestingly, the SMR in *ferro*magnetic insulators has very rarely been investigated, and only recently some results on EuS/Pt, EuO/Pt bilayers have been reported [4, 5]. In a joint collaboration with the Forschungszentrum Jülich and the University of Konstanz, we implemented the metastable ferromagnetic semiconductor EuO with a Curie temperature of 69 K and studied the SMR in *in-situ* prepared EuO/W thin film bilayers [6].

Epitaxial, bulk-like EuO thin films with a thickness of about 40 nm were grown on single crystalline, (001)-oriented yttria-stabilized zirconia (YSZ) substrates using oxide molecular beam epitaxy with subsequent *in-situ* deposition of 4 nm thin W strips through a shadow mask onto the EuO film via electron beam evaporation. For comparison, we fabricated a reference sample solely consisting of W-strips on YSZ. For magnetotransport measurements, we used a standard 4-point dc measurement technique in a 3D-vector magnet cryostat with a variable temperature insert and applied a charge current bias of 10 µA together with a current reversal method to eliminate any spurious thermal signals. We first performed angle-dependent magnetoresistance (ADMR) measurements, where the orientation of an external magnetic field with constant magnitude was varied in three orthogonal rotation planes (ip, oopj, oopt) while the sample's longitudinal (ρ_{long}) and transverse resistivity ρ_{trans} was recorded as a function of the rotation angles α, β, and γ (Fig. 1). For the bare W reference sample (blue open symbols), we only observe a $\cos^2$-dependence for the oopj and oopt rotations with a maximum magnetoresistance $MR = 4 \times 10^{-4}$ for $\mathbf{h} \parallel \mathbf{n}$, typical for an ordinary magnetoresistance (OMR). For EuO/W (black symbols), we find an additional $\cos^2$-dependence for the ip rotation, having a maximum $MR = 5 \times 10^{-5}$ at $\mathbf{h} \parallel \mathbf{j}$. This angle dependence and position of the maximum (i.e. its phase) is consistent with the SMR in ferrimagnetic insulators where the magnetization follows the external magnetic field [1].

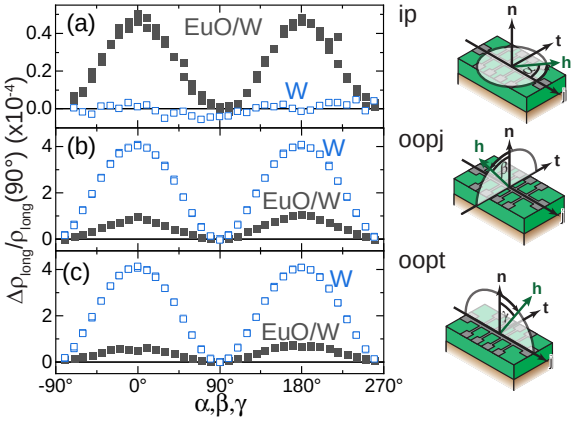

Figure 1: Longitudinal resistivity at $T = 15$ K for EuO/W (black squares) and W (open blue squares) while rotating an external magnetic field of 2 T (a) in-plane (ip), (b) out-of-plane perpendicular to **j** (oopj), and (c) out-of-plane perpendicular to **t** (oopt). The illustrations on the right show the rotation planes with respect to sample and current direction **j**. For EuO/W, we observe in all rotation planes an angle-dependence of ρ_{long}, consistent with the combined action of SMR and OMR. For the bare W layer, there is no angle-dependence visible in the ip rotation, confirming that the EuO/W interface is necessary to observe the SMR signature.

[1] We acknowledge financial support by the German Research Foundation via Germany's Excellence Strategy – EXC-2111 – 390814868 and project AL 2110/2-1.

[2] Peter Grünberg Institut, Forschungszentrum Jülich and Department of Physics, University of Konstanz, Germany

[3] P.R. and M.M. acknowledge financial support by the DFG via TRR 160 (Project C9).

Utilizing $\rho_{\text{long}} = \rho_0 + \rho_1 (1 - m_t^2)$ and $\rho_{\text{trans}} = \rho_2 m_n + \rho_3 m_j m_t$ with $m_{t,n,j}$ being the projections of the magnetization orientation $\mathbf{m}$ in EuO onto the $\mathbf{t}, \mathbf{n}, \mathbf{j}$ directions, we extracted the resistive coefficients ρ_0, ρ_1 and ρ_2 (Fig. 2(a)). With decreasing T, the SMR amplitudes ρ_1/ρ_0 and ρ_2/ρ_0 increase and the values for ρ_1/ρ_0 seem to saturate at low temperatures. Moreover, both amplitudes vanish above the Curie temperature $T_c \approx 69\,\text{K}$, determined from magnetization measurements (Fig. 2(b)). In a detailed quantitative analysis [6], we calculated the complex spin mixing conductance $G_{\uparrow\downarrow} = G_r + iG_i$ of the EuO/W interface (Fig. 2(c)). In most previous reports G_i is neglected due to the assumption $G_i \ll G_r$. This is valid for ferrimagnetic and antiferromagnetic insulators, where compensation effects can drastically reduce G_i. For our *ferro*magnetic insulator EuO, however, we need to account for G_r and G_i separately, which leads to contributions of G_i to ρ_1/ρ_0.

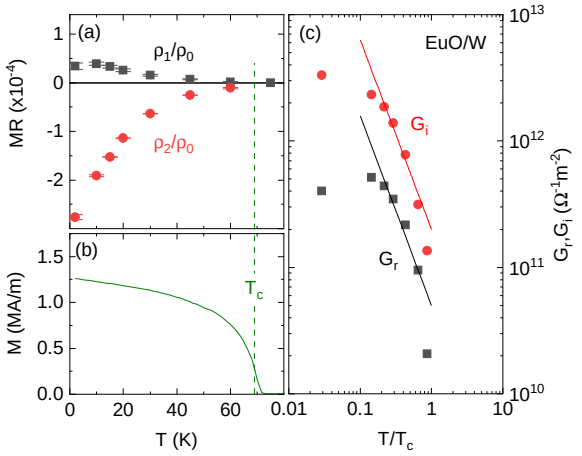

Figure 2: (a) ρ_1/ρ_0 (black) and ρ_2/ρ_0 (red) in EuO/W as a function of temperature T. (b) Remanent magnetization M of EuO/W after field cooling. (c) Real (G_r, black squares) and imaginary part (G_i, red circles) of the spin mixing interface conductance. The black and red lines indicate a $(T/T_c)^{-3/2}$ dependence.

For low T, we find $G_r = 4 \times 10^{11}\ \Omega^{-1}\text{m}^{-2}$ and $G_i = 3 \times 10^{12}\ \Omega^{-1}\text{m}^{-2}$. These values agree well with results in EuS/Pt [4], but are significantly reduced compared to $G_r = 4 \times 10^{14}\ \Omega^{-1}\text{m}^{-2}$ for the $Y_3Fe_5O_{12}$/Pt interface [1]. This indicates a lower coupling between the conduction electrons in the metal and the localized ones of the Eu^{2+} magnetic moments. The temperature dependence of G_r and G_i is explained by thermal fluctuations in the magnetic lattice, described by $G_r \approx (1 - 2n/s)G_r^{T=0}$ and $G_i \approx (1 - n/s)G_i^{T=0}$ with n the density of magnons and s the saturation magnetization per unit cell in units of $\hbar$. In the limit of a 3-dim ferromagnet with parabolic magnon band dispersion and an intermediate T/T_c range, both G_r and G_i should follow a $(T/T_c)^{-3/2}$ law, i.e. scale inversely as the number of magnons. Indeed for $0.1 < T/T_c < 0.7$, the extracted G_r and G_i agree well with a $(T/T_c)^{-3/2}$ dependence (black and red lines in Fig. 2(c)), further confirming the theoretical model. For the whole temperature range, we find $G_i > G_r$ consistent with recent experiments in EuS/Pt interfaces [4]. Our results confirm that in ferromagnetic insulators a new regime for spin-transfer torque experiments can be established, where the field-like symmetry is the dominant contribution.

References

[1] H. Nakayama, M. Althammer, Y.-T. Chen, K. Uchida, Y. Kajiwara, D. Kikuchi, T. Ohtani, S. Geprägs, M. Opel, S. Takahashi, R. Gross, G. E. W. Bauer, S. T. B. Goennenwein, and E. Saitoh, Physical Review Letters **110**, 206601 (2013).

[2] J. Fischer, O. Gomonay, R. Schlitz, K. Ganzhorn, N. Vlietstra, M. Althammer, H. Huebl, M. Opel, R. Gross, S. T. B. Goennenwein, and S. Geprägs, Phys. Rev. B **97**, 014417 (2018).

[3] K. Ganzhorn, J. Barker, R. Schlitz, B. A. Piot, K. Ollefs, F. Guillou, F. Wilhelm, A. Rogalev, M. Opel, M. Althammer, S. Geprägs, H. Huebl, R. Gross, G. E. W. Bauer, and S. T. B. Goennenwein, Physical Review B **94**, 094401 (2016).

[4] J. M. Gomez-Perez, X.-P. Zhang, F. Calavalle, M. Ilyn, C. González-Orellana, M. Gobbi, C. Rogero, A. Chuvilin, V. N. Golovach, L. E. Hueso, F. S. Bergeret, and F. Casanova, Nano Letters **20**, 6815–6823 (2020).

[5] K. Mallick, A. A. Wagh, A. Ionescu, C. H. W. Barnes, and P. S. Anil Kumar, Applied Physics Letters **116**, 202405 (2020).

[6] P. Rosenberger, M. Opel, S. Geprägs, H. Huebl, R. Gross, M. Müller, and M. Althammer, Applied Physics Letters **118**, 192401 (2021).

Spin Reorientation in the Kagome Ferromagnet Fe_3Sn_2

G. He, L. Peis, R. Stumberger, R. Hackl [1]
L. Prodan, V. Tsurkan, N. Unglert, L. Chioncel, I. Kézsmárki [2,3]

Magnets having exotic ground states attract a lot of attention not only for their fundamental properties but also for the increasing number of applications. In many cases, the properties may be tuned by small modifications of the band structure such as semiconductors or through the thickness of thin-film layers. In Fe_3Sn_2 for instance, in thin films the magnetic anisotropy rather than the Dzyaloshinskii-Moriya interaction triggers the emergence of magnetic bubbles at room temperature similar to skyrmions. Fe_3Sn_2 is a ferromagnet where the Fe atoms sit on planes of a Kagome network perpendicular to the crystallographic c-axis as shown in Fig. 1 (a) and (b). Fig. 1 (c) shows the eponymous Japanese basket. Fe_3Sn_2 has a very high Curie temperature, $T_C = 670\,K$, which hinders measurements in the paramagnetic phase. Yet, there are indications of a temperature-driven spin reorientation from out-of-plane at high temperatures towards in-plane at temperatures below approximately 100 K, which has been found earlier in Mössbauer [1, 2], x-ray [3] and transport studies [4]. Optical absorption experiments [5] reveal an additional feature in the 10 meV range below 150 K and associate it with this spin reorientation. Similarly, transport and magnetisation experiments performed on our own samples and in Ref. [6] suggest a cross-over close to $T_r \approx 100\,K$. The question arises as to the driving interaction behind this transition.

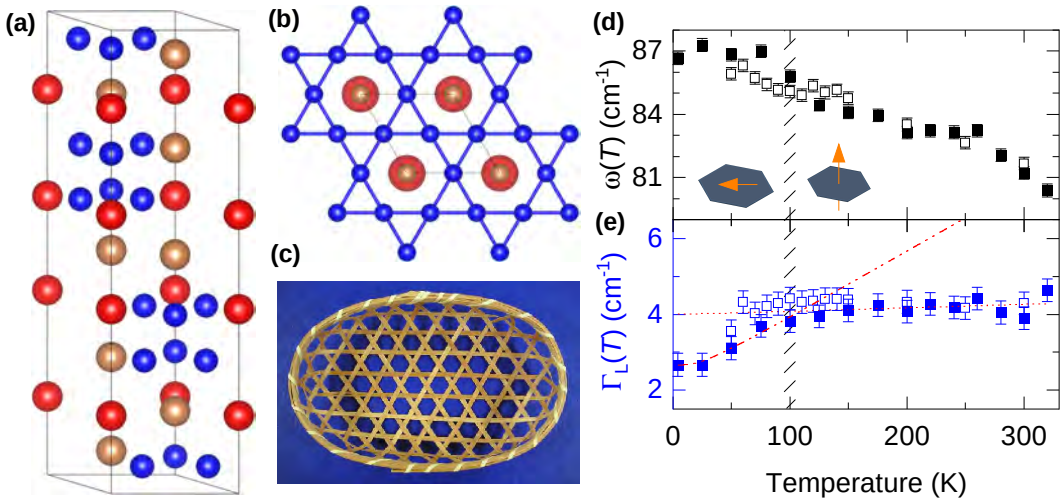

Figure 1: Fe_3Sn_2: Structure and results. (a) Crystal structure of Fe_3Sn_2. The Fe atoms (blue spheres) form a Kagome network separated by Sn atoms (braun and red spheres). (b) Planar Kagome network of the Fe atoms. The Sn atoms in the center of the hexagons are not sitting in the same plane. (c) Japanese basket from which the name is borrowed. (d) Energy $\omega(T)$ (upper panel) and linewidth $\Gamma_L(T)$ (lower panel) of the lowest A_{1g} mode. Full and open symbols represent data from different runs. The direction of the Fe spins (orange arrows) above and below the reorientation temperature $T_r \approx 100\,K$ (hatched area) is indicated with respect to the Kagome plane.

Already the origin of the rather complex itinerant magnetism of Fe_3Sn_2 remains elusive. The theoretical approaches either favor flat-band ferromagnetism [7] or a competition between potential and kinetic energy [8]. The latter case is reminiscent of the magnetism in Fe(Se,Te) where itinerant and nearly localized spins coexist [9, 10]. Yet, it is unlikely that the mag-

[1] Financial support from the German Research Foundation (DFG) through the coordinated programme TRR80 (Projekt-ID 107745057), projects HA2071/8-1, HA2071/12-1 (R.H.), and the Alexander von Humboldt Foundation (G.H.) is greatfully acknowledged.

[2] Institut für Physik, Universität Augsburg, Germany

[3] Financial support from the German Research Foundation (DFG) through TRR80 (Projekt-ID 107745057) is greatfully acknowledged.

netism in Fe_3Sn_2 can be observed directly in a similar way as in FeSe since the two-magnon excitations typical for antiferromagnets [11] do not exist here. However, indirect signatures of spin order, the spin reorientation or the interaction between spin, lattice and electrons may be expected, in particular gaps between flatbands such as in the optical experiments [5] or phonon renormalization effects as in MnSi [12]. Here, we focus on the role of the lattice and analyze the phonons.

In Fe_3Sn_2 4 A_{1g} and 5 E_g Raman-active phonons were observed [13] which all but one exhibit conventional temperature dependences described by anharmonic decay. Only the mode at the lowest energy (87 cm^{-1} in the zero temperature limit) displays deviations from the expected behavior. Fig. 1 (d) shows the temperature dependences of energy and linewidth of the fully symmetric A_{1g} phonon at 87 cm^{-1}. The energy $\omega(T)$ and the linewidth $\Gamma_L(T)$ were derived by fitting Lorentzian functions to the spectra [13]. While most of the phonon energies harden slightly around the transition [hatched area in Fig. 1 (d)], the linewidths do not experience T_r and vary according to the Klemens model for symmetric anharmonic decay [14] in the entire temperature range. Only the linewidth of the mode at 87 cm^{-1} has a distinct anomaly close to 100 K. Above T_r, $\Gamma(T)$ is essentially constant and becomes smaller by approximately 35% below T_r. Obviously, the phonon decay rate and thus the linewidth $\Gamma_L(T)$ increase exponentially with temperature up to T_r according to

$$\Gamma_L(T) = \Gamma_{L,0}\left(1 + \frac{2\lambda_{\mathrm{ph-ph}}}{\exp(\frac{\hbar\omega_0}{2k_BT}) - 1}\right), \tag{1}$$

where $\Gamma_{L,0}$ and ω_0 are the phonon linewidth and energy, respectively, at $T = 0$ and $\lambda_{\mathrm{ph-ph}}$ is the coupling parameter when an optical phonon at $\mathbf{k} = 0$ decays into two acoustic modes at $\pm\mathbf{k}$ and $\omega_0/2$. Above T_r, this decay channel seems to be blocked.

Usually, the phonon decay occurs through the lattice deformation or the electron-phonon coupling or both. Here, we speculate that at least the A_{1g} mode at 87 cm^{-1} couples also to the Fe spin. Below T_r with the spins in the plane [see Fig. 1 (d) upper panel] the coupling is strong. Above with the spins pointing out of the plane this coupling is weaker because of the phonon eigenvector. Due to demagnetization effects it is energetically more favorable if the spins are in the plane. This argues in favor of a magnetism to finally drive the transition.

References

[1] G. Le Caër, B. Malaman, and B. Roques, J. Phys. F: Met. Phys. **8**, 323–336 (1978).
[2] B. Malaman, C. Fruchart, and G. Le Caër, J. Phys. F: Met. Phys. **8**, 2389 (1978).
[3] L. A. Fenner, A. A. Dee, and A. S. Wills, J. Phys. Condens. Matter **21**, 452202 (2009).
[4] Q. Wang, S. Sun, X. Zhang, F. Pang, and H. Lei, Phys. Rev. B **94**, 075135 (2016).
[5] A. Biswas, O. Iakutkina, Q. Wang, H. C. Lei, M. Dressel, and E. Uykur, Phys. Rev. Lett. **125**, 076403 (2020).
[6] K. Heritage, B. Bryant, L. A. Fenner, A. S. Wills, G. Aeppli, and Y.-A. Soh, Adv. Funct. Mater. **30**, 1909163 (2020).
[7] A. Mielke, J. Phys. A **24**, 3311 (1991).
[8] Z. Lin, J.-H. Choi, Q. Zhang, W. Qin, S. Yi, P. Wang, L. Li, Y. Wang, H. Zhang, Z. Sun, L. Wei, S. Zhang, T. Guo, Q. Lu, J.-H. Cho, C. Zeng, and Z. Zhang, Phys. Rev. Lett. **121**, 096401 (2018).
[9] Z. P. Yin, K. Haule, and G. Kotliar, Nature Mater. **10**, 932–935 (2011).
[10] I. Leonov, S. L. Skornyakov, V. I. Anisimov, and D. Vollhardt, Phys. Rev. Lett. **115**, 106402 (2015).
[11] A. Baum, H. N. Ruiz, N. Lazarević, Y. Wang, T. Böhm, R. Hosseinian Ahangharnejhad, P. Adelmann, T. Wolf, Z. V. Popović, B. Moritz, T. P. Devereaux, and R. Hackl, Commun. Phys. **2**, 14 (2019).
[12] H.-M. Eiter, P. Jaschke, R. Hackl, A. Bauer, M. Gangl, and C. Pfleiderer, Phys. Rev. B **90**, 024411 (2014).
[13] G. He, L. Peis, R. Stumberger, L. Prodan, V. Tsurkan, N. Unglert, L. Chioncel, I. Kézsmárki, and R. Hackl, physica status solidi (b) 2100169 (2021).
[14] P. G. Klemens, Phys. Rev. **148**, 845–848 (1966).

Perseverance of the Coherent Fermi Surface in a Layered Organic Metal Near the Bandwidth-Controlled Mott Transition

M. V. Kartsovnik, S. Oberbauer, W. Biberacher [1]

The Mott insulating instability of the normal metallic state, one of the most profound consequences of electronic correlations in narrow-band conductors, has been under extensive investigation the last two decades. It is, thus, all the more amazing that no clarity has been achieved on such fundamental issue as the Fermi surface coherence and the evolution of the quasiparticle lifetime near the bandwidth-controlled Mott metal-insulator transition (MIT). For example, a number of theoretical works [1–3] proposed a dramatic enhancement of scattering, resulting in a pseudogap in the archetypal quasi-two-dimensional antiferromagnetic Mott insulator κ-(BEDT-TTF)$_2$Cu[N(CN)$_2$]Cl, hereafter referred to as κ-Cl. Other theories argued against the pseudogap formation in exactly half-filled band systems [4, 5], which is the case of this system. At the same time, a decisive experimental test probing the Fermi surface properties at a controlled variation of the correlation strength has been lacking. Magnetic quantum oscillations, being critically sensitive to scattering, should be very helpful for clarifying this issue. We have, therefore, carried out a study of quantum oscillations of magnetoresistance (Shubnikov-de Haas, SdH effect) in the metallic state of κ-Cl approaching the first-order MIT. The position of the compound on the phase diagram was tuned by applying precise controlled quasi-hydrostatic pressure.

We have succeeded in the observation of the SdH oscillations in κ-Cl in the pressure interval $20 - 100$ MPa, that includes both the purely normal metallic (NM) domain of the phase diagram and the transient region of the first-order transition where the NM and the antiferromagnetic insulating (AFI) states coexist in the bulk of the crystal. Examples of the oscillatory component of the resistance, normalized to the monotonic field-dependent background, $R_{\rm osc}/R_{\rm bg}$ are shown in Fig. 1(a). Remarkably, clear oscillations are seen even at a pressure $P = 21$ MPa, at which the NM phase occupies only a tiny volume fraction of the sample, well below 1%. Keeping in mind that SdH oscillations are a fingerprint of a well-defined Fermi surface, our observation gives a firm evidence of a narrow continuous path for coherent charge carriers even at the very edge of stability of the metallic state.

The fast Fourier transform (FFT) of the signal reveals two fundamental frequencies F_α and F_β (see Fig. 1(b)). These frequencies correspond to the classical orbit α and magnetic-breakdown orbit β on the Fermi surface, respectively, as shown in the lower inset in Fig. 1(b). In the following we focus on the β oscillations, which dominate the SdH spectrum and characterize the entire Fermi surface.

Qualitatively, the observation of the β oscillations even deep inside the AFI/NM coexistence region appears to be, by itself, a signature of a large coherent Fermi surface. On a quantitative level, the effect of a finite quasiparticle lifetime τ on the oscillation amplitude is usually described in terms of the Dingle factor $R_{\rm D} = \exp(-2\pi^2 k_{\rm B} T_{\rm D}/\hbar\omega_c)$ [6], where $k_{\rm B}$ is the Boltzmann constant, $\omega_c = eB/m_c$ is the cyclotron frequency, e the elementary charge, B the magnetic-field strength, m_c the effective cyclotron mass, and $T_{\rm D} = \hbar/2\pi k_{\rm B}\tau$ the Dingle temperature. A pseudogap, which arises from the enhanced scattering of quasiparticles on short-range antiferromagnetic fluctuations, should effectively increase $T_{\rm D}$. Thus, an analysis of the B-dependence of the SdH amplitude, yielding $T_{\rm D}$, may give a crucial test of a pseudogap formation.

As seen in Fig. 1(a), the field dependence of the SdH amplitude is nonmonotonic. The modulation originates from a weak warping of the cylindrical Fermi surface typical of strongly

[1] The work was supported in part by the German Research Foundation, project KA 1652/5-1

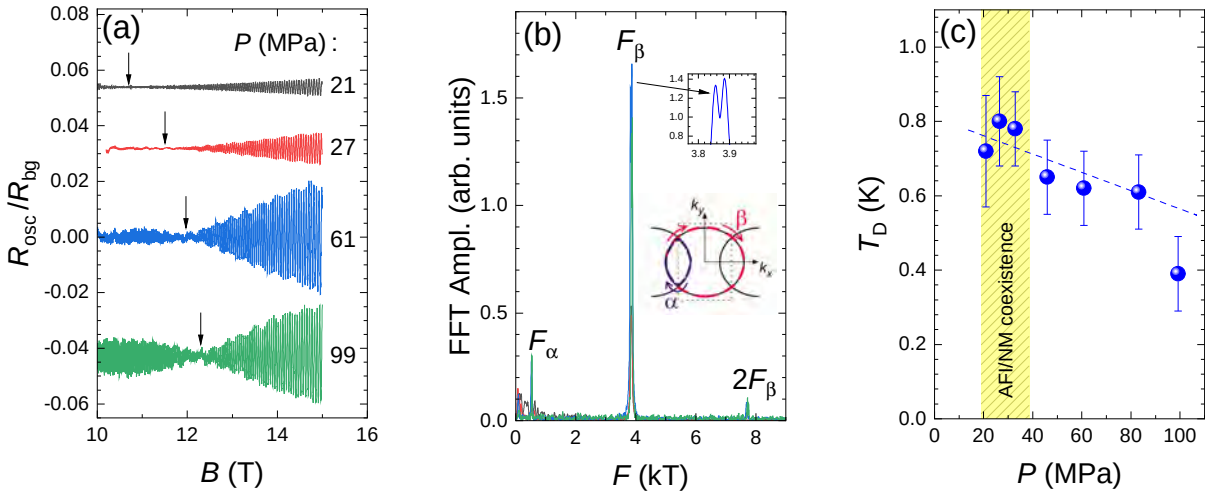

Figure 1: (a) Shubnikov-de Haas oscillations of the interlayer resistance of κ-Cl at different pressures recorded at $T = 70\,\mathrm{mK}$. The oscillatory component of the resistance R_{osc} is normalized to the monotonic B-dependent background component R_{bg}. The arrows point to the beat nodes originating from the weak warping of the Fermi surface cylinder. (b) FFT spectra of the curves shown in (a). Upper inset: close-up of the β-peak in the $P = 99\,\mathrm{MPa}$ spectrum, revealing the splitting caused by the Fermi surface warping. Lower inset: Fermi surface of κ-Cl with the classical closed orbit α (blue) and magnetic-breakdown orbit β (red). (c) Dingle temperature T_{D} of the κ-Cl sample versus pressure P. The dashed line is a guide to the eye. The shaded area is the AFI/NM coexistence region separating the low-P purely insulating and the high-P purely metallic regions.

anisotropic layered organic metals [7]. This is also reflected in a splitting of the β peak in the FFT spectrum, see upper inset in Fig. 1(b). Therefore, our analysis of the field-dependent amplitude incorporated, besides the standard exponential Dingle factor, the beating effect caused by the Fermi-surface warping, as described quantitatively by P. Grigoriev [8, 9]. The resulting Dingle temperature determined for different pressures is shown in Fig. 1(c).

The obtained values, $T_{\mathrm{D}} \lesssim 1\,\mathrm{K}$, which results in $\tau \gtrsim 10^{-12}\,\mathrm{s}$, are typical for clean crystals of organic metals [7]. With the exception of the point at 100 MPa, T_{D} stays constant within the experimental error bar. In particular, it is insensitive to the nucleation of the insulating phase, thus ruling out a dramatic enhancement of scattering in the coexistence region predicted in some works [10].

Taking all the points in Fig. 1(c), there is a weak trend of increasing T_{D} with lowering the pressure. Evaluating the change in the scattering rate directly from the Dingle temperature variation $\Delta T_{\mathrm{D}} \simeq 0.5\,\mathrm{K}$ in the displayed pressure range, one would obtain an extremely weak effect: $\Delta(1/\tau) \simeq 4 \times 10^{11}\,\mathrm{s}^{-1}$ or 0.26 meV in energy units. This is two orders of magnitude smaller than the anticipated pseudogap scale $\delta_{\mathrm{PG}} \sim 20\,\mathrm{meV}$ [1]. We thus conclude that the pseudogap formation in the present material is highly unlikely and the large Fermi surface remains fully coherent even deep in the AFI/NM coexistence region.

References

[1] J. Merino, and O. Gunnarsson, Phys. Rev. B **89**, 245130 (2014).
[2] J. Kang, S.-L. Yu, T. Xiang, and J.-X. Li, Phys. Rev. B **84**, 064520 (2011).
[3] A. Tanaka, Phys. Rev. B **99**, 205133 (2019).
[4] C.-D. Hébert, P. Sémon, and A.-M. S. Tremblay, Phys. Rev. B **92**, 195112 (2015).
[5] H. Bragança, S. Sakai, M. C. O. Aguiar, and M. Civelli, Phys. Rev. Lett. **120**, 067002 (2018).
[6] D. Shoenberg. *Magnetic Oscillations in Metals* (Cambridge University Press, Cambridge, 1984).
[7] M. V. Kartsovnik, Chem. Rev. **104**, 5737 (2004).
[8] P. D. Grigoriev, M. V. Kartsovnik, W. Biberacher, N. D. Kushch, and P. Wyder, Phys. Rev. B **65**, 060403 (2002).
[9] P. D. Grigoriev, Phys. Rev. B **67**, 144401 (2003).
[10] H. Park, K. Haule, and G. Kotliar, Phys. Rev. Lett. **101**, 186403 (2008).

Dynamics of Non-Equilibrium Heat Distribution in Rare-Earth-Doped Crystals at sub-Kelvin Temperatures

A. Meyer, R. Gross, N. Kukharchyk [1]

The rapid development of quantum computing platforms in recent years attracts interest to the quantum information field in both science and industry. However, quantum processors alone are not sufficient to fulfil all the promises made by researchers and companies, as they rely on a quantum infrastructure in which the quantum processor units are embedded [1, 2]. A controllable quantum memory is an essential element of such future infrastructure [3]. Electronic spin ensembles are among the most promising candidates to realize the quantum memory elements [4]. A great example of such spin ensembles are the rare earth ions, which have transitions in both the optical and microwave frequency regimes, and, respectively, allow to convert quantum information between optical and microwave carriers. Inhomogeneously broadened transitions in rare earth spin ensembles provide a unique possibility to realize a multi-mode quantum memory that could simultaneously store multiple quantum signals of frequency-detuned modes.

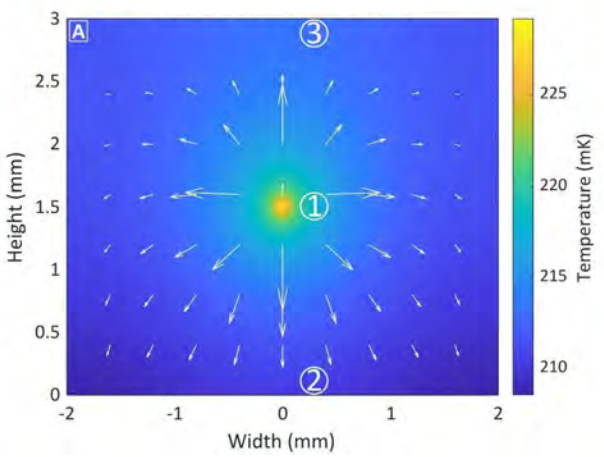

Figure 1: Colour plot of simulated heat source in the centre of the crystal and subsequent heat gradient inside of the crystal. The thermal distribution has been recorded after 50 µs ot the heating with a power of 1.4 µW. The crystal is thermally anchored to a sample holder at its lower boundary. White arrows depict the heat flow. Numbers in the circles point out the measurement points for the curves shown in Fig. 2.

Even when quantum information is stored in the isolated and well-controlled environment, the spins eventually relax to their ground state. The spin-lattice relaxation process leads to excitation of phonons, i.e. it heats up the host-crystal. Optical and microwave signals, which are routinely used for spin state manipulation, also may lead to non-equilibrium phononic excitations. Rarely observable at higher temperatures, these processes become significant below temperatures of 1 K when the heat capacity and thermal conductivity of the host crystal are strongly reduced. In numerous recent studies of the rare-earth spin ensembles at millikelvin temperatures, a divergence between actual spin temperature and that of a cryostat has been reported. Moreover, the phonon bottleneck effect has been observed in several studies [5–7], and its influence on the coherence and storage times of the quantum memories has been observed [5]. Presence of the phonon bottleneck effect tells us that the phononic bath temperature exceeds that of the spin system and may lead to excitations in the thermally polarized spin bath, which results in reduced coherence times.

The models for heat capacity and thermal conductivity have been mastered over the years, and behaviour of dilute spins in crystalline media is well-known. In the light of the rapidly developing quantum technologies, it is of great importance to understand the temporal dynamics of these sub-systems (spin ensembles and phonon bath) and their interactions at millikelvin temperatures.

[1] We acknowledge financial support from the Deutsche Forschungsgesellschaft via Germany's Excellence Strategy (EXC-2111-390814868).

In this study, we aim to characterize thermal dynamics inside of a typical host crystal Y_2SiO_5 at millikelvin temperatures. We use relevant models for spin relaxation and heat dynamics at millikelvin temperatures to create an effective thermodynamic model for spin-doped crystals. Subsequently, we implement these models with a commercially available multi-physics software to investigate time and spatial dependencies of the temperature distribution within the quantum memory devices.

The temporal evolution of heat distribution depends on the crystal properties and geometry of the excited volume. Typically, only a small fraction of spins interacts with the excitation signals resonantly. Some part of the these signals may be resonantly absorbed by phonon bath. We take geometry of the optical excitation within a crystal into account, and use it to model a heat source which induces excitation of the phonon bath, see Fig. 1. We have selected the geometry of experiment to match that with the available optical coherence study at millikelvin temperatures, see Ref. 5 for details. That study provides the most detailed experimentally derived information about the effective temperatures of different subsystems of the crystal at millikelvin temperatures.

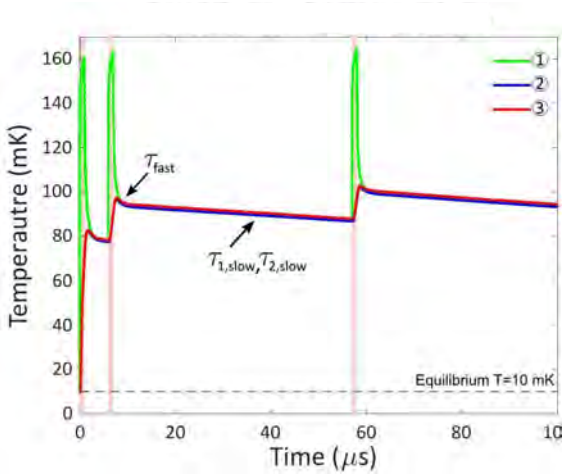

Figure 2: Simulated temperature response of the stimulated echo sequence at selected measurement points (1 - center, 2 - thermally contacted border with Kapitza resistance, 3 - insulated crystal edge, see Fig. 1). The temperature relaxation has been found to follow the triple-exponential decay. The first fast decay with a time constant τ_{fast} represents the thermal evolution after the disappearance of the excitation till an intermediate thermal gradient is reached. The subsequent slow exponents are related to slow thermal relaxation, which is related to the existence of the thermal boundary.

In particular, we have simulated the thermal dynamics of the crystal when a stimulated echo ($\pi/2 - \pi/2 - \pi/2$) sequence is applied. From the simulation, we are able to identify thermal relaxation time constants, which are in the order of 1 µs, 454 µs, and 835 µs. Example of the temperature change due to the stimulated echo sequence is demonstrated in Fig. 2.

Our results are of great importance for the community working with spin ensemble quantum memories at millikelvin temperatures. We provide a deeper insight into the thermodynamics of crystalline hosts in relation to the quantum thermodynamics of spin ensembles, which leads to a better understanding of decoherence sources and temperatures of various sub-systems.

References

[1] E. Altman, K. R. Brown, G. Carleo, and et al., PRX Quantum **2**, 017003 (2021).
[2] D. Awschalom, K. K. Berggren, H. Bernien, and et al., PRX Quantum **2**, 017002 (2021).
[3] C. Simon, M. Afzelius, J. Appel, and et al., The European Physical Journal D **58**, 1 (2010).
[4] A. Kinos, D. Hunger, R. Kolesov, and et al., arXiv:2103.15743 (2021).
[5] N. Kukharchyk, D. Sholokhov, A. A. Kalachev, and P. A. Bushev, arXiv:1910.03096 (2018).
[6] N. Kukharchyk, D. Sholokhov, O. Morozov, S. L. Korableva, A. A. Kalachev, and P. A. Bushev, Opt. Express **28**, 29166–29177 (2020).
[7] R. P. Budoyo, K. Kakuyanagi, H. Toida, Y. Matsuzaki, W. J. Munro, H. Yamaguchi, and S. Saito, Applied Physics Express **11**, 043002 (2018).

Microwave Spectroscopy of Rare Earth Spin Ensembles at Zero Magnetic Field

A. Strinic, K.G. Fedorov, R. Gross, N. Kukharchyk [1]

Recent advances in the development of quantum processors show exceptional potential of superconducting circuits which operate in the microwave regime and in the absence of external magnetic fields. While the research on quantum memories mainly focuses on the development of optical quantum memories in the field of quantum communication, a realization of a quantum memory operating in the microwave frequency range and around zero magnetic field would allow for superconducting quantum processors to interact with other quantum systems [1]. In this regard, rare-earth doped crystals are highly attractive, as they exhibit long optical and spin coherence times and posses transitions in the microwave range [2, 3].

In order to identify suitable transitions which can be addressed within a quantum memory scheme, we have conducted microwave spectroscopy on a ^{167}Er:^{7}LiYF$_4$ crystal in a magnetically shielded environment, i.e. at near-zero magnetic field. Microwave spectra were recorded with a vector network analyzer, while the crystal was placed on a meander-shaped superconducting microwave transmission line and cooled down to 10 mK in a dilution refrigerator. Transmission spectra were taken in the frequency range from 2 GHz to 4 GHz, where simulation results indicated hyperfine transitions of ^{167}Er-ions. In the following, we concentrate on the frequency range between 3.1 GHz and 3.2 GHz and compare measured results to our simulations.

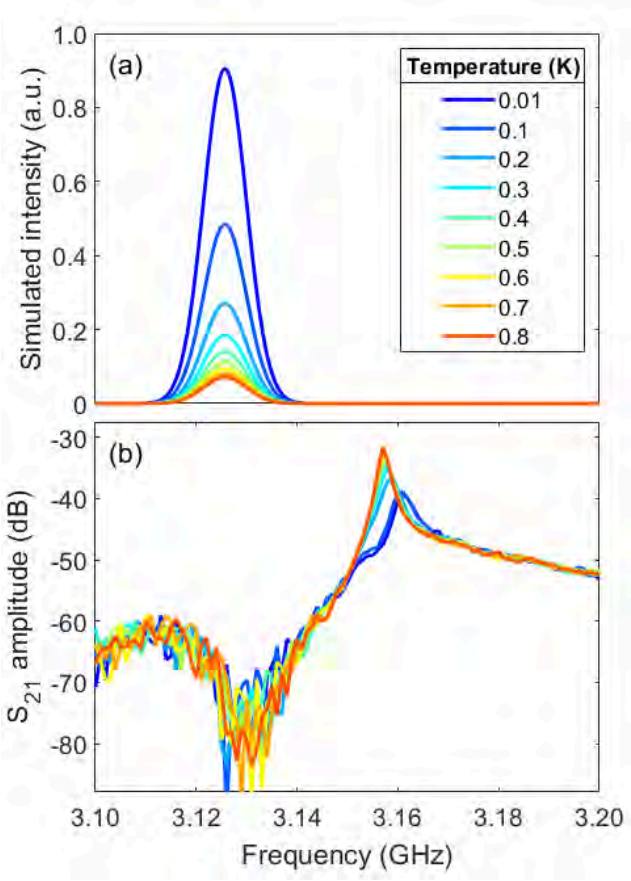

Figure 1: Temperature dependence of (a) simulated absorption and (b) measured microwave transmission spectra in the range from 3.1 GHz to 3.2 GHz. The color coding in the legend refers to (a) and (b).

In order to characterize the transitions of the ^{167}Er-ions, transmission spectra were recorded at temperatures varied from 10 mK up to 800 mK. The simulated microwave absorption is calculated via the Easyspin Matlab package and is based on g-tensor and hyperfine tensors of the respective system [4]. The temperature dependence of the simulated absorption and the measured transmission of ^{167}Er:^{7}LiYF$_4$ in the temperature range between 10 mK and 800 mK are shown in Fig. 1(a) and (b), respectively.

Fig. 1(a) indicates the temperature dependence of the simulated intensity of the absorption at 3.125 GHz. With increasing temperature, the absorption decreases, as is expected due to

[1] We acknowledge support by the German Research Foundation via Germany's Excellence Strategy (EXC-2111-390814868).

the change of energy level population of the spin ensemble. Fig. 1(b) shows the temperature dependence of the microwave transmission measured as S_{21} magnitude, in the same frequency range. While a dip can be seen at the desired frequency in the measured transmission, a temperature dependent trend is observed in the neighboring resonance, which is accompanied by a frequency shift from 3.161 GHz at 10 mK to 3.157 GHz at 800 mK.

The intensity of the simulated absorption peak for increasing temperature and the temperature dependence of the frequency shift of the measured resonance peak are given in Fig. 2. The course of the temperature dependence of both plots coincides well, underlining the assumption that the respective hyperfine transitions are coupled to the neighboring resonance. As the temperature increases, the population of the energy levels of the spin ensemble changes according to the Boltzmann distribution. This leads to a decrease in the coupling efficiency of the transition to the resonance. Finally, the resonance shifts to lower frequency, i.e. its initial state. This effect can be reproduced by power dependent measurements as well, where the population distribution is deliberately changed by applying microwave fields at higher powers to the spin ensemble. In this case, the frequency of the resonance shifts back after a time associated with the relaxation rates of the involved hyperfine levels.

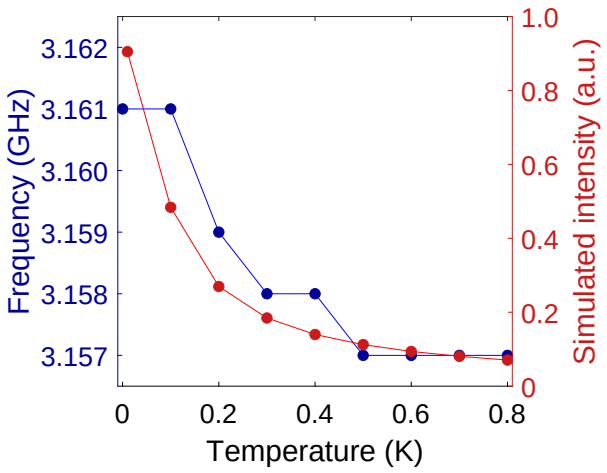

Figure 2: Temperature dependence of the simulated intensity of the absorption peak at 3.125 GHz (red) and the frequency shift (blue) of the measured resonance at 3.161 GHz.

In summary, we have investigated a rare-earth spin ensemble coupled to a microwave transmission line at near-zero magnetic field via microwave spectroscopy. This configuration is especially interesting for the development of microwave quantum memories based on rare-earth spin ensembles which could be interfaced to a superconducting quantum processor. Via temperature dependent measurements on ^{167}Er:^{7}LiYF$_4$ crystals, we have demonstrated the coupling of hyperfine transitions to a neighboring resonance at 3.161 GHz and compared the findings to theoretical simulations.

References

[1] Z.-L. Xiang, S. Ashhab, J. Q. You, and F. Nori, Rev. Mod. Phys. **85**, 623–653 (2013).
[2] M. Zhong, M. P. Hedges, R. L. Ahlefeldt, J. G. Bartholomew, S. E. Beavan, S. M. Wittig, J. J. Longdell, and M. J. Sellars, Nature **517**, 177–180 (2015).
[3] N. Kukharchyk, D. Sholokhov, O. Morozov, S. L. Korableva, A. A. Kalachev, and P. A. Bushev, New J. Phys. **20**, 023044 (2018).
[4] S. Stoll, and A. Schweiger, J. Magn. Reson. **178**, 42–55 (2006).

Mechanical Frequency Control in Inductively Coupled Electromechanical Systems

T. Luschmann, P. Schmidt, F. Deppe, A. Marx, R. Gross, H. Huebl [1,2]

The opto-mechanical interaction couples displacement of a mechanical mode to resonance frequency of an optical resonator. This setting is key for the realization of ultra-sensitive force detectors and investigation of quantum mechanics in the literal sense [1]. However, this interaction can also be realized in the microwave frequency regime using superconducting circuits. Recently, the concept of inductively coupled electromechanics, where mechanical displacement is transduced into a change of resonator inductance, and hence, resonance frequency, has been demonstrated [2–4]. We realize this concept by integrating a direct-current superconducting quantum interference device (dc-SQUID) into a coplanar waveguide (CPW) microwave resonator. Besides the advantage of having large optomechanical coupling rates, this concept also allows for tuning of the mechanical resonance frequency which is the focus of this report.

The device investigated here is shown in Fig. 1 (a)-(c). A $\lambda/4$ superconducting CPW resonator is short-circuited to ground via a dc-SQUID at one end (cf. Fig. 1b). The inductance of the SQUID is flux-dependent, allowing for control of the resonance frequency via an out-of-plane oriented applied magnetic field, B_{OOP}. To enable the electromechanical interaction, parts of the SQUID loop are suspended, forming two nanomechanical string oscillators (cf. Fig. 1c). The displacement of the strings modulates the effective area of the SQUID and, therefore, alters the magnetic flux threading the loop. This causes a displacement-dependence of the SQUID's inductance and results in a displacement dependent resonance frequency of the microwave resonator. In this experiment, we use a combination of the out-of-plane and in-plane magnetic fields. The former allows to tune the static inductance of the SQUID via controling the flux Φ_{b}, while the latter (B_{IP}) is used to realize an enhanced electromechanical interaction.

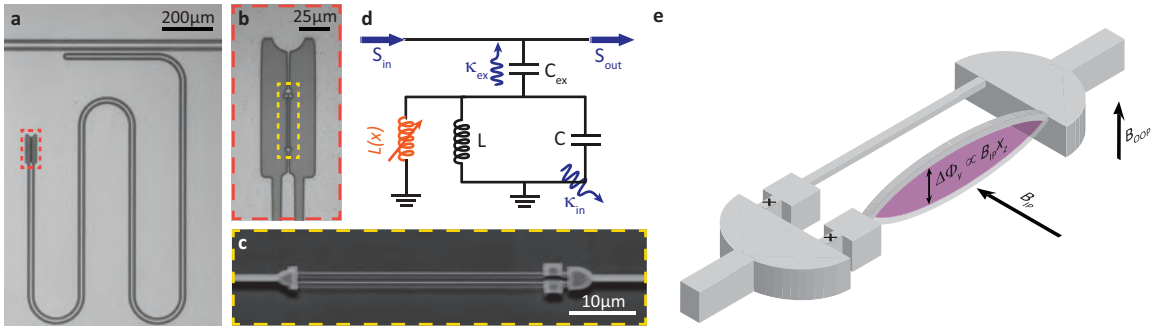

Figure 1: (**a**) Optical micrograph image of the $\lambda/4$ coplanar-waveguide resonator coupled to a feedline (top) and short-circuited to ground via a flux-dependent inductance formed by a dc-SQUID (orange box). (**b**) Magnified view of the dc-SQUID with freely suspended strings. (**c**) Tilted scanning electron micrograph image of a suspended SQUID structure similar to the one used in this work. Note that the actual device features nanostrings of 20 µm length. (**d**) Equivalent circuit representation of the device. The CPW resonator is described by means of an effective capacitance C and inductance L, forming an LC-oscillator. Additionally, the circuit contains a dynamic inductance (orange), whose magnitude depends on the time-varying displacement $x(t)$ of the mechanical element. (**e**) Illustration of the SQUID with incorporated nanostrings and relevant magnetic field directions. The shading illustrates how the motion of the nanostring modulates the flux-threaded area of the SQUID-loop due to an in-plane magnetic field B_{IP}.

[1]This project has received funding from the European Union's Horizon 2020 program (No. 736943) and from the Deutsche Forschungsgemeinschaft under Germany's Excellence Strategy (EXC-2111-390814868).

[2]We acknowledge theoretical support by Alvaro Sanchez, Department of Physics, Universitat Autonoma de Barcelona, 08193 Bellaterra, Catalonia, Spain

In order to investigate the impact of the electromechanical system on the mechanical subsystem's frequency, Ω_m, we analyze the properties of the mechanical resonator as function of Φ_b and the in-plane bias field B_{IP}. To this end, we record a thermal displacement spectrum of the anti-Stokes field. This allows us to determine Ω_m as function of Φ_b and B_{IP}. The extracted mechanical resonance frequencies are plotted in Fig. 2.

The mechanical resonance frequency Ω_m approximately shows a parabolic tuning behavior with respect to the applied flux bias. We observe a maximum tuning of roughly 1 kHz at the maximum applied in-plane field, $B_{IP} = 35\,\mathrm{mT}$. We compare these results with the theoretical prediction by Ref. 5. The presented model precisely describes our experimental findings (solid lines are fits). However, an analysis of the determined fit parameters (see inset) reveals that the uncoupled resonance frequency Ω_0 increases by several hundred Hz as B_{IP} is increased, an effect that is not accounted for by the theoretical model. The change in mechanical frequency depending on the bias flux Φ_b penetrating the SQUID loop, as modelled in Fig. 2, is well understood as a consequence of the Lorentz force acting on the oscillating nanostring. It originates from a change in the SQUIDs circulating current due to the displacement of a mechanical element, which in turn experiences an effective spring stiffening. Our comprehensive study of the mechanical resonance frequency allows us to quantitatively account for this Lorentz force based mechanism. Comparing this quantitative model with our experimental data, we can distinguish and quantify the additional, field-dependent frequency shift $\Delta\Omega_0$, which is not accounted for by the theoretical model. To explain the origin of the observed effect, we draw parallels to vibrating reed experiments, which were able to measure the stiffness of the flux line lattice (FLL) in type-II superconductors and its influence on mechanical properties [6]. In particular, the FLL can exhibit quasi-elastic properties, couple to the motion of the atomic lattice and hence influence the mechanical resonance frequency. For more details we refer the reader to Ref. 7, where we discuss and rule out other possible origins for the additional frequency shift and elaborate on flux line lattice elasticity as the most probable cause.

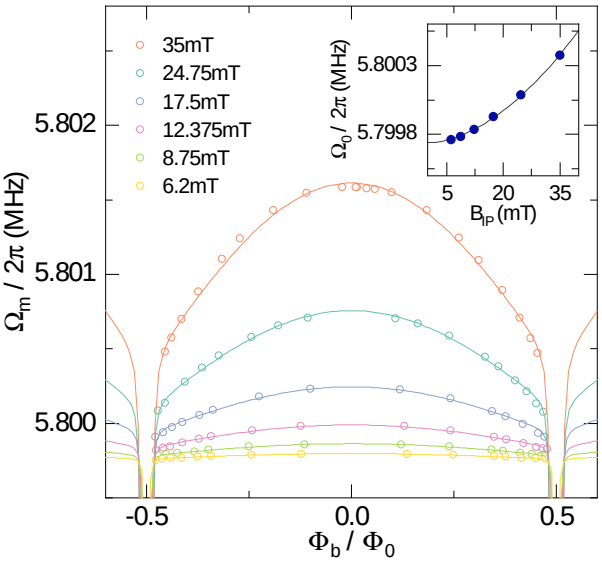

Figure 2: Extracted mechanical resonance frequency as a function of the applied bias flux through the SQUID loop, measured at different in-plane fields B_{IP} ranging from 6.2 mT to 35 mT. Lines are fits to the data according to a model from Ref. 5. The inset shows Ω_0 as a function of the applied in-plane field as extracted from the fits as well as a power-law fit (black line) revealing $\Omega_0 \propto B_{IP}^{1.81}$.

References

[1] M. Aspelmeyer, T. J. Kippenberg, and F. Marquardt, Reviews of Modern Physics **86**, 1391–1452 (2014).
[2] I. C. Rodrigues, D. Bothner, and G. A. Steele, Nature Communications **10**, 5359 (2019).
[3] P. Schmidt, M. T. Amawi, S. Pogorzalek, F. Deppe, A. Marx, R. Gross, and H. Huebl, Communications Physics **3**, 233 (2020).
[4] D. Zoepfl, M. L. Juan, C. M. F. Schneider, and G. Kirchmair, Physical Review Letters **125**, 023601 (2020).
[5] O. Shevchuk, G. A. Steele, and Y. M. Blanter, Physical Review B **96**, 014508 (2017).
[6] E. H. Brandt, P. Esquinazi, and H. Neckel, Journal of Low Temperature Physics **63** (1986).
[7] T. Luschmann, P. Schmidt, F. Deppe, A. Marx, A. Sanchez, R. Gross, and H. Huebl, Submitted for publication (2021). arXiv:2104.10577 [quant-ph].

Simulation of Dissipation in a Superconducting Quantum Annealer

Y. Nojiri, K. E. Honasoge, D. Bazulin, Q. Chen, F. Fesquet, F. Kronowetter, M. Renger, K. G. Fedorov, A. Marx, F. Deppe, R. Gross [1]

Adiabatic quantum computation is a field of research which has attracted a lot of attention from scientists and engineers. This approach promises an efficient solution of various important optimization problems. A scalable quantum annealing device can be realized with superconducting qubits and Josephson ring modulators (JRM) by realizing a strong ZZ coupling [1, 2]. Here, we study a theoretical model for such superconducting quantum annealer and investigate the influence of dissipation therein. In particular, we investigate the energy relaxation and dephasing effects of the Y and Z eigenmodes.

The circuit diagram of the model under consideration is depicted in Fig. 1. The respective model Hamiltonian is

$$\begin{aligned}\hat{H}_{\text{JRM Coupler}} =& 4E_C\hat{N}_X^2 + 4E_C\hat{N}_Y^2 + 4E_{C,Z}\hat{N}_Z^2 - E_{Ja}\cos\left(\hat{\Phi}_X\right) - E_{Jb}\cos\left(\hat{\Phi}_Y\right) \\ & - 4E_{\text{JRM}}\cos\left(\frac{\hat{\Phi}_X}{2}\right)\cos\left(\frac{\hat{\Phi}_Y}{2}\right)\cos\left(\hat{\Phi}_Z\right)\cos\left(\frac{\Phi_{\text{ext}}}{4}\right), \end{aligned} \tag{1}$$

where E_C and $E_{C,Z}$ are the charge energies of the X and Y, and Z eigenmodes, respectively. Energies E_{Ja} and E_{Jb} are the Josephson energies of the X and Y modes, and E_{JRM} is the Josephson energy of the JRM coupler. The operators $\hat{N}_{X,Y,Z}$ and $\hat{\Phi}_{X,Y,Z}$ are dimensionless charge and flux operators of each mode, while Φ_{ext} is the dimensionless external magnetic flux. The key feature in this model is an existence of the third parasitic mode (Z mode), which is inherent to the JRM coupler [3], while two other modes are the qubit modes (X and Y).

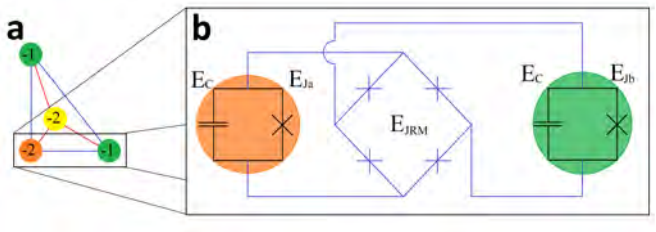

Figure 1: Part **a** shows a Lechner-Hauke-Zoller (LHZ) plaquette for a scalable quantum annealing protocol [1], where qubits are coupled with a JRM coupler. Part **b** shows the circuit diagram for the two-qubit building block based on the transmon qubits (orange and green areas) coupled via the JRM in the center.

By restricting the Hilbert space of our system to computational subspaces, we can recover the Ising spin glass formulation of adiabatic quantum annealing

$$\hat{H}_p = \sum_{k=1}^{3} b_k\hat{\sigma}_z^{(k)} + \sum_{k\neq l}^{3} J_{kl}\hat{\sigma}_z^{(k)}\hat{\sigma}_z^{(l)}, \tag{2}$$

where the coupling strengths are defined as $J_{XY} = E_C E_{\text{JRM}}/2(\sqrt{E_{Ja}+E_{\text{JRM}}}\sqrt{E_{Jb}+E_{\text{JRM}}})$ and $J_{mZ} = \sqrt{E_C E_{C,Z} E_{\text{JRM}}}/\sqrt{E_{Jm}+E_{\text{JRM}}}$ for $m = X, Y$ [2]. Here, we simulate the annealing protocol, which follows the time evolution $\hat{H}(t/\tau) = t/\tau\hat{H}_P + (1-t/\tau)\hat{H}_0$, where $\hat{H}_0 = \sum_{k=1}^{2} a_k\hat{\sigma}_x^{(k)} + b_3\hat{\sigma}_z^{(3)}$ and τ is the annealing time. Hence, we do not drive the Z mode, but only the qubit modes. To account for the dissipation, energy relaxation of the particular mode m is calculated with the following Lindblad master equation

$$\dot{\hat{\rho}} = -i\left[\hat{H}\left(\frac{t}{\tau}\right), \hat{\rho}\right] + \gamma_1\left(\hat{a}_m\hat{\rho}\hat{a}_m^\dagger - \frac{1}{2}\{\hat{a}_m, \hat{\rho}\}\right), \tag{3}$$

[1] We acknowledge support by the German Research Foundation via Germany's Excellence Strategy (EXC-2111-390814868), Elite Network of Bavaria through the program ExQM, EU Flagship project QMiCS (Grant No. 820505), and the German Federal Ministry of Education and Research via the project QUARATE (Grant No. 13N15380).

while the dephasing effects are estimated by

$$\dot{\hat{\rho}} = -i\left[\hat{H}\left(\frac{t}{\tau}\right), \hat{\rho}\right] + \gamma_\phi\left(\hat{a}_m^\dagger \hat{a}_m \hat{\rho} \hat{a}_m^\dagger \hat{a}_m - \frac{1}{2}\left\{\hat{a}_m^\dagger \hat{a}_m, \hat{\rho}\right\}\right), \tag{4}$$

where $\hat{a}_m^{(\dagger)}$ is the annihilation (creation) operator of the eigenmode $m = Y, Z$, and $\gamma_1 = 1/T_1$ and $\gamma_\phi = 1/T_\phi$ are the energy relaxation and dephasing rates, respectively. The infidelity is defined as infidelity $= 1 - |\langle\phi_0(t)|\,\hat{\rho}(t)\,|\phi_0(t)\rangle|$, which is a measure of how far the evolving state $\hat{\rho}(t)$ from the instantaneous ground state $|\phi_0(t)\rangle$ of the Hamiltonian.

The simulation results are shown in Fig. 2. We observe a general increase of the infidelities, which show 0.014 for no dissipation case, 0.060 for the Y eigenmode with only energy relaxation, 0.199 with only dephasing, 0.071 for the Z eigenmode with only energy relaxation, and 0.252 with only dephasing at the end of the protocol. This is related to a closing energy gap between the ground state and the first excited state. The energy relaxation case degrades the annealing results slightly larger than the ideal case because the qubit can still relax to its ground state, which is actually not the ground state of the whole problem Hamiltonian due to the ZZ interaction. The large infidelities of the dephasing are rather counter-intuitive because the relative phases of the energy eigenstates should not carry any information [4]. Furthermore, we observe that finite dissipation in the Z mode tends to increase the infidelity more than dissipation in the Y mode. This trend can be explained by the fact that the ZZ interaction strength between the Z mode and X, Y modes is stronger (60 MHz) than between the X and Y modes (35 MHz).

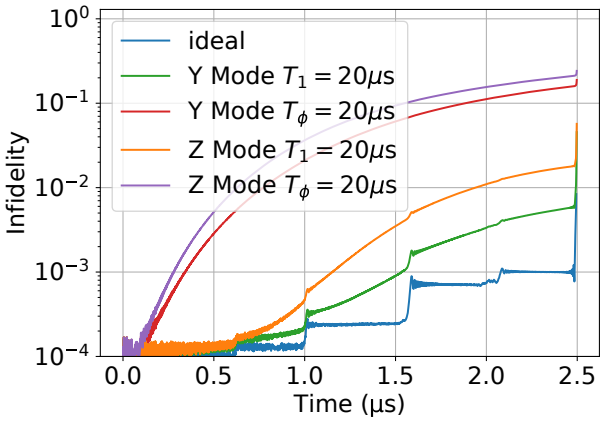

Figure 2: Temporal evolution of the infidelity for different cases: ideal case (blue), Y mode under energy relaxation (green), Y mode under dephasing (red), Z mode under relaxation (orange), and Z mode under dephasing (purple). The infidelities at the end of the protocol are 0.014, 0.060, 0.199, 0.071, and 0.252, respectively.

In summary, we have simulated the transmon qubits coupled with a JRM with a parasitic eigenmode under the influence of dissipation. Dephasing greatly increases the infidelity of the desired ground state, where further investigation is needed. Furthermore, the Z mode tends to degrade the annealing result more than the Y mode in both dissipation cases. Our work is an important step towards understanding noisy quantum annealing protocols with LHZ-type of architecture.

References

[1] W. Lechner, P. Hauke, and P. Zoller, Science Advances **1** (2015).
[2] M. Leib, P. Zoller, and W. Lechner, Quantum Science and Technology **1**, 015008 (2016).
[3] T. Roy. *Multimode Superconducting Circuits as Building Blocks for a Programmable Quantum Processor*. Ph.D. thesis, Department of Condensed Matter Physics and Materials Science Tata Institute of Fundamental Research, Mumbai (2018).
[4] Q. Deng, D. V. Averin, M. H. Amin, and P. Smith, Scientific Reports **3**, 1–6 (2013).

Application–Oriented Research

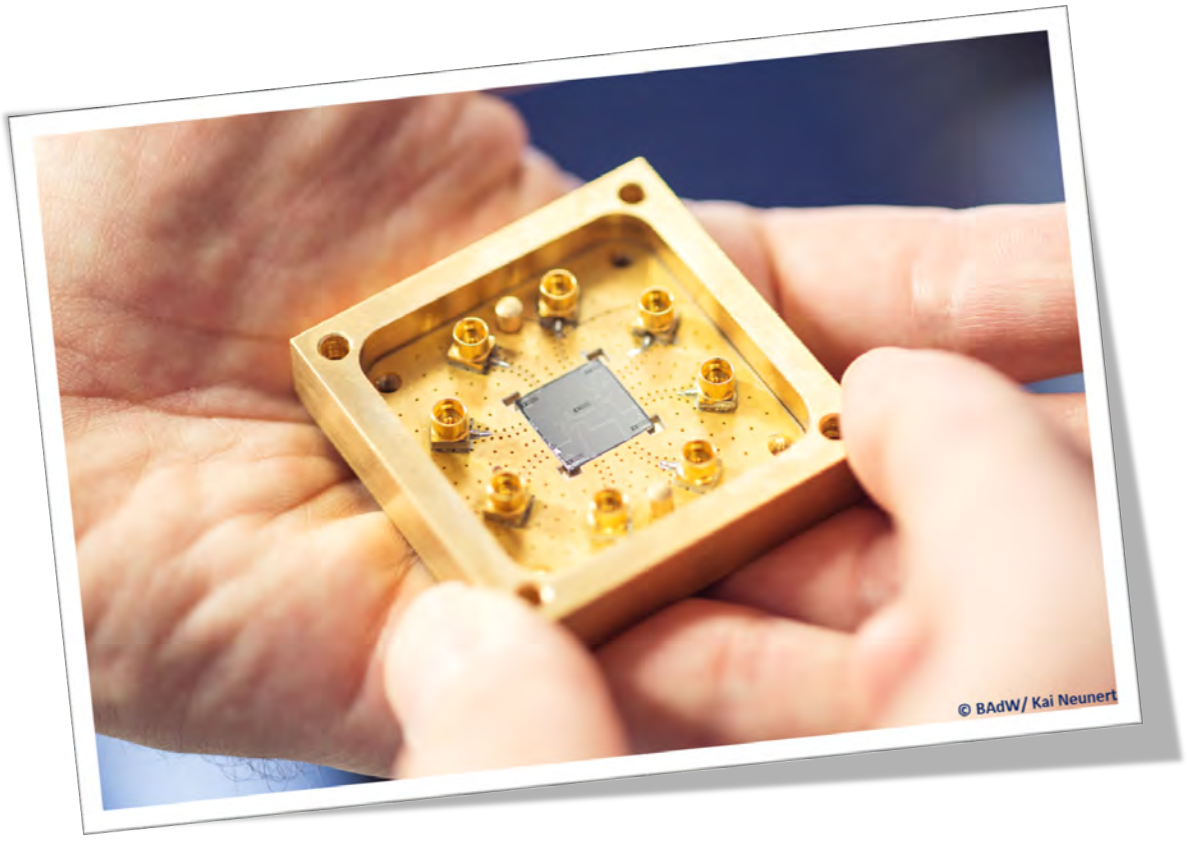

Rapid Calibration of Superconducting Qubits Without Qubit Reset

M. Werninghaus, S. Filipp [1]
D. J. Egger [2]

Quantum computers rely on thorough characterization in order to allow for high precision control and reliable operations. Characterizing quantum information processing devices and calibrating the unitary gates that are required for their operation is, however, a measurement intensive task. Quantum gates can be calibrated using error amplifying gate sequences [1] and black-box optimization algorithms inspired from optimal control which are particularly measurement intensive [2–4]. In particular, noisy quantum processors that rely on error mitigation techniques involving pulses of varying lengths, are strongly affected by the time required to calibrate and characterize each of the quantum gates. In this context the most measurement intensive task is often determining the gate fidelity which is typically done with Randomized Benchmarking (RB) [5].

The time consumption of such measurements is largely owed to the qubits being reset to the ground state in between consecutive measurements to guarantee a known and well defined initial state. The easiest way to reset a qubit is by waiting several times the decay time (T_1) so that the energy stored in the qubit relaxes to the environment. As T_1 times increase beyond 100 μs, this qubit reset mechanism becomes inefficient and lengthens the time needed to acquire data. Qubit reset schemes, both conditional [6, 7] and unconditional on the qubit state [8–10], have therefore been developed. However, such reset mechanisms require additional hardware and/or calibration.

Alternatively, the outcome of a projective measurement can be used as the initial state of the next operation. In this operation mode, named *restless tune-up*, data is gathered at elevated trigger rates without resetting the qubit back into its ground state. This allows data to be collected at a rate of the order of 100 kHz, limited only by the pulse lengths, when characterizing a quantum processor or calibrating the unitary gates. Such a rapid data gathering is essential for data intensive optimal control schemes [4].

Restless measurements have been used to successfully tune-up superconducting qubit gates with sequences of Clifford gates which ideally always compose to a state flip of the qubit [11]. However, we find that, when measuring pulse sequences which compose to arbitrary operations, a distortion appears in the measured data.

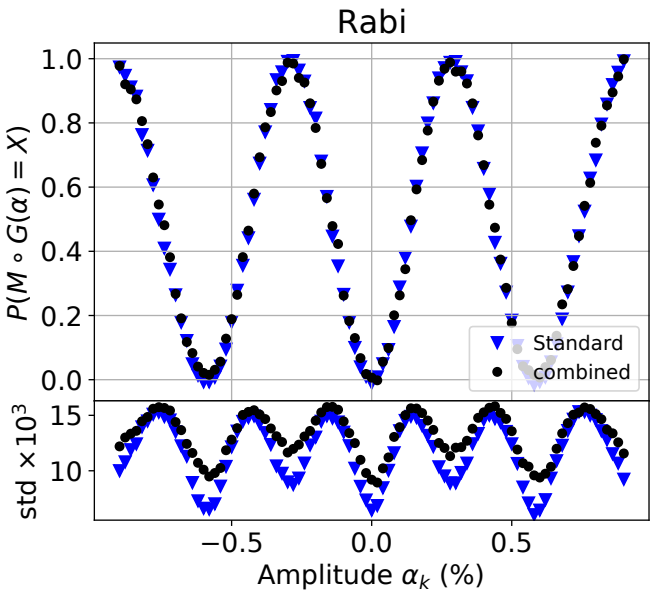

Figure 1: Rabi Oscillations measured both using conventional measurements with ground state initialization (blue triangles) and restless measurements (black dots). The subplot at the bottom shows the standard deviation of the individual measurement points.

[1]This work was supported by the European Commission Marie Curie ETN QuSCo (Grant No. 765267), the IARPA LogiQ program under contract W911NF-16-1-0114-FE, and the ARO under contract W911NF-14-1-0124.
[2]IBM Quantum, IBM Research Zurich, Switzerland

This is a direct result of the initial state
not being initialized in the qubit ground state, which in turn makes conventional data processing methods inaccurate. In our recent work [12] we show the processing steps required to efficiently and accurately analyze restless single-shot data and how to overcome the distortions to generalize the method to a broad range of experiments. We demonstrate the benefits of the method by measuring Rabi oscillations and Randomized Benchmarking, see Fig. 1 and Fig. 2. Using our method, we can execute these measurements at 250-fold and 50-fold increased data-acquisition rates, respectively, while achieving identical measurement signatures.

We expect this method to be of great benefit when completing measurement intensive calibration tasks, until active reset of qubits is readily available. The increased measurement speed has already proven highly beneficial when performing high-dimensional qubit pulse optimization algorithms, enabling the investigation of complicated pulse shapes to improve qubit gate performance [4]. We further have demonstrated the usability of the procedure for multi-qubit measurements by performing two-qubit RB, and albeit the 25-fold increased acquisition rate in this case is not as large as in single qubit measurements, the measurement time is still drastically reduced.

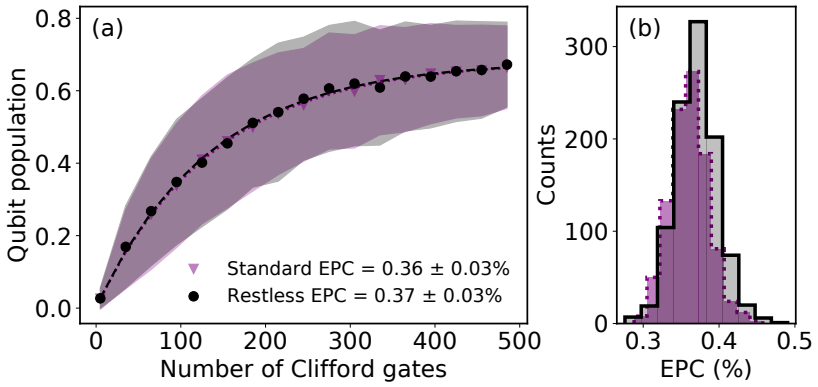

Figure 2: Randomized benchmarking of single-qubit gates measured with a 1 kHz and a 50-kHz repetition rate. (a) The dots and the shaded areas show the average and the standard deviation, respectively, of all 200 realizations of random Clifford sequences. The averages are fitted to the function $A + (B - A)\alpha^{N_c}$, with absolute weights given by the standard error of the mean. A, B, and α are fit parameters. The measured EPC is $(1 - \alpha)/2$. (b) The distribution of 1000 measurements of the Error per Clifford. Each measurement is obtained by randomly selecting 100 of the 200 sequences and fitting the mean as in (a). The mean and standard deviation of the distribution in (b) are in the legend in (a).

References

[1] S. Sheldon, E. Magesan, J. M. Chow, and J. M. Gambetta, Phys. Rev. A **93**, 60302 (2016).
[2] D. J. Egger, and F. K. Wilhelm, Phys. Rev. Lett. **112**, 1–5 (2014).
[3] J. Kelly, R. Barends, B. Campbell, Y. Chen, Z. Chen, B. Chiaro, A. Dunsworth, a. G. Fowler, I. C. Hoi, E. Jeffrey, A. Megrant, J. Mutus, C. Neill, P. J. J. O'Malley, C. Quintana, P. Roushan, D. Sank, A. Vainsencher, J. Wenner, T. C. White, A. N. Cleland, and J. M. Martinis, Phys. Rev. Lett. **112**, 240504 (2014).
[4] M. Werninghaus, D. J. Egger, F. Roy, S. Machnes, F. K. Wilhelm, and S. Filipp, npj Quantum Information **7** (2021).
[5] Phys. Rev. Lett. **106**, 180504 (2011).
[6] D. Ristè, J. G. van Leeuwen, H.-S. Ku, K. W. Lehnert, and L. DiCarlo, Phys. Rev. Lett. **109**, 50507 (2012).
[7] L. C. G. Govia, and F. K. Wilhelm, Phys. Rev. Applied **4**, 54001 (2015).
[8] K. Geerlings, Z. Leghtas, I. M. Pop, S. Shankar, L. Frunzio, R. J. Schoelkopf, M. Mirrahimi, and M. H. Devoret, Phys. Rev. Lett. **110**, 1–5 (2013).
[9] D. Egger, M. Werninghaus, M. Ganzhorn, G. Salis, A. Fuhrer, P. Müller, and S. Filipp, Phys. Rev. A **10**, 044030 (2018).
[10] P. Magnard, P. Kurpiers, B. Royer, T. Walter, J.-C. Besse, S. Gasparinetti, M. Pechal, J. Heinsoo, S. Storz, A. Blais, and A. Wallraff, Phys. Rev. Lett. **121**, 060502 (2018).
[11] M. A. Rol, C. C. Bultink, T. E. O'Brien, S. R. de Jong, L. S. Theis, X. Fu, F. Luthi, R. F. L. Vermeulen, J. C. de Sterke, A. Bruno, D. Deurloo, R. N. Schouten, F. K. Wilhelm, and L. DiCarlo, Phys. Rev. Applied **7**, 041001 (2017).
[12] M. Werninghaus, D. Egger, and S. Filipp, PRX Quantum **2**, 020324 (2021).

Direct Implementation of a Quantum Perceptron [1]

Federico Roy, Max Werninghaus, Stefan Filipp [1]

The field of machine learning has seen significant advances due to the development of neural networks, which are able to approximate any functional relation between a set of input and output variables. At the same time, quantum computing has entered an era where some problems may be more efficiently computed on a quantum rather than classical hardware. At the interface of these two fields lie quantum neural networks (QNNs), that may be able to combine the advantages of both worlds.

A classics perceptron (Fig. 1(a)) takes a number of binary inputs $x_i \in \{0,1\}$, each with an associated weight w_i, and outputs a value $y = f(x)$, where f is a non-linear function of of $x \equiv \sum_i w_i x_i + b$. In a quantum generalization of the perceptron [2], the binary variables can be naturally represented by qubit states $|0\rangle$ and $|1\rangle$. The action of the perceptron can then be represented by a gate U, whose effect on the output qubit depends on the states of the input qubits:

$$|x_1 x_2 \ldots\rangle_{\text{in}} \otimes |0\rangle_{\text{out}} \xrightarrow{U} |x_1 x_2 \ldots\rangle_{\text{in}} \otimes |y\rangle_{\text{out}},$$

where $|y\rangle_{\text{out}} = \sqrt{1-|c(x)|^2}|0\rangle + c(x)|1\rangle$ and the excitation amplitude $c(x)$ is a continuous non-linear function, as depicted in Fig. 1(b).

We implement a single-input quantum perceptron in a superconducting circuit device with two fixed-frequency transmon qubits, with bare frequencies ω_{in} and ω_{out}, interacting via a tunable coupler. To realize the step-like response function $c(x)$ we apply an adiabatic chirped pulse to the output qubit [3].

Under perfect adiabatic conditions, as illustrated in Fig. 1(c), and if the initial and the final detuning have the same sign, the two basis states $|0\rangle$ and $|1\rangle$ remain unchanged by the pulse (up to accumulated phases). If they have opposite signs, the states are flipped. Smooth response functions $|c(\Delta)|^2$ arise naturally from imperfect adiabaticity of the chirp pulse.

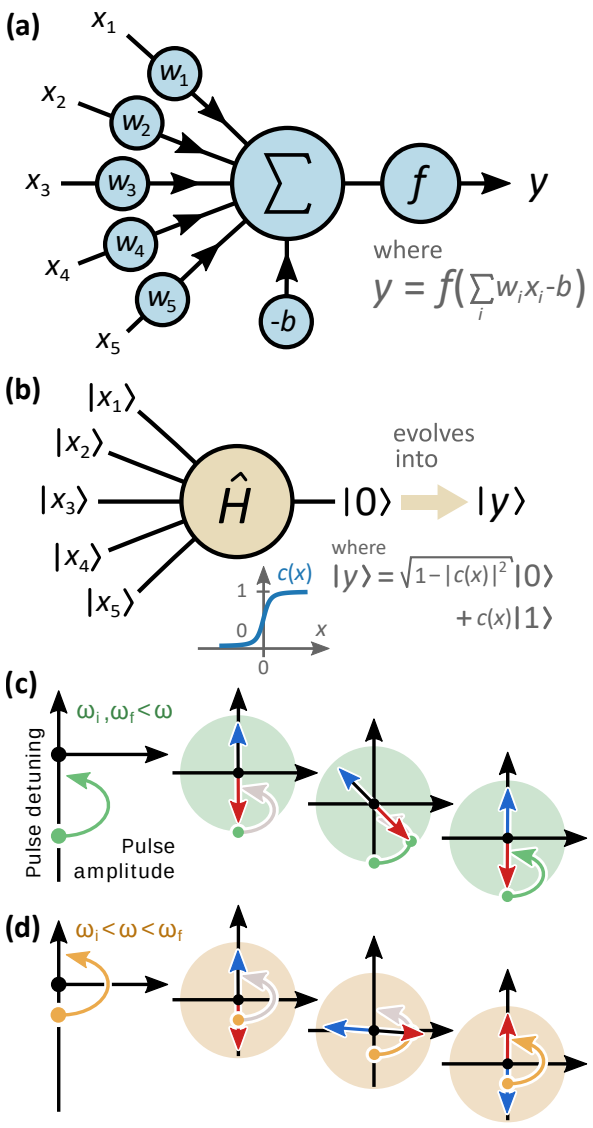

Figure 1: (a) Schematic representation of a classical perceptron with $n = 5$ inputs. The perceptron output y is given by a non-linear activation function $f(\cdot)$ applied to the sum of input values $x_1, ..., x_n$ individually weighted by $w_1, ..., w_n$ and biased by a term b. A quantum analog (b) can be constructed, where the inputs are encoded in quantum states $|x_1\rangle, ..., |x_n\rangle$ of n qubits and an output qubit, starting in the ground state, undergoes an evolution determined by the inputs values, leading to an excited population of $|c(x)|^2$. (c,d) Illustration of the effect of an adiabatic chirped pulse with initial and final frequencies ω_i and ω_f on a qubit with a frequency ω. (c) If the initial and final detunings have the same sign, the basis states $|0\rangle$ and $|1\rangle$ are unchanged (up to a phase). (d) If the signs are opposite, the states get swapped.

[1]We acknowledge support by the European Union, agreements No. 765267 (QuSCo) and No. 828826 (FET-Open Quromorphic), the BMBF program GeCQoS (FKZ 13N15680), and by the DFG (EXC2111 - 390814868).

Furthermore, by subjecting the system to a ZZ interaction between the two qubits,

$$H_{\text{int}} = J|1\rangle\langle 1|_{\text{in}} \otimes |1\rangle\langle 1|_{\text{out}}, \tag{1}$$

we implement a linear dependence of the output qubit frequency on the input $\tilde{\omega}_{\text{out}} = \omega_{\text{out}} + Jx_1$. Hence, we achieve the mapping

$$\Delta = \omega_{\text{f}} - \tilde{\omega}_{\text{out}} = w_1 x_1 + b, \tag{2}$$

where $b = \omega_{\text{f}} - \omega_{\text{out}}$ and $w_1 = -J$. Thus, we implement a quantum perceptron with response function $c(\Delta)$.

By controlling the final pulse frequency ω_{f} and the coupling strength J, we can tune the bias b and weight w_1 independently, as demonstrated in Fig. 2, allowing for trainability of the network. Fig. 2(a) shows the measured effect of the pulse on the qubit state as a function of the bias b for several pulse lengths T. In these measurements, the qubit is initialized in its ground state and its excited state population p_{e} after the pulse is observed to follow a step-like curve, where the slope of the transition increases with the pulse length due to non-adiabatic effects. The effect of the ZZ coupling between the output and the input qubit is a shift of the S-shaped activation function dependent on the input qubit being in the excited state, as demonstrated in Fig. 2(b).

We envisage that this demonstration of the basic operation of a quantum perceptron will guide future research towards the implementation of practical quantum neural networks.

We acknowledge major contributions to this work by Marek Pechal, Samuel Wilkinson, Gian Salis and Michael Hartmann.

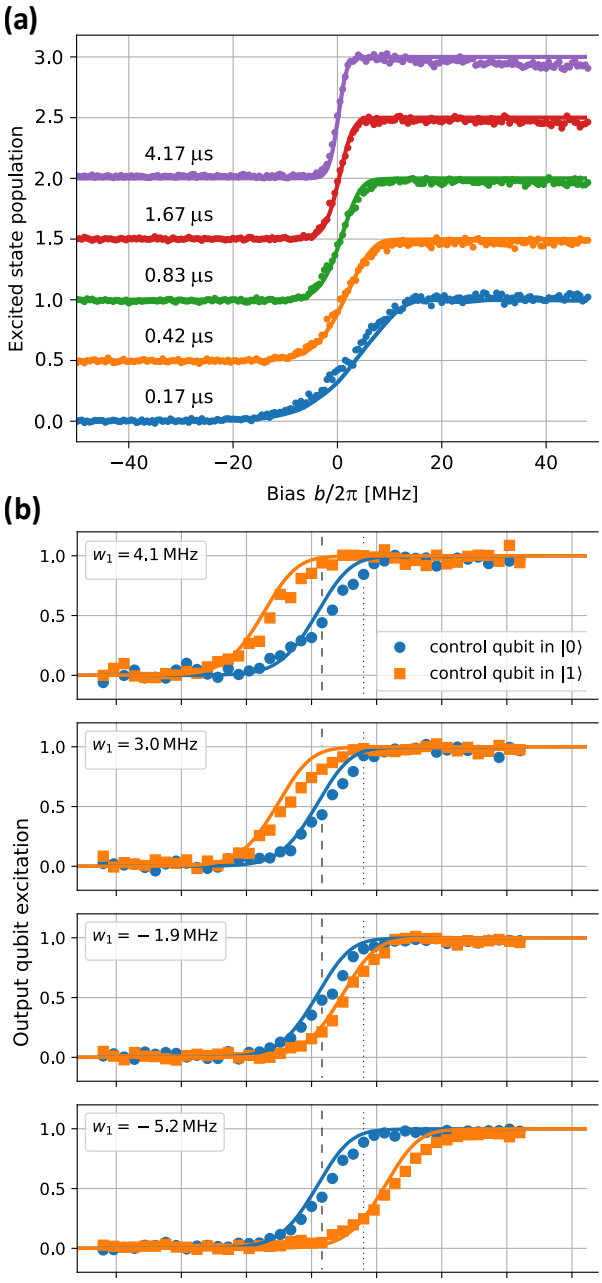

Figure 2: (a) The quantum perceptron activation functions: The excited state population of the output qubit as a function of its final detuning Δ after an adiabatic chirped pulse is applied on the ground state of the two-qubit system. Results for different pulse lengths T are offset for better visibility. The characteristic width of the activation function is inversely proportional to the pulse lengths T. Solid lines result from a simulation of unitary evolution under the adiabatic drive, with no fit parameters. (b) Frequency shift, $-w_1$, of the activation function dependending on the state of the input qubit, for the pulse length of $T = 1.67\,\mu$s. Both the magnitude and sign of this shif can be varied by tuning the coupler frequency. In these plots, the output qubit excitations are rescaled to correct for relaxation and readout imperfections, in order to highlight the agreement of the curve's shape with the simulation results.

References

[1] M. Pechal, F. Roy, S. A. Wilkinson, G. Salis, M. Werninghaus, M. J. Hartmann, and S. Filipp (2021). arXiv:2111.12669.

[2] E. Torrontegui, and J. J. García-Ripoll, Europhysics Letters **125**, 30004 (2019).

[3] M. Roth, N. Moll, G. Salis, M. Ganzhorn, D. J. Egger, S. Filipp, and S. Schmidt, Phys. Rev. A **99**, 022323 (2019).

Towards Quantum Local Area Networks

M. Renger, W. Yam, S. Gandorfer, O. Gargiulo, F. Fesquet, K. Honasoge, F. Kronowetter, D. Bazulin, Q. Chen, Y. Nojiri, A. Marx, R. Gross, K. G. Fedorov, F. Deppe [1]

Rapid progress in the field of superconducting quantum information processing triggers a general demand in efficient ways to transfer quantum microwave states between distant nodes. In particular, a concept of quantum local area networks (QLANs) for controlled exchange of such quantum states is important for future distributed quantum computing. Superconducting coaxial cables combined with cryogenic links connecting distant quantum processors in spatially separated dilution refrigerators offer a natural way to accomplish this task.

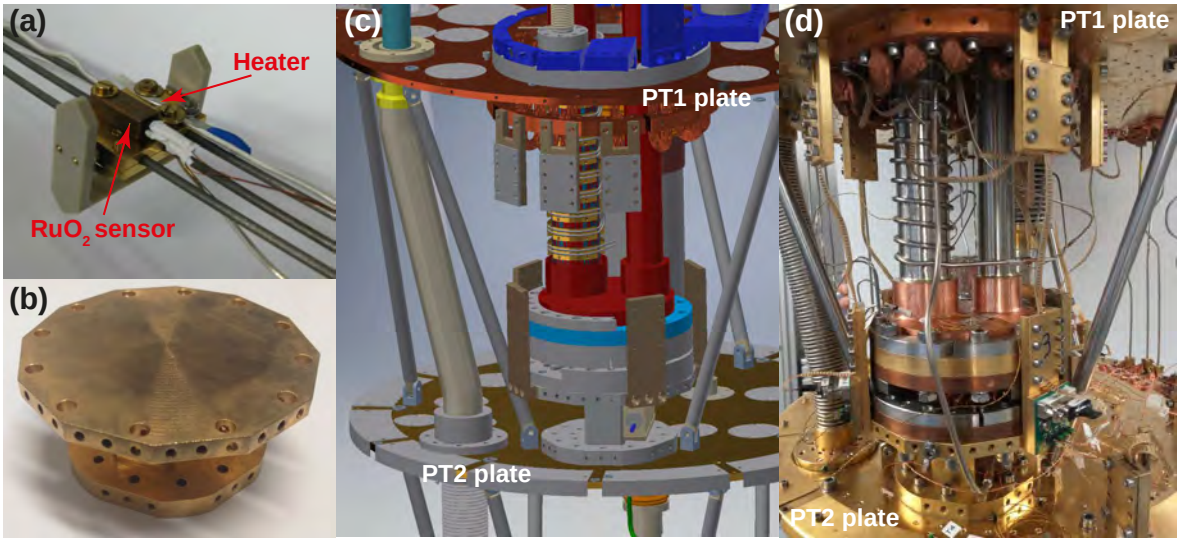

Figure 1: (a) Holder for the superconducting coaxial cables passing through the cryogenic link. A RuO_2 sensor and a 100 Ω heater are installed for controlled local heating. (b) Adapter component for the Alice PT2 plate and the copper braids used for mechanical decoupling. (c) CAD drawing for the integration of the PT420 cold head into the Alice cryostat. (d) Photograph of the finally mounted PT420 cold head.

At WMI, we are testing a prototype for such a cryogenic link, in cooperation with Oxford Instruments Nanotechnology Ltd. (OINT). Our cryogenic link has a length of 6.5 m and consists of a commercial cryostat provided by OINT (Bob) and a home-built dry dilution refrigerator (Alice). An intermediate cold network node (Eve), operated with a cryomech PT415 cold head, provides additional cooling power at the center of the link. The innermost tube of the cryolink contains three 2 m long superconducting coaxial cables, combined in a continuous, 6 m long microwave superconducting transmission line. The cables are attached to 13 holders, where each holder contains a gold-plated copper feedthrough which is thermalized by two silver wires. The innermost holder, shown in Fig. 1(a), is additionally equipped with a sensor and heater. In the first test cooldown, we have found that we are limited by the cooling power provided by the PT410 cold head in Alice. As the result, we have decided to upgrade Alice with a PT420 cold head to gain additional 1 W of cooling power at the PT2 stage. A main building block of the thermal coupling for the new cold head is shown in Fig. 1(b). This component is central for establishing strong thermal coupling between the PT2 Alice plate and the PT420 cold head, while suppressing mechanical (vibrational) coupling. A CAD drawing for the new thermal coupling is shown in Fig. 1(c). The final assembly is depicted in Fig. 1(d).

A first benchmark cooldown for the modified Alice fridge demonstrated a PT1 temperature of

[1] We acknowledge support by the German Research Foundation via Germany's Excellence Strategy (EXC-2111-390814868), Elite Network of Bavaria through the program ExQM, EU Flagship project QMiCS (Grant No. 820505), and the German Federal Ministry of Education and Research via the project QUARATE (Grant No. 13N15380).

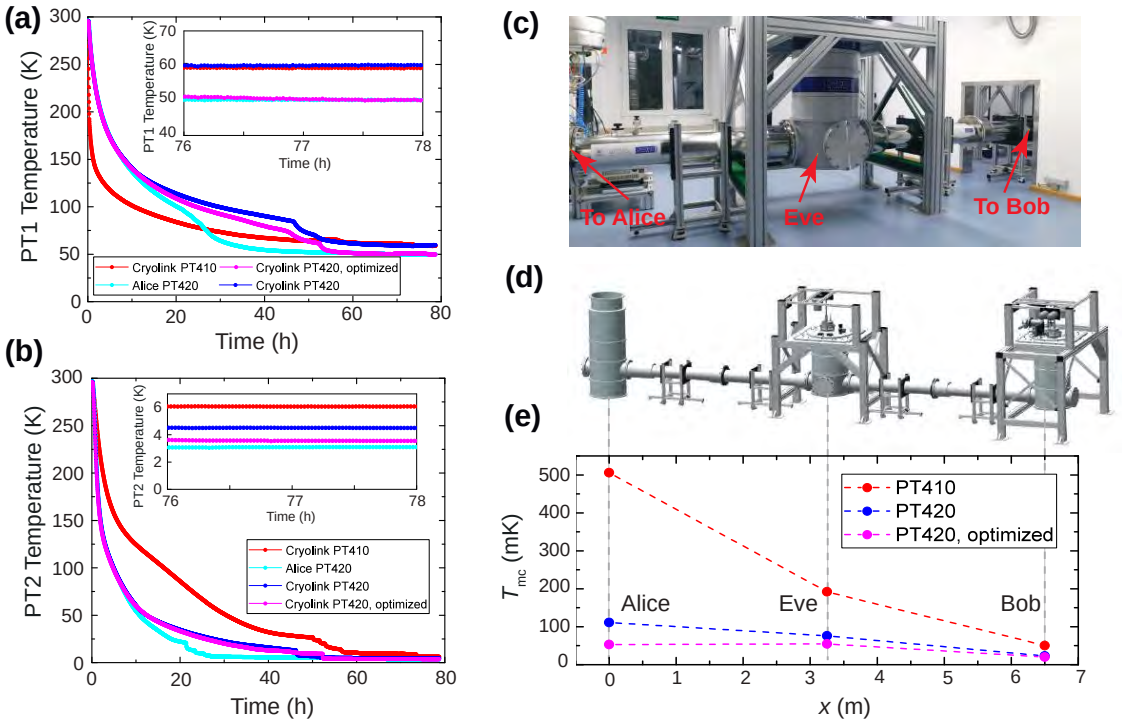

Figure 2: (a) Alice PT1 temperature for the cryolink cooldown with the PT410 cold head (red), PT420 cold head (blue) and PT420 cold head after removing thermal leaks (magenta). The cyan line shows the respective data from the Alice test cooldown with the PT420 cold head (without the cryolink attached). The inset shows the steady state temperatures. (b) Respective results for the Alice PT2 plate. (c) Photograph of the cryolink, indicating the location of Alice, Eve and Bob. (d) CAD model of the cryolink. Grey dashed lines show the position of the respective mixing chamber thermometers. (e) Gradient of the mixing chamber temperature T_{mc} over the link.

$T_{PT1} = 49\,K$ and a PT2 temperature of $T_{PT2} = 3\,K$, thereby providing a significant improvement of the precooling performance (see Fig. 2(a), cyan line). Within this test cooldown, the heat load of the cryolink is estimated by externally heating the PT2 stage, from which we expect $T_{PT2} = 3.6\,K$ with the cryolink attached. In the end, we tested the completely assembled cryolink set-up shown in Fig. 2(c), leading to $T_{PT1} = 59\,K$ and $T_{PT2} = 4.6\,K$. Despite significant improvement in comparison to the PT410 cold head, the PT2 temperature has been still above the required 4.15 K for Helium liquefication. Thus, the system must be further optimized by removing thermal leaks between the link segments. The latter efforts have led to a drastic increase of the cryolink performance, as we reached the steady state temperatures $T_{PT1} = 49\,K$ and $T_{PT2} = 3.6\,K$. This result enabled stable operation of both fridges with the base temperatures of 52 mK (Alice) and 20 mK (Bob). The corresponding temperature at the center of the cryolink was 55 mK (Eve). The results from all cooldowns are summarized in Fig. 2(a) and (b). The respective insets show the final steady state temperatures. We observe that T_{PT1} is limited by thermal coupling to the room temperature shield, whereas for T_{PT1} the limiting factor is the cooling power provided by the cold head. Figure 2(e) shows the temperature gradient over the cryolink, where the sensor positions are indicated in Fig. 2(d). The slight deviations from the expected linear gradient result from residual heat leaks.

The demonstrated QLAN prototype is readily available for testing of various microwave quantum communication protocols [1, 2] towards distributed quantum computing.

References

[1] S. Pogorzalek *et al.*, Nat. Commun. **10**, 2604 (2019).
[2] K. G. Fedorov *et al.* Accepted for publication in Science Advances, arXiv:2103.04155 (2021).

Microwave Quantum Key Distribution in Open-Air

F. Fesquet, F. Kronowetter, M. Renger, K. Honasoge, Q. Chen, Y. Nojiri, O. Gargiulo, A. Marx, R. Gross, F. Deppe, K. G. Fedorov [1]

Quantum communication with continuous-variables (CV) has been of great interest in the last decades. This particularly includes topics such as quantum teleportation or quantum key distribution (QKD). The latter has attracted a lot of attention due to the promise of unconditionally secure communication. At the same time, quantum communication in the microwave domain has also made significant advances due to its connection to the thriving field of superconducting quantum circuits [1, 2]. Furthermore, one can try to exploit low absorption losses of propagating microwave signals in open-air scenarios in order to investigate feasibility of purely microwave QKD protocols. Here, we present a short summary of our studies on a possible implementation of an open-air microwave CV-QKD protocol.

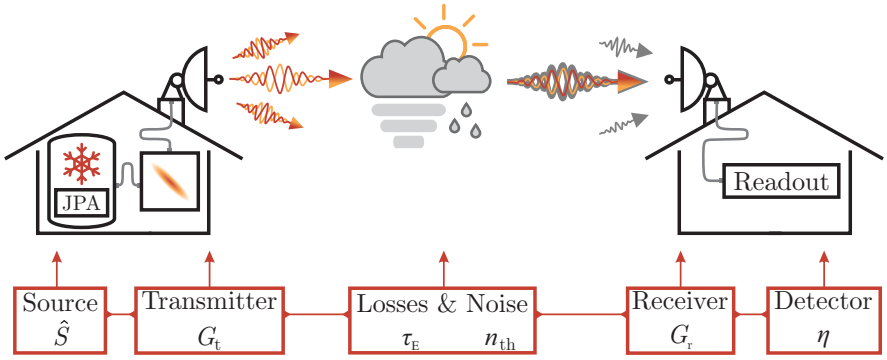

Figure 1: Schematics of main components for an open-air microwave CV-QKD implementation. Source denotes a squeezing generator, typically implemented with a JPA. Transmitter and receiver correspond to antennae with the gain G_t and G_r, respectively. Atmospheric absorption losses are quantified using transmissivity τ_E with a thermal background noise of n_{th} photons. Readout is modelled as a homodyne detector with an overall quantum efficiency η.

We focus on the specific CV-QKD protocol introduced in Ref. 3 in the microwave range. In this protocol, an emitter Alice encodes a classical Gaussian-distributed key within a sequence of displaced squeezed states and send them to a receiver Bob. The latter obtains an estimation of Alice's encoded key by using local homodyne measurements in a certain projection basis. Each key element, or symbol, is encoded either into a q-squeezed or p-squeezed state. Security of this protocol can be estimated by using the secret key quantity, which is measured in units of bits per symbol and represents the amount of secure information communicated.

In Fig. 1 we present a generic scheme for our open-air microwave CV-QKD protocol. The displaced squeezed states encoding the information of Alice are generated at milli-Kelvin temperatures by using a flux-driven Josephson parametric amplifier (JPA) in conjunction with a cryogenic directional coupler [4, 5]. From there, microwave antennae serve as an interface between the cryogenic quantum states and ambient open-air environment. For antennae, a central figure of merit is the passive antenna gain G, allowing to minimize geometric attenuation of microwave signals during communication. Here, we consider an idealized case when the total gain of receiving and transmitting antennae fully compensates for geometric losses. In the latter case, the main obstacle for the microwave CV-QKD is posed by atmospheric absorption losses and room temperature noise. In order to model the case of maximal security, all thermal noise and losses are attributed to a potential eavesdropper. We describe the ef-

[1] We acknowledge support by the German Research Foundation via Germany's Excellence Strategy (EXC-2111-390814868), Elite Network of Bavaria through the program ExQM, EU Flagship project QMiCS (Grant No. 820505), and the German Federal Ministry of Education and Research via the project QUARATE (Grant No. 13N15380).

fect of these losses and noise by using the following input-output relation for a bosonic field operator $\hat{a}$ based on the beam splitter model

$$\hat{a}' = \sqrt{\tau_E}\,\hat{a} + \sqrt{1-\tau_E}\,\hat{h}, \tag{1}$$

where $1-\tau_E$ represents the atmospheric absorption in dB. Here, we estimate microwave atmospheric specific attenuation for ideal dry weather with corresponding values of 6.3×10^{-3} dB/km. Furthermore, we model environmental mode $\hat{h}$ as a thermal state with an average number of noise photons n_{th} obeying the Planck distribution. Lastly, we model signals readout as a microwave homodyne detector with an overall quantum efficiency η. We account for the latter as additional noise photons on the received microwave signals.

Finally, we numerically calculate the secret key versus a communication distance d between Alice and Bob for various initial squeezing levels, for both direct reconciliation case (DR) and reverse reconciliation (RR). The resulting graphs are shown in Fig. 2. Remarkably, we observe a positive secret key (i.e., unconditionally secure communication) over a finite communication distances of up to 200 m, in both DR and RR cases for our microwave communication protocol. Thus, these results indicate feasibility of microwave CV-QKD in open-air conditions. No major distinction in communication distances is observed between these two reconciliation cases, although DR yields higher secure communication distance at low squeezing levels. This behaviour originates from presence of the bright microwave thermal background, where the effects of coupled noise largely outweigh the effects of losses. Furthermore, from our numerical calculations, we find microwave CV-QKD to be robust against weather imperfections such as rain, or fog. In particular, we observe in these cases that maximal secure communication distances are almost unchanged compared to the ideal dry weather conditions.

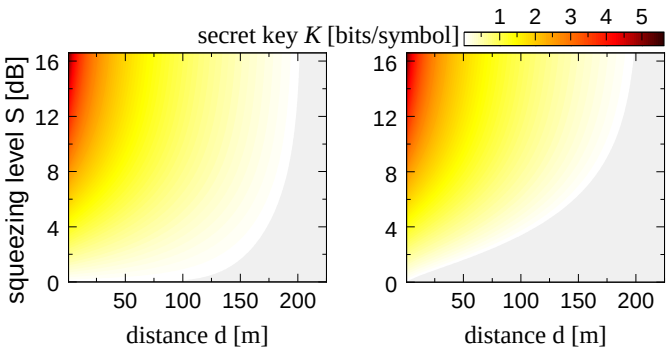

Figure 2: Microwave secret keys for DR (left) and RR (right) versus the squeezing level S (measured in dB below the vacuum limit) and communication distance d for ideal detection quantum efficiency $\eta = 1$. We assume ideal squeezed states with the environmental noise photon level $n_{\mathrm{th}} = 1250$ and transmission losses $\tau_E \simeq 6.3 \times 10^{-3}$ dB/km for the carrier frequency of 5 GHz. Grey areas represent the regions of insecure keys.

In summary, our theoretical analysis indicates large potential for microwave CV-QKD in the near-term future by using established technology of superconducting circuits.

References

[1] S. Pogorzalek, K. G. Fedorov, M. Xu, A. Parra-Rodriguez, M. Sanz, M. Fischer, E. Xie, K. Inomata, Y. Nakamura, E. Solano, A. Marx, F. Deppe, and R. Gross, Nat. Commun. **10**, 2604 (2019).

[2] C. J. Axline, L. D. Burkhart, W. Pfaff, M. Zhang, K. Chou, P. Campagne-Ibarcq, P. Reinhold, L. Frunzio, S. M. Girvin, L. Jiang, M. H. Devoret, and R. J. Schoelkopf, Nat. Phys. **14**, 705–710 (2018).

[3] N. J. Cerf, M. Lévy, and G. V. Assche, Phys. Rev. A **63**, 052311 (2001).

[4] L. Zhong, E. P. Menzel, R. Di Candia, P. Eder, M. Ihmig, A. Baust, M. Haeberlein, E. Hoffmann, K. Inomata, T. Yamamoto, Y. Nakamura, E. Solano, F. Deppe, A. Marx, and R. Gross, New J. Phys. **15**, 125013 (2013).

[5] K. G. Fedorov, L. Zhong, S. Pogorzalek, P. Eder, M. Fischer, J. Goetz, E. Xie, F. Wulschner, K. Inomata, T. Yamamoto, Y. Nakamura, R. Di Candia, U. Las Heras, M. Sanz, E. Solano, E. P. Menzel, F. Deppe, A. Marx, and R. Gross, Phys. Rev. Lett. **117**, 020502 (2016).

Frequency Degenerate Josephson Mixer for Quantum Illumination

F. Kronowetter, F. Fesquet, K. Honasoge, M. Renger, Y. Nojiri, Q. Chen, O. Gargiulo, A. Marx, R. Gross, F. Deppe, K. G. Fedorov [1]

In quantum illumination, a joint measurement of the signal and idler beams enables a quantum advantage in target detection, as compared to the ideal classical radar [1]. This advantage is predicted to exist for the case of weak quantum signals in a bright thermal background region, which potentially contains a weakly reflecting target. In contrast to classical approaches, the joint measurement exploits non-classical correlations between the signal and idler modes. A promising detector proposal allowing for a theoretical 3 dB quantum advantage consists of a frequency degenerate Josephson mixer (JM) combined with a single photon detector [2].

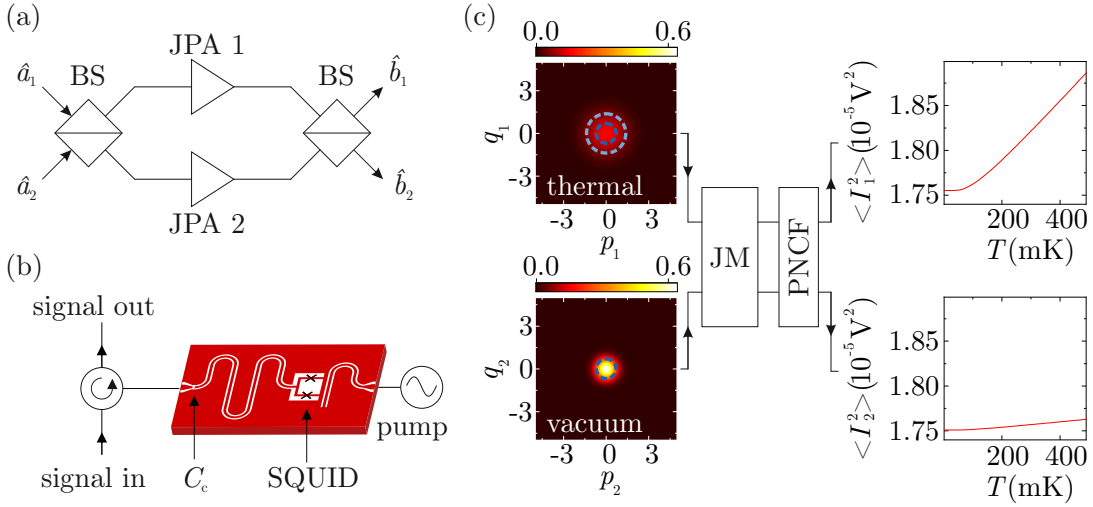

Figure 1: (a) Schematic of the JM circuit. Two modes, described by bosonic operators $\hat{a}_1$ and $\hat{a}_2$, are superimposed on a hybrid ring beam splitter (BS). Subsequently, the respective signals enter JPA1 & JPA2 and are recombined by a second BS to form the output signals with bosonic operators $\hat{b}_1$ and $\hat{b}_2$. **(b)** Schematic structure of a flux-driven JPA consisting of a coplanar waveguide resonator coupled to a circulator via a coupling capacitor C_c. A pump tone is coupled inductively to a dc-SQUID at the opposite end of the resonator. **(c)** PNCF simulation for a thermal state, controlled by T, as input 1 (top) to the JM and a vacuum state as input 2 (bottom). The dashed blue $1/e$-contours of the Wigner functions illustrate the increased variance of a thermal state (light blue) compared to the vacuum (dark blue).

The circuit layout of such frequency-degenerate JM consists of two 180° hybrid ring beam splitters and two custom-made flux-driven Josephson parametric amplifiers (JPAs), as depicted in Fig. 1(a). In both signal lines, a circulator connected to the respective JPA separates the incoming and outgoing signals, as shown in Fig. 1(b). We operate both JPAs in the frequency degenerate mode by pumping them at twice the resonance frequency. The JPAs are set to perform a phase-sensitive amplification with identical gains G but along orthogonal directions in phase space. In this case, this circuit implements, in theory, a well-known input-output relation for the JM,

$$\begin{aligned} \hat{b}_1 &= \sqrt{G_{\mathrm{JM}}}\hat{a}_1 + \sqrt{G_{\mathrm{JM}}-1}\hat{a}_2^\dagger, \\ \hat{b}_2 &= \sqrt{G_{\mathrm{JM}}}\hat{a}_2 + \sqrt{G_{\mathrm{JM}}-1}\hat{a}_1^\dagger, \end{aligned} \tag{1}$$

where G_{JM} denotes the effective JM gain, with $\sqrt{G_{\mathrm{JM}}} = \frac{1}{2}\left(\sqrt{G} + \sqrt{G}^{-1}\right)$. One approach to

[1] We acknowledge support by the German Research Foundation via Germany's Excellence Strategy (EXC-2111-390814868), Elite Network of Bavaria through the program ExQM, EU Flagship project QMiCS (Grant No. 820505), and the German Federal Ministry of Education and Research via the project QUARATE (Grant No. 13N15380).

verify this input-output relation is by using photon number conversion factor (PNCF) measurements. The PNCF relates measured quadrature voltages at room temperatures to photon numbers at a certain reference point within the experimental setup via varying well-known and controlled thermal states. In practice, one can use a cryogenic heatable attenuator, which acts as black body radiator emitting thermal radiation through coaxial RF cables. The attenuator is placed in one of the input lines. The emitted power is determined by the temperature of the attenuator which can be controlled by an attached heater and temperature sensor. We assume vacuum as an input to the second JM input. In this case, by using Eq. 1, we can derive the following expressions for the in-phase variances of electromagnetic field quadratures $I_{1,2}$,

$$\begin{aligned}\langle I_1^2\rangle &= \frac{\kappa\, G_\mathrm{A}}{4}\left[G_\mathrm{JM}\coth\left(\frac{hf}{2k_\mathrm{B}T}\right)+(G_\mathrm{JM}-1)+(1-\frac{1}{G_\mathrm{A}})(1+2n_\mathrm{H})\right],\\ \langle I_2^2\rangle &= \frac{\kappa\, G_\mathrm{A}}{4}\left[G_\mathrm{JM}+(G_\mathrm{JM}-1)\coth\left(\frac{hf}{2k_\mathrm{B}T}\right)+(1-\frac{1}{G_\mathrm{A}})(1+2n_\mathrm{H})\right],\end{aligned} \tag{2}$$

where κ is the PNCF, G_A is the overall gain of the detection chain, h is the Planck constant, f is the signal frequency, k_B is the Boltzmann constant, T is the temperature of the heatable attenuator connected to input 1 of the JM and n_H the input noise photon number associated with the amplification chain. Similar relations can be derived for the out-of-phase quadratures $Q_{1,2}$.

Fig. 1(c) depicts the simulated dependence of the two I-quadratures on a thermal state at input port 1 (top) and vacuum state at input port 2 (bottom) of the JM. We assume typical PNCF values of $\kappa = 1.7\,(\mathrm{mV})^2\,/G_\mathrm{A}$ and the amplification gain of $G_\mathrm{A} = 100\,\mathrm{dB}$. The JM gain of $G_\mathrm{JM} = 1.1$ is chosen to be slightly larger than unity. The carrier frequency of $f = 5.5\,\mathrm{GHz}$ is a typical value for flux-driven JPAs and the $0.5\,(1-1/G_\mathrm{A})\,n_\mathrm{H} = 20$ added noise photons can be routinely achieved with commercially available low noise cryogenic amplifiers. As result, we expect a weak temperature dependence of the measured quadrature voltages $\langle I^2\rangle$ for output 2 and a significantly stronger dependence, well-known from the Planck spectroscopy, for output 1, which provides means to experimentally verify correctness of the JM transformation.

Another approach to experimentally investigate the JM transformation is to apply coherent tones to the inputs of the JM. In addition to the signal power dependencies which can be acquired via PNCF, phase and amplitude can be well controlled and tested for coherent input tones. For a displaced vaccum bipartite state, where $\alpha_{1,2} = |\alpha_{1,2}|e^{i\Theta_{1,2}}$ is a complex number describing the displacement amplitude with displacement angles $\Theta_{1,2}$ of input field 1 and 2, respectively, the expectation value of the annihilation operator $\langle\hat{b}_1\rangle$ for output 1 is

$$\langle\hat{b}_1\rangle = \left(|\alpha_1|e^{i\Theta_1}\right)\sqrt{G_\mathrm{JM}} + \left(|\alpha_2|e^{-i\Theta_2}\right)\sqrt{G_\mathrm{JM}-1}. \tag{3}$$

In conclusion, we derived two approaches to experimentally test the transformation implemented by the frequency degenerate JM. Related verification of the JM transformations will be an important milestone for realization of the microwave quantum radar.

References

[1] G. Sorelli, N. Treps, F. Grosshans, and F. Boust. Detecting a target with quantum entanglement. arXiv:2005.07116 [quant-ph] (2021).

[2] U. Las Heras, R. Di Candia, K. G. Fedorov, F. Deppe, M. Sanz, and E. Solano, Scientific Reports **7**, 9333 (2017).

Improving the 1 dB-Compression in Multi-SQUID Josephson Parametric Amplifiers

O. Gargiulo, M. Renger, S. Gandorfer, F. Fesquet, K. Honasoge, F. Kronowetter, D. Bazulin, Q. Chen, Y. Nojiri, A. Marx, R.Gross, K. G. Fedorov, F. Deppe [1]

Superconducting Josephson Parametric Amplifiers (JPAs) are used to produce squeezed vacuum states. They can be applied as elementary building blocks for more involved quantum communication protocols in the microwave regime, such as remote state preparation [1] or quantum teleportation [2]. JPAs are designed by coupling a $\lambda/4$-wavelength resonator to a Direct Current Superconducting Quantum Interference Device (DC-SQUID). This system enables a 3-wave mixing process, when the SQUID is driven by an alternating magnetic flux. In the end, this nonlinear process can be exploited to achieve phase-sensitive amplification and produce propagating squeezed microwaves. Here, we characterize new JPA devices fabricated within the QMiCS project by our Finnish partner (VTT). These samples consist of single SQUID (JPA 1) and double SQUID (JPA 2) devices.

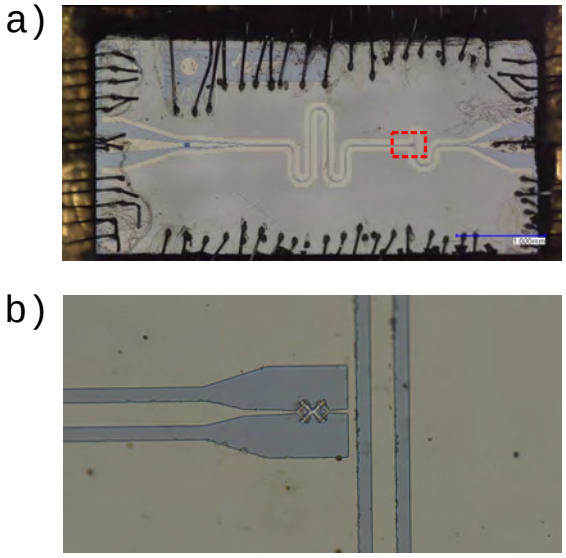

Figure 1: VTT JPA. **a)** Microscope image of the double SQUID JPA2. **b)** Zoom in the SQUID area (red dotted rectangle in **a**).

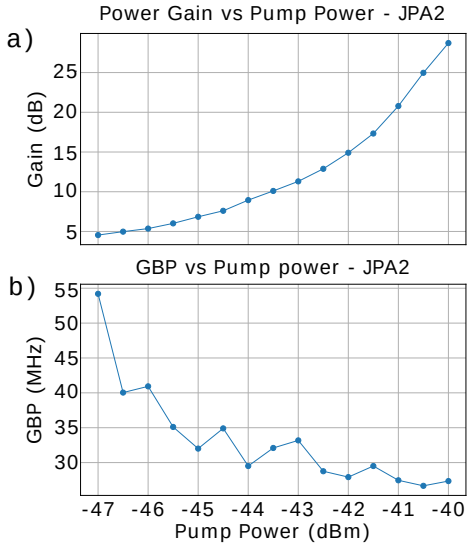

Figure 2: Performance of JPA 2 at 5.567 GHz as a function of the pump power at the JPA pump port and for an estimated input power of -130 dBm at the JPA signal port. **a)** Nondegenerate power gain. **b)** Gain-bandwidth product.

The JPA 2 consists of two SQUIDs in series (see Fig. 1b), each with half the critical current of the single SQUID sample. By keeping the other design parameters identical, we expect to obtain devices with the same gain but smaller nonlinearity in the double SQUID JPA 2.

According to theory [3], the JPA 1 dB-compression point should increase as a function of αN^2, where α takes into account fabrication uncertainties and N is the number of SQUIDs. We expect an improvement of maximum 6 dB for $N = 2$. Both JPAs are placed inside a gold-plated oxigen-free high-conductivity copper sample boxes, bonded to alumina PCBs. They are then fixed inside of cylindrical aluminum boxes for magnetic shielding. This system is then mounted inside a dry dilution refrigerator with a base temperature of 26 mK. For JPA 1 (JPA 2), we measure a maximum resonance frequency of 5.87 GHz (5.85 GHz). We characterize JPA 1 (JPA 2) at 5.596 GHz (5.567 GHz). Both working points are chosen in a way that one obtains an

[1] We acknowledge support by the German Research Foundation via Germany's Excellence Strategy (EXC-2111-390814868), Elite Network of Bavaria through the program ExQM, EU Flagship project QMiCS (Grant No. 820505), and the German Federal Ministry of Education and Research via the project QUARATE (Grant No. 13N15380).

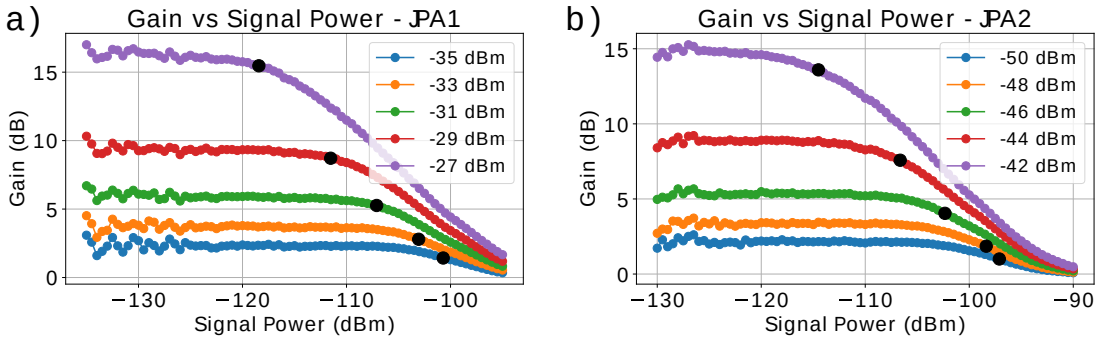

Figure 3: Compression measurement. Shown is the nondegenerate power gain as a function of signal power at JPA input port. **a)** JPA 1 measurements. **b)** JPA 2 measurements. The effect of compression is systematically studied as a function of the applied pump power at the JPA port (in the legend). Black dots indicate the respective 1 dB-compression point.

equal derivative of $\Delta f_{JPA}/\Delta\Phi \approx 4.25\,\mathrm{GHz}/\Phi_0$. We measure nondegenerate gains up to 22.5 dB (27.5 dB) for JPA 1 (JPA 2). These values are comparable to those of earlier JPAs, fabricated at WMI or NEC. Note that the working points are not chosen to achieve maximum gain. The nondegenerate power gain (G) as a function of the pump power for JPA2 is shown in Fig. 2a.

Next, we study the bandwidth of JPA 2 as a function of the pump power. For each fixed pump power, we fit a Lorentzian to the amplitude gain as a function of the input signal frequency and extract the full-width-half-maximum bandwidth (Δf). For a reliable comparison to the JPAs previously used, we calculate the gain-bandwidth product (GBP = $\sqrt{G}\cdot\Delta f$) for each pump power, which is around 27 MHz and constant within 10 % above 7 dB of gain. The result is plotted in Fig. 2b and it is close to the GBP of other devices used at WMI [4].

Finally, we measure the compression properties of both JPAs by varying the power of a coherent input signal for fixed pump powers. The result of these measurements are depicted in Fig. 3. The 1 dB-compression point for JPA 1 coincides well with the 1 dB-compression point of single-SQUID JPAs previously measured at WMI. By comparing the curves at equal gain values, we observe that the 1 dB-compression point for the double-SQUID sample JPA 2 is approximately 3.5 dB higher than that of JPA1.

The demonstrated improvement in 1 dB-compression point is an important contribution for various microwave quantum communication and information processing protocols. For example, larger 1 dB-compression in JPAs allows for larger quantum teleportation codebooks, and respectively, lower no-cloning fidelity thresholds [2]. The latter is the key for unconditional communication security and lowering it is crucial for many practical quantum key distribution applications.

References

[1] S. Pogorzalek, K. Fedorov, M. Xu, A. Parra-Rodriguez, M. Sanz, M. Fischer, E. Xie, K. Inomata, Y. Nakamura, E. Solano, A. Marx, F. Deppe, and R. Gross, Nature Commun. **10**, 2604 (2019).

[2] K. G. Fedorov, M. Renger, S. Pogorzalek, R. Di Candia, Q. Chen, Y. Nojiri, K. Inomata, Y. Nakamura, M. Partanen, A. Marx, R. Gross, and F. Deppe, arXiv.org - accepted for publication in Science Advances (2021).

[3] X. Zhou, V. Schmitt, P. Bertet, D. Vion, W. Wustmann, V. Shumeiko, and D. Esteve, Phys. Rev. B **89**, 214517 (2014).

[4] L. Zhong, E. P. Menzel, R. Di Candia, P. Eder, M. Ihmig, A. Baust, M. Haeberlein, E. Hoffmann, K. Inomata, T. Yamamoto, Y. Nakamura, E. Solano, F. Deppe, A. Marx, and R. Gross, New J. Phys. **15**, 125013 (2013).

Implementation of CC Phase Gates with a Three-Qubit Coupler

Federico Roy, Niklas Glaser, Ivan Tsitsilin, Gerhard Huber [1]

Quantum computing technologies enter the era of noisy intermediate scale quantum (NISQ) devices, where problems in quantum chemistry and optimization tasks can be tackled. The underlying algorithms, e.g., Variational Quantum Eigensolver (VQE) or Quantum Approximate Optimization Algorithm (QAOA), rely on the entanglement over many qubits. Superconducting circuit quantum devices are promising candidate for achieving these tasks, as large coherence times and fast single- and two-qubit gate operations have been demonstrated. However, the commonly used architectures suffer from low connectivity between the qubits, as they rely only on two-qubit entangling gates. The logical operations needed for the generation of the desired quantum state lead to a substantial overhead, which could be reduced by directly employing multi-qubit entangling gates.

We investigate how strong multi-qubit interactions can be harnessed in a system, where three fixed-frequency transmon-qubits [1] (Q1, Q2, Q3) are strongly capacitively coupled via a squid-type tunable transmon coupler [2] (*TC*). A schematic of this three-qubit circuit, including weak direct couplings between the qubits is shown in Fig. 1a. This setup can be realized by the design presented in Fig. 1b.

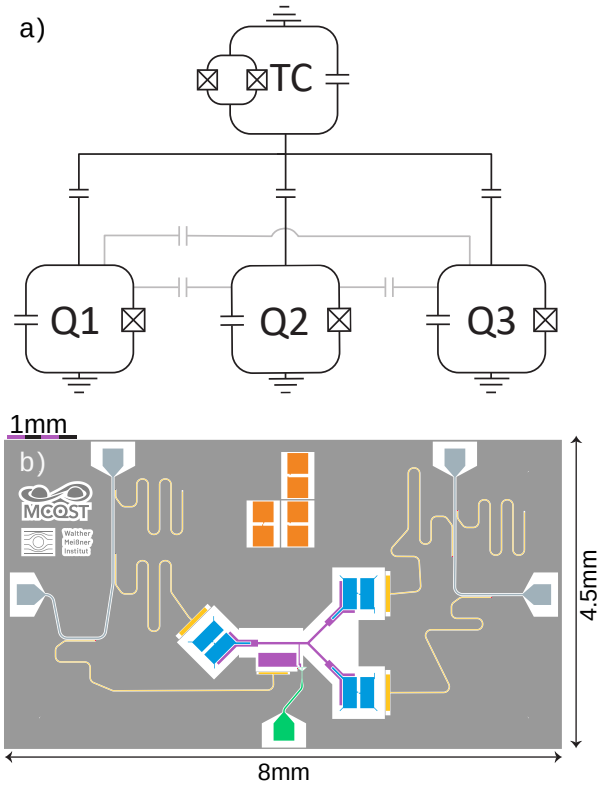

Figure 1: a) Circuit architecture used to generate three-body interactions and the CCPhase gate. Q1, Q2 and Q3 are fixed frequency qubits as implemented by a Transmon-type superconducting circuit. Each qubit is coupled capacitively to a tunable coupler element, where the tunability is realized by a SQUID-loop, i.e. a loop with two Josephson Junctions. Smaller stray capacitive coupling appears between the qubits. b) Full chip of the three qubit-coupler with qubits and control lines. Qubits are shown in blue. The coupler islands are shown in purple, the test structures in orange and the readout plus test resonators in yellow. The flux line for the coupler is shown in green. In grey are the feed-lines used to send and acquire microwave signals.

Gate operation – With this setup we aim to implement a controlled-controlled-phase (CCPHASE) gate, where the interactions between the energy levels are harnessed in the form of frequency shifts. We have therefore extended the pulse scheme, recently demonstrated for the implementation of controlled-phase (CPHASE) gates, where only two-qubits are connected [3, 4].

During the adiabatic frequency sweep of the tunable coupler, non-computation coupler states with higher excitation numbers interact with the computational states. As eigenstates are followed adiabatically this can result in frequency shifts χ_{ijk} up to multiples of the strong coupling strength between coupler and qubits (Fig. 2a).

[1]This project has received support by the European Union, agreements No 765267 (QuSCo) and No 828826 (FET-Open Quromorphic), the BMBF project GeCQoS (FKZ 13N15680), and the DFG under Germany's Excellence Strategy (EXC2111 - 390814868).

In the frame of reference of the qubits, the effective Hamiltonian in the computational-subspace reads

$$\tilde{H}/\hbar = \sum_{ijk} \chi_{ijk} |ijk\rangle\langle ijk| \tag{1}$$

with the computational states $ijk \in \{011, 101, 110, 111\}$. The evolution under $\tilde{H}$ leads to a state dependent phase acquisition

$$\phi_{ijk} = \int_0^\tau \chi_{ijk}(t)\, \mathrm{dt}, \tag{2}$$

needed for the CCPHASE gate. For an efficient control of the desired collected phases four frequency sweeps of the coupler, with different pulse durations t_i, are performed, interleaved by single-qubit pulses. Fig. 2b shows an exemplary pulse sequence for the implementation of the CCPhase gate, where the τ_i of the frequency sweeps are chosen to only collect a phase $\phi_{111} = \pi$ on the $|111\rangle$ state, while effectively collecting no phase on the other states. After calibration, this gate scheme allows to realize arbitrary gate phases on all states, by adjusting the timings t_i. For example, Fig. 2c shows required timings for realizing respective CCPhase(ϕ_{111}) gates, where the total gate time, including single-qubit pulse, lays between 200 ns and 270 ns. From simulations, which include decoherence, fidelities above 99% are expected for this gate scheme.

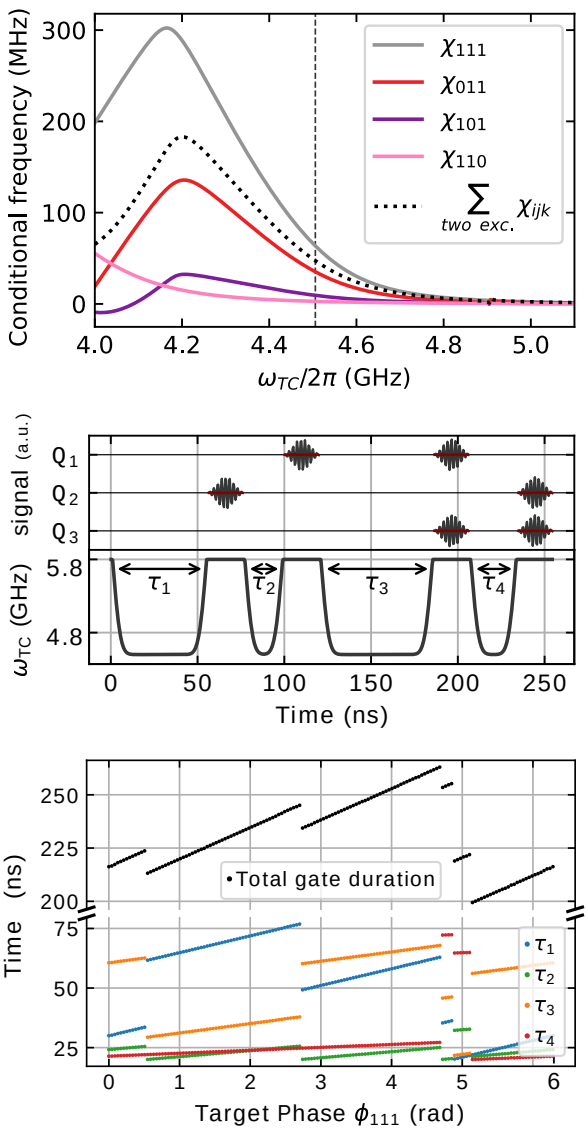

Figure 2: a) Frequency shifts of the excited computational eigenstates depending on the tunable coupler frequency. The black dashed line indicates the sum of the two-excitation shifts. The grey dotted line indicates the minimum coupler frequency in the pulse sequence below. b) CCPhase pulse scheme. (top) Microwave drives inducing bit flips on individual qubits. (bottom) Frequency modulation of the tunable coupler, reaching a minimum value of 4.5 GHz. c) Phase collection times for a parametric CCPhase gate. (top) Total gate time required to reach respective phases, including single qubit pulses. (bottom) Widths of the individual phase collection pulses. The jumps arise due to extra $2k\pi$ degree of freedom in choosing phases.

References

[1] J. Koch, T. M. Yu, J. Gambetta, A. A. Houck, D. I. Schuster, J. Majer, A. Blais, M. H. Devoret, S. M. Girvin, and R. J. Schoelkopf, Physical Review A **76**, 042319 (2007).

[2] D. C. McKay, S. Filipp, A. Mezzacapo, E. Magesan, J. M. Chow, and J. M. Gambetta, Physical Review Applied **6**, 064007 (2016).

[3] M. C. Collodo, J. Herrmann, N. Lacroix, C. K. Andersen, A. Remm, S. Lazar, J.-C. Besse, T. Walter, A. Wallraff, and C. Eichler, Phys. Rev. Lett. **125**, 240502 (2020).

[4] Y. Xu, J. Chu, J. Yuan, J. Qiu, Y. Zhou, L. Zhang, X. Tan, Y. Yu, S. Liu, J. Li, F. Yan, and D. Yu, Phys. Rev. Lett. **125**, 240503 (2020).

Materials, Thin Film and Nanotechnology, Experimental Techniques

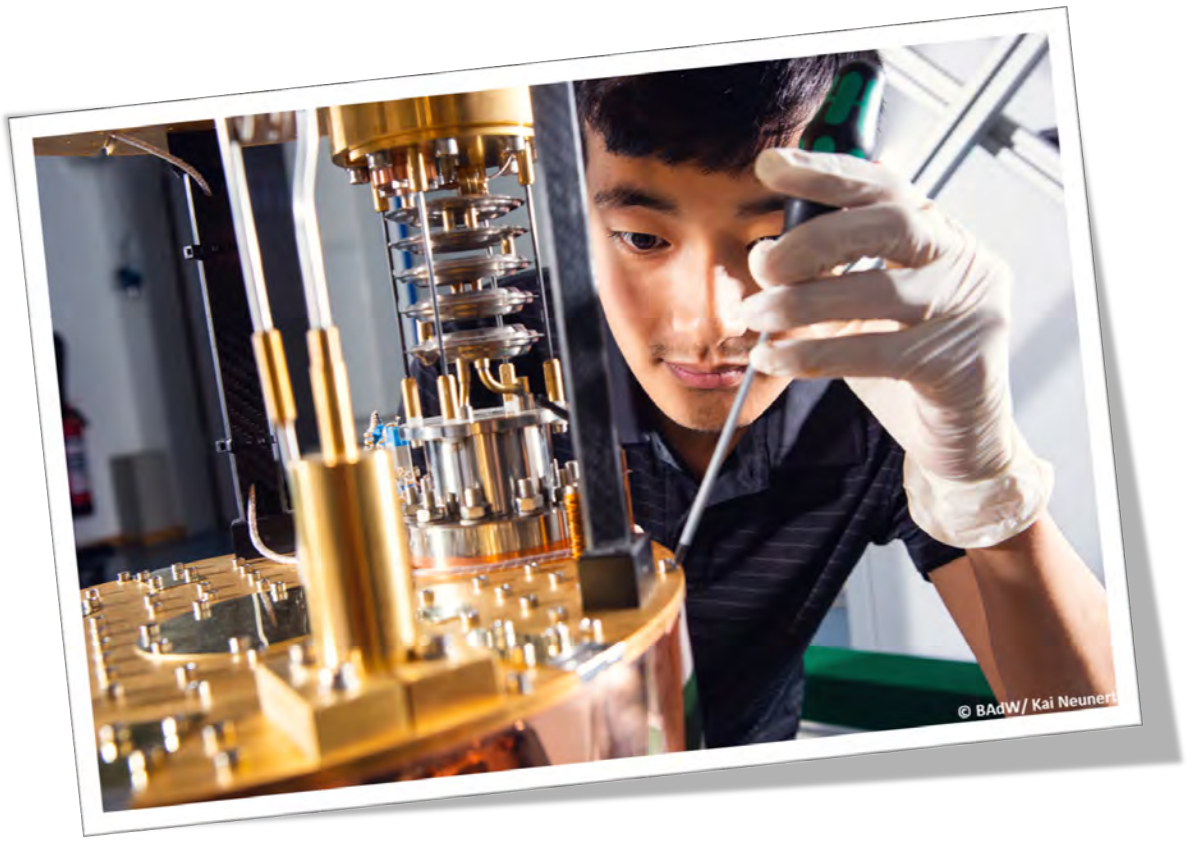

Development of a Fabrication Process for High Coherence Qubits

L. Koch, N. Bruckmoser, L. Hölscher, I. Tsitsilin, G. Huber, K. Honasoge, Y. Nojiri, T. Luschmann, S. Geprägs, S. Filipp[1]

Superconducting circuits for quantum computing are currently in the noisy intermediate scale quantum (NISQ) era. To get beyond this era, fabrication methods for high coherence qubits and large scale circuits need to be developed. In order to meet the goal of high coherence qubits we have tested new cleaning methods for silicon wafers and metal surfaces and have optimized the deposition of superconducting aluminum and niobium thin films taking advantage of the new PLASSYS UHV deposition system. To quantify the effect of the different fabrication techniques on losses [1] we have measured the internal quality factor of $\lambda/4$ coplanar waveguide resonators (CPW) which are shorted at one end and open at the other. CPWs are highly sensitive sensors for so called two level systems (TLS), which are the main loss channel in current superconducting processors. To allow for multiplexing several CPWs are capacitively coupled to a common feedline. A schematic of our CPW layout is shown in Fig.(1).

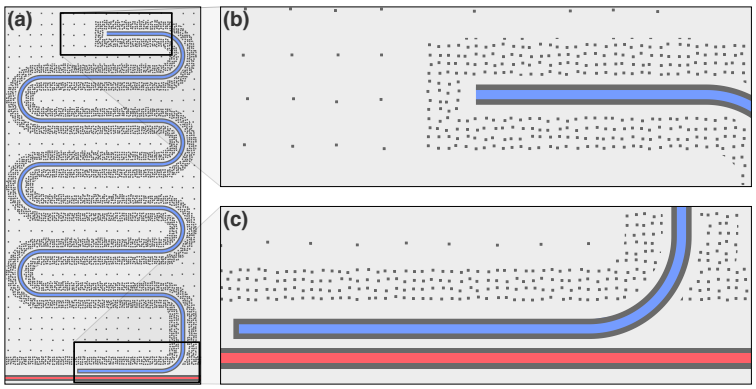

Figure 1: Layout of a superconducting $\lambda/4$ CPW resonator. **(a)** Hanging resonator (blue) coupled to a feedline colored in red. The resonator is shorted at the top **(b)** and open at the feed line **(c)**.

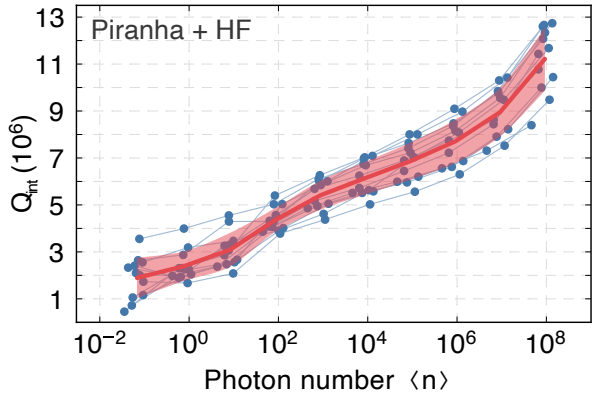

Figure 2: Dependence of the internal quality factor on the mean photon number for twelve resonators from 4 GHz to 5.2 GHz. The blue dots display the measured Q_i, the red curve shows the average internal quality factor with the standard deviation (transparent red).

A typical power sweep over the internal quality factors of twelve niobium resonators on a single chip is shown in Fig.(2). The resonance frequency of the CPWs are equally spaced between 4 GHz and 5.2 GHz, allowing to identify losses at relevant transmon qubit frequencies. By optimizing the fabrication parameters we have been able to improve the internal quality factor of aluminium resonators to over $1 \cdot 10^6$ and niobium resonators to over $3 \cdot 10^6$. The aforementioned optimized fabrication techniques have then been transferred to a transmon qubit [2] fabrication process to fabricate the niobium ground planes of the qubit chips. Additionally, a so called bandaging process [3] as well as a new double layer resist stack for lift-off processes have been developed and optimized. Using these techniques the aluminium Josephson junctions as well as the aluminium bandages have been fabricated.

The layout of single fixed frequency qubit chips is shown in Fig.(3). The qubits reached 150 µs

[1]This project has received support by the BMBF program No. 13N15680 (GeCQoS), and by the DFG under Germany's Excellence Strategy (EXC2111 - 390814868).

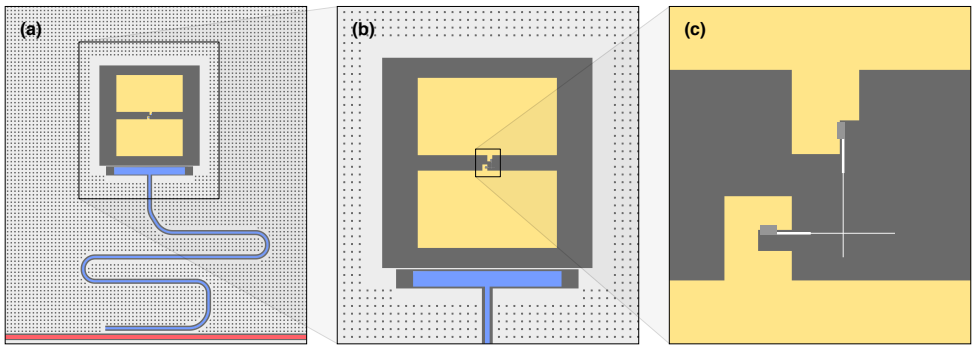

Figure 3: Layout of a transmon qubit. **(a)** Fixed-frequency transmon qubit (yellow) coupled to a resonator colored in blue. **(b)** The coupling between the qubit and resonator is mediated over a large capacitance. **(c)** Detailed view of the design of the Al strips (white) and the bandages (light gray). The overlap of the strips define the Josephson junction via an Al/AlOx/Al trilayer.

of T_1 and $T_{2,E}$ times, as shown in Fig.(4).
To not only be able to fabricate highly coherent single qubits but also larger superconducting processors, additionally a fabrication process for so called air bridges [4] has been developed. Air bridges are 3D structures that can span across CPWs enabling a more complex routing of signal lines as well as providing the best possible suppression of slot line modes. A scanning electron microscope (SEM) image of an air bridge spanning across a CPW is shown in Fig.(5).

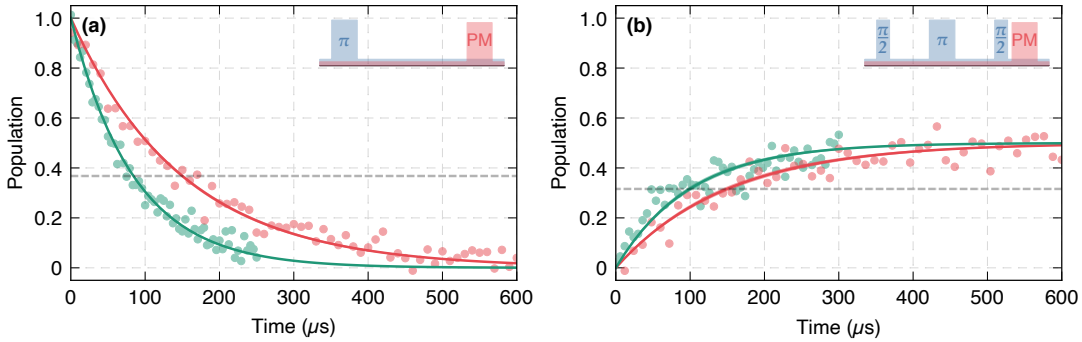

Figure 4: Decoherence measurement data for two niobium-based qubits with Al/AlOx/Al Josephson junctions. **(a)** Measured T_1 time of 84 µs (green) and 150 µs (red). **(b)** Measured $T_{2,E}$ for the same qubits. The fits correspond to 100 µs (green) and 150 µs (red).

References

[1] C. R. H. McRae, H. Wang, J. Gao, M. R. Vissers, T. Brecht, A. Dunsworth, D. P. Pappas, and J. Mutus, Review of Scientific Instruments **91**, 091101 (2020).
[2] J. Koch, T. M. Yu, J. Gambetta, A. A. Houck, D. I. Schuster, J. Majer, A. Blais, M. H. Devoret, S. M. Girvin, and R. J. Schoelkopf, Physical Review A **76**, 042319 (2007).
[3] A. Dunsworth, A. Megrant, C. Quintana, Z. Chen, R. Barends, B. Burkett, B. Foxen, Y. Chen, B. Chiaro, A. Fowler *et al.*, Applied Physics Letters **111**, 022601 (2017).
[4] Z. Chen, A. Megrant, J. Kelly, R. Barends, J. Bochmann, Y. Chen, B. Chiaro, A. Dunsworth, E. Jeffrey, J. Mutus *et al.*, Applied Physics Letters **104**, 052602 (2014).

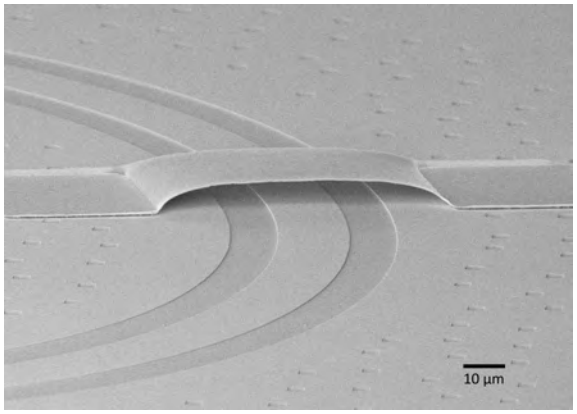

Figure 5: SEM image of an air bridge spanning across a resonator.

Fabrication of Low-Loss Coplanar Resonators

K.E. Honasoge, Y. Nojiri, L. Koch, T. Luschmann, F. Kronowetter, F. Fesquet, M. Renger, A. Marx, F. Deppe, R. Gross, K.G. Fedorov [1]

Superconducting coplanar waveguide (CPW) resonators enable the realization of a wide range of experiments in circuit quantum electrodynamics (QED) architectures. Utilizing CPW resonators, circuit-QED systems have been employed in quantum information processing for fundamental studies of quantum physics and building of superconducting quantum computer prototypes. These advances have enabled development of more intricate devices such as Josephson Parametric Amplifiers (JPAs), Josephson Parametric Converters (JPCs), and single photon detectors (SPDs) for for operations with propagating quantum microwaves.

In circuit-QED, superconducting CPW resonators have several advantages. They can be designed to operate at frequencies between $4 - 12\,\mathrm{GHz}$ by adjusting their lengths [1]. A respective resonator external quality factor (Q_{ext}) is controlled by capacitance C between the resonator input and an external transmission line, as shown in Fig.1. Overcoupled resonators ($Q_{\mathrm{ext}} < Q_{\mathrm{int}}$) are typically used as various sources of quantum light and undercoupled resonators ($Q_{\mathrm{ext}} > Q_{\mathrm{int}}$) are often used as quantum memories. For most applications, it is desirable to have the internal quality factors (Q_{int}) as high as possible.

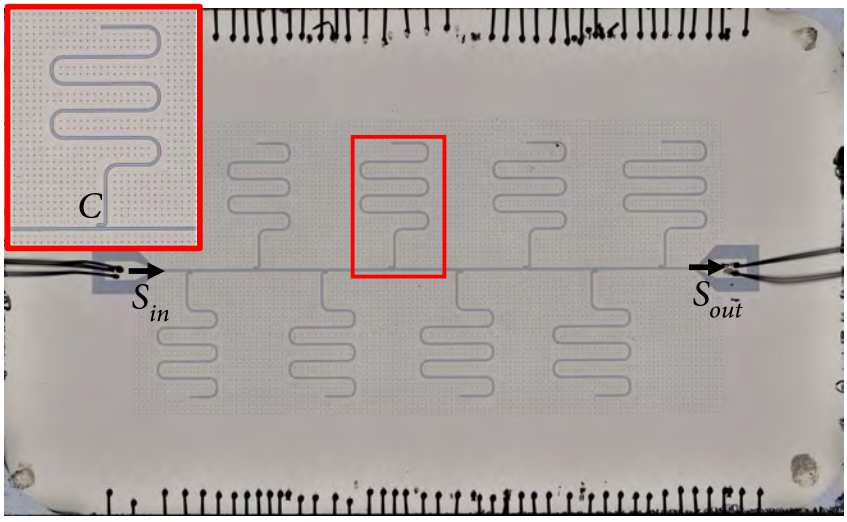

Figure 1: A processed Niobium chip with several CPW resonators wirebonded to a printed circuit board (not visible). S_{in} and S_{out} show the signal input and output. Red inset shows a single resonator.

In the framework of the quantum radar project (nickname: QUARATE), we require various superconducting devices with low-loss resonators, such as JPAs or JPCs. The challenge in reaching respective high internal quality factors arises from the presence of numerous loss channels. One the dominant loss channels is due to presence of two-level fluctuators (TLSs) in various parts of our CPWs. These TLSs lead to energy relaxation and significantly limit Q_{int}. The key regions of importance are the substrate-metal (S-M), substrate-vacuum (S-V), and metal-vacuum (M-V) interfaces. Extensive cleaning measures must be taken during fabrication to mitigate TLS occurrence at such interfaces. Here, we report that we are able to reach high internal quality factors in homemade CPW resonators.

Our resonator fabrication process relies on a series of surface treatments of silicon substrate chips prior to the lithography step. These cleaning processes ensure clean S-M and S-V interfaces. After pre-cleaning of high resistivity ($R_{\square} > 10\,\mathrm{k\Omega}$) silicon chips, we perform oxidation in a hot Piranha (Sulfuric acid + Hydrogen peroxide) solution. This step also removes any

[1] We acknowledge support by the German Research Foundation via Germany's Excellence Strategy (EXC-2111-390814868), Elite Network of Bavaria through the program ExQM, EU Flagship project QMiCS (Grant No. 820505), and the German Federal Ministry of Education and Research via the project QUARATE (Grant No. 13N15380).

organic contaminants and ensures a thick oxide layer on top of the chip. Then, the chips are processed in a buffered hydrofluoric (HF) acid solution which strips the oxide layer off the silicon and exposes a clean layer of the silicon surface, ensuring a clean S-M interface for the following steps. Then, the chips are transferred into our PLASSYS MEB 550 S4-I UHV system for metal deposition. After deposition of niobium/aluminum films, the chips are spin-coated with an optical resist and patterned with the optical writer 4 PICO *PicoMaster* 200. Finally, the chips are developed and chemically wet-etched with MicroChemicals AZ© 726 MIF (or dry-etched with sulfur hexafluoride and argon) for aluminium (niobium) films, respectively. After fabrication, the chips are packaged for microwave measurements at milli-Kelvin temperatures.

Microwave cryogenic measurements are performed using a Vector Network Analyzer (VNA), which obtains complex scattering parameters as a function of frequency and power. The respective resonator quality factors are extracted through an analytic fit of the measured response [2] [3]. Fig. 2 illustrates our cryogenic measurement results of the CPW resonator internal quality factors for various types of fabrication processes. Here, the etched resonators outperform the lift-off resonators as they have a cleaner S-M interface without resist residues, as it is the case for the lift-off resonators. Among the etched resonators, the Niobium resonators have higher internal quality factors ($\approx 9 \times 10^5$), as compared to the Aluminium ($\approx 3.5 \times 10^5$).

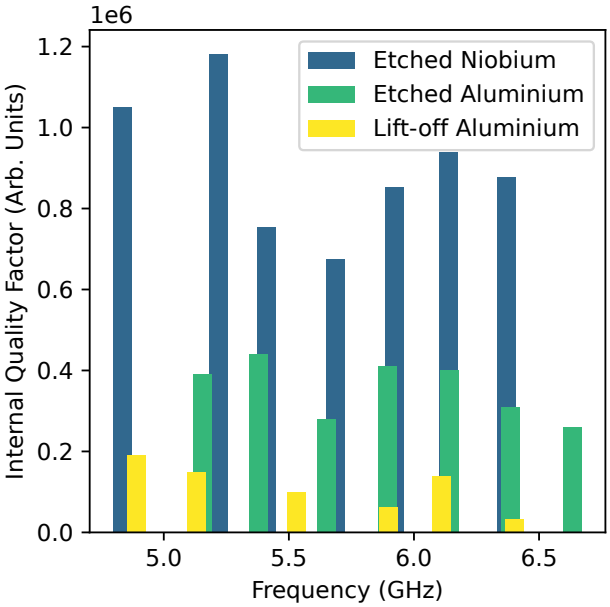

Figure 2: Summary of internal quality factors of fabricated CPW resonators measured in the single-photon regime.

In conclusion, we have tested various surface cleaning techniques in order to optimize of CPW resonators and reach the respective internal quality factors on the order of $Q_{\text{int}} \sim 10^6$. This progress establishes a solid foundation for fabrication of superconducting resonator-based devices for various projects in the fields of quantum computing, quantum communication, and quantum illumination, among others.

References

[1] M. Göppl, A. Fragner, M. Baur, R. Bianchetti, S. Filipp, J. M. Fink, P. J. Leek, G. Puebla, L. Steffen, and A. Wallraff, Journal of Applied Physics **104**, 113904 (2008).

[2] S. Probst, F. Song, P. A. Bushev, A. V. Ustinov, and M. Weides, Review of Scientific Instruments **86**, 024706 (2015).

[3] Q.-M. Chen, M. Pfeiffer, M. Partanen, F. Fesquet, K. E. Honasoge, F. Kronowetter, Y. Nojiri, M. Renger, K. G. Fedorov, A. Marx, F. Deppe, and R. Gross. The scattering coefficients of superconducting microwave resonators: I. Transfer-matrix approach. arXiv:2109.07762 [quant-ph] (2021).

New Bluefors LD 400 Dry Dilution Refrigerator with Rapid Sample-Loading System

F. Haslbeck, A. Marx, R. Gross, S. Filipp [1]

A key effort in the rapidly advancing field of quantum computing is the scaling of systems from a handful of quantum bits (qubits) to hundreds or more. Upscaling quantum computers based on superconducting qubits increases the complexity of the chips and the demands on the quality of their fabrication. As the chips also need to be operated at milli-Kelvin temperatures, electronic components for cryogenic temperatures need to be developed and characterized. Therefore, a fast turnaround and short cooldown time to milli-Kelvin temperatures is necessary for an efficient optimization of fabrication processes as well as for fast characterization measurements. These requirements are fully met by the newly installed Bluefors LD 400 dry dilution refrigerator with its rapid sample-loading system. The system was funded by the Deutsche Forschungsgemeinschaft and was installed in August 2021 in the quantum lab at WMI as shown in Fig. 1.

Figure 1: New Bluefors LD 400 dry dilution refrigerator after installation in the quantum lab at WMI. The control unit is on the left side and the vacuum can hosting the fridge that is cooled to milli-Kelvin temperatures on the right side. The samples are in the gold plated probe shown in the center which is attached to an automated lifting mechanism that loads the probe into the refrigerator.

Instead of warming up the entire system to exchange the samples as typically performed with dilution refrigerators, this system remains cold and only the probe containing the samples is exchanged. Thereby, the cool-down time is reduced to approximately eight hours compared to 24 hours needed to cooldown the entire system. Likewise, the warm-up time of the probe is only one hour compared to 12 hours for the entire system. The lift mechanism with the gold plated probe as shown in Fig. 1 is manually attached to the refrigerator. The automated loading mechanism moves the probe step by step into the system to allow for thermal equilibration at each temperature stage. Although the probe needs to be compact to minimize its thermal load, a large sample space with a diameter of 72 mm and a height of 280 mm is available as shown in Fig. 2 (left) which allows to install several samples simultaneously.

[1] This infrastructure has been funded by the DFG as part of the "Major Research Instrumentation" program (Art. 91b).

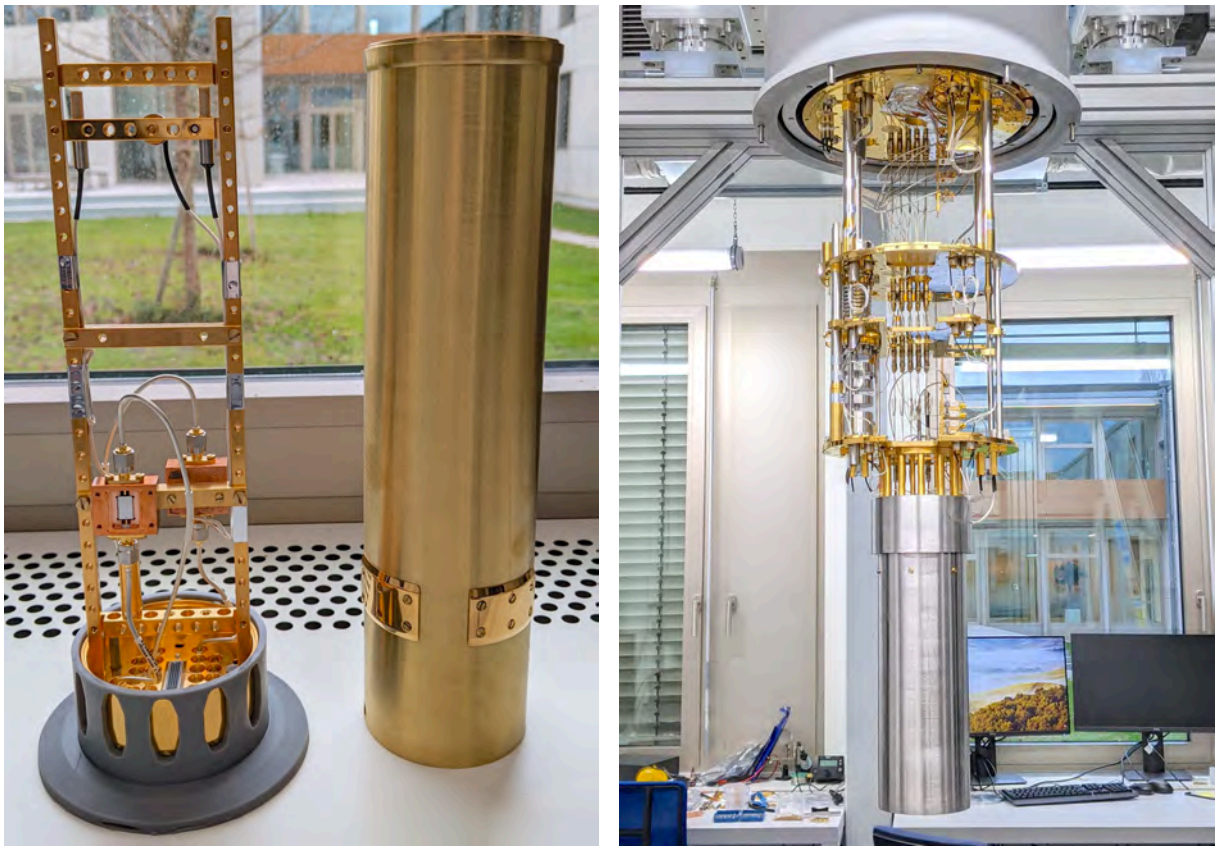

Figure 2: Left: Open sample probe with two sample boxes. The left sample box is open to show the chip with dimensions $10 \times 6\,\mathrm{mm}^2$. Right: Open dilution refrigerator. The gold plated copper plates are at different temperatures with 4 K, 1 K, 100 mK, and 8 mK from top to bottom. The double layer cryophy shield is attached to the coldest stage and shields the sample space from magnetic field noise.

Superconducting qubits are very susceptible to magnetic field noise and need to be carefully shielded from the environment. Therefore, the sample space is shielded by two concentric cylinders made from cryophy as shown in Fig. 2 (right). Cryophy is a nickel-iron soft magnetic alloy optimized for cryogenic temperatures that shields magnetic fields with frequencies from DC to 1 kHz by four orders of magnitude in our setup. Furthermore, the Bluefors LD 400 offers additional space on the $\sim$ 300 mm-wide plates for cryogenic electronics such as amplifiers, circulators, and isolators. The system is furthermore equipped with 16 input and four output microwave lines that support frequencies from DC up to 40 GHz.

The dilution unit provides a cooling power of 450 μW at 100 mK (16 μW at 20 mK) and reaches a base temperature of < 8 mK. The system is equipped with a pulse tube refrigerator (Cryomech PTR 420 with 2 W cooling power at 4 K). The cool-down and warm-up can be done completely automatic. Oil-free pumps and compressors in the gas handling unit guarantee minimal maintenance requirements with service intervals up to three years. An internal cold-trap allows continuous operation of the system without the need of cryogenic liquids to operate.

Optical Cryostats - A Versatile Tool for Investigating Materials, Magnetization Dynamics, and Hybrid Systems

H. Huebl, T. Luschmann, L. Liensberger, M. Müller, L. Niekamp, M. Opel, S. Geprägs, M. Althammer, M. Weiler, and R. Gross [1]

We recently commissioned two optical cryostats, one with and one without magnetic field capabilities. Both cryostats are 'dry' systems, i.e. they do not rely on a liquid helium supply but operate with a pulse tube cooler. This allows for automated experiments under stable conditions. The cryostats are funded by the DFG excellence cluster 'Munich Center for Quantum Science and Technology (MCQST)' and are specifically tailored for studies in the research areas 'quantum sensing' and 'quantum materials'. Members of the MCQST community have access to these cryostats.

Figure 1: Magneto-optical cryostat with an added (homemade) optical imaging system for the precise positioning of samples. Image: Jan Greune/MCQST

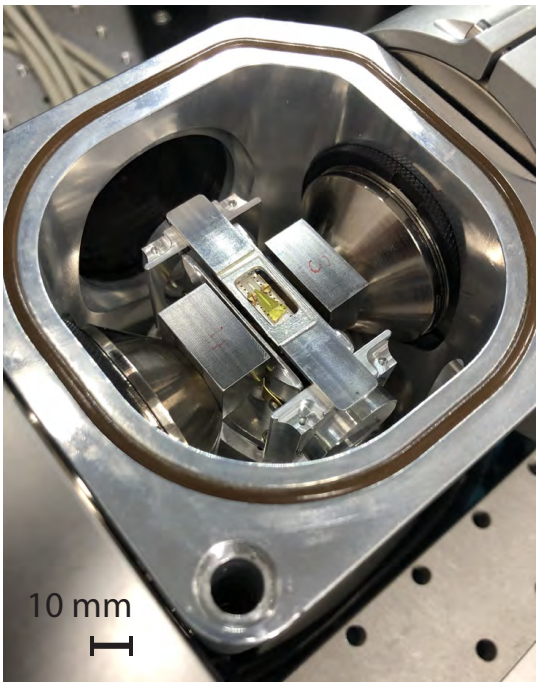

Figure 2: Optical image of the inside of the magneto-optical cryostat. Inside the vaccum vessel, two magnet pole-shoes face the thermal shields protecting the sample environment from thermal radiation. The sample is placed on a printed circuit board, which is bolted to a cold-finger sitting on the *xyz*-positioner (see Fig. 3 for details).

The systems are designed for research requiring optical access and/or a vacuum environment. Our in-house added microscope imaging (Fig. 1) allows in combination with the movable sample stage (Fig. 2) to precisely place microstructures with respect to the optical signal path. Thus, we are able to investigate e.g. the impact of the sample geometry or spatially map a response quantity.

For various quantum sensing and quantum material related projects, an additional stimulus in the form of broadband radio-frequency and microwave radiation is essential. In particular, projects studying magnetization dynamics, hybrid quantum systems based on magnonic and phononic excitations, light matter interaction in solid state systems, as well as nanomechanical elements and optical circuits are expected to benefit from this addition to the system. As shown in Fig. 2, the available sample space inside the cryostats is rather limited and the optical access from the top restricts microwave cable routing, requiring an innovative solution for the sample holder. We decided to design and realize a custom made microwave delivery concept with microwave lines connected to the printed circuit

[1] Financial Support by the German Research Foundation via Germany's Excellence Strategy (EXC-2111-390814868) is gratefully acknowledged.

board (PCB) from the bottom side. Figure 3 shows the microwave board within the assembly. In this configuration, the microwave signal line has to transit through the body of the PCB, while maintaining excellent microwave transmission properties. We implemented this in form of a 4-layer PCB to obtain continuous ground planes and minimally disturb the line impedance of 50 Ω.

Figure 3 a) shows a finite element simulation of the the microwave electric field visualizing the transfer of the signal from the bottom to the top layer and vice versa, which overlays a rendering of the PCB cut vertically along the position of the signal line. As shown in Fig. 3 a), the fields are confined to the respective side of the PCB and transition through the board at the designed locations. Using this complex board design allows to connect the microwave lines from the 'bottom'-side and enable broadband microwave delivery in this confined sample environment. Experimentally, we have demonstrated a broadband transmission of up to 18 GHz.

The installation of the dry-cryostats in combination with the optical assembly and the microwave signal delivery sets us in an excellent position to study multiple aspects of quantum sensing, quantum materials, and hybrid quantum systems.

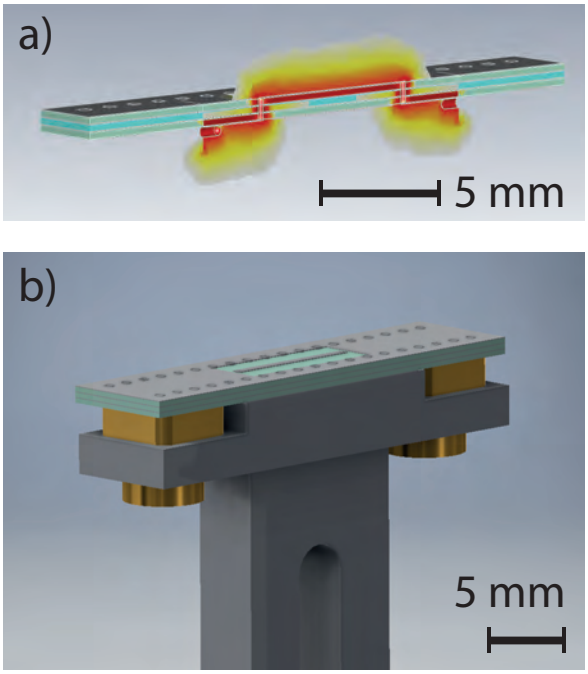

Figure 3: Rendering of the microwave printed circuit board and cold-finger acting as sample mount. Panel a) shows a finite element modeling of the the 4-layer microwave printed circuit board with allows to connect to flexible microwave coaxial lines from the bottom and deliver the microwave signal to the top layer and sample. The dimensions of the PCB are $4 \times 20\,\mathrm{mm}^2$. Panel b) displays the assembly including the board, cold finger and microwave connectors.

Experimental Facilities

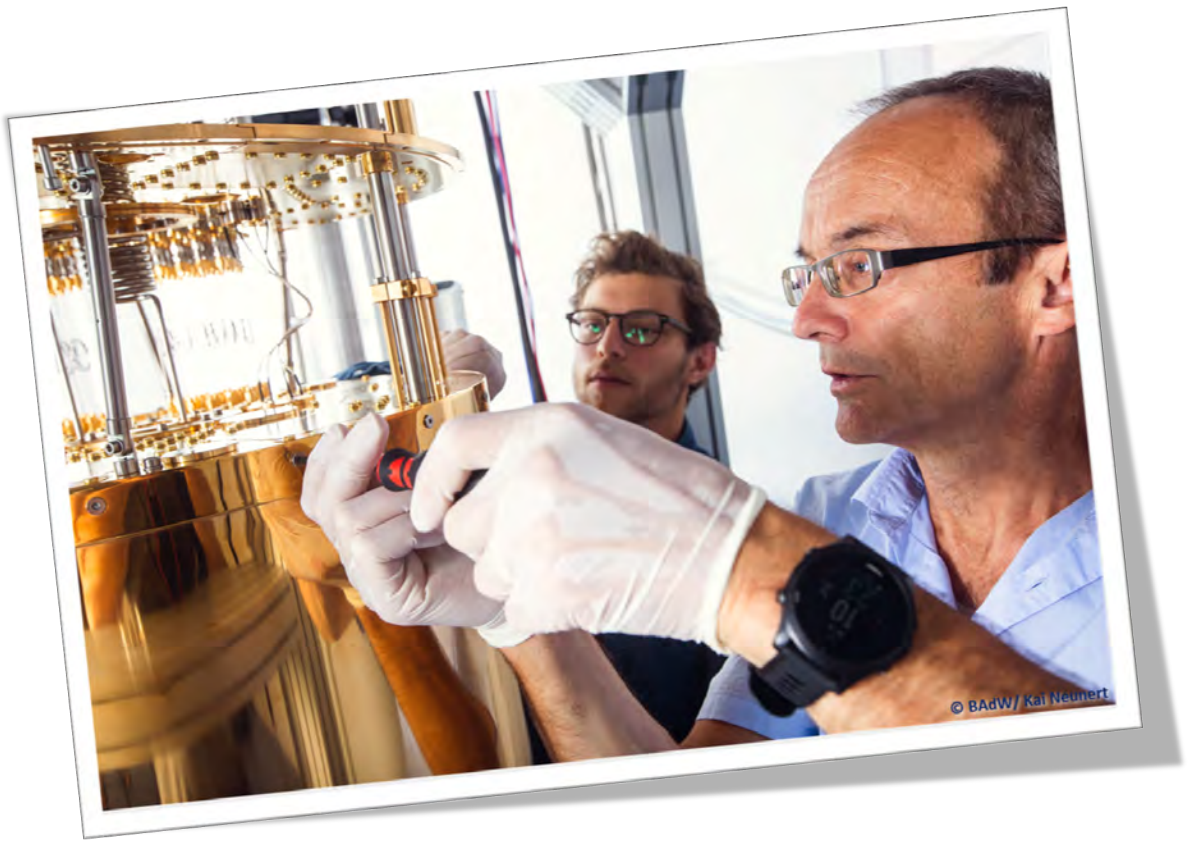

Overview of Key Experimental Facilities and Infrastructure

In the following basic information on the key experimental facilities and components of the technical infrastructure installed at the Walther-Meißner-Institute (WMI) is given.

UHV Laser-MBE

The WMI operates an UHV Laser-Molecular Beam Epitaxy (L-MBE) system for the growth of complex oxide heterostructures. The system has been designed to meet the special requirements of oxide epitaxy. The UHV cluster tool consists of the following main components:

- central transfer chamber;
- load-lock chamber with a heater system for substrate annealing;
- laser deposition chamber with a KrF excimer laser, *in-situ* reflection high energy electron diffraction (RHEED) system, laser substrate heating system, and atomic oxygen/nitrogen source; the RHEED system has been modified to allow for the operation at high oxygen partial pressure up to 0.5 mbar;
- surface characterization chamber with UHV scanning atomic force microscope (Omicron);
- metallization chamber with a four heart electron gun system and a liquid nitrogen cooled sample stage. The sample holder can be tilted for shadow evaporation.

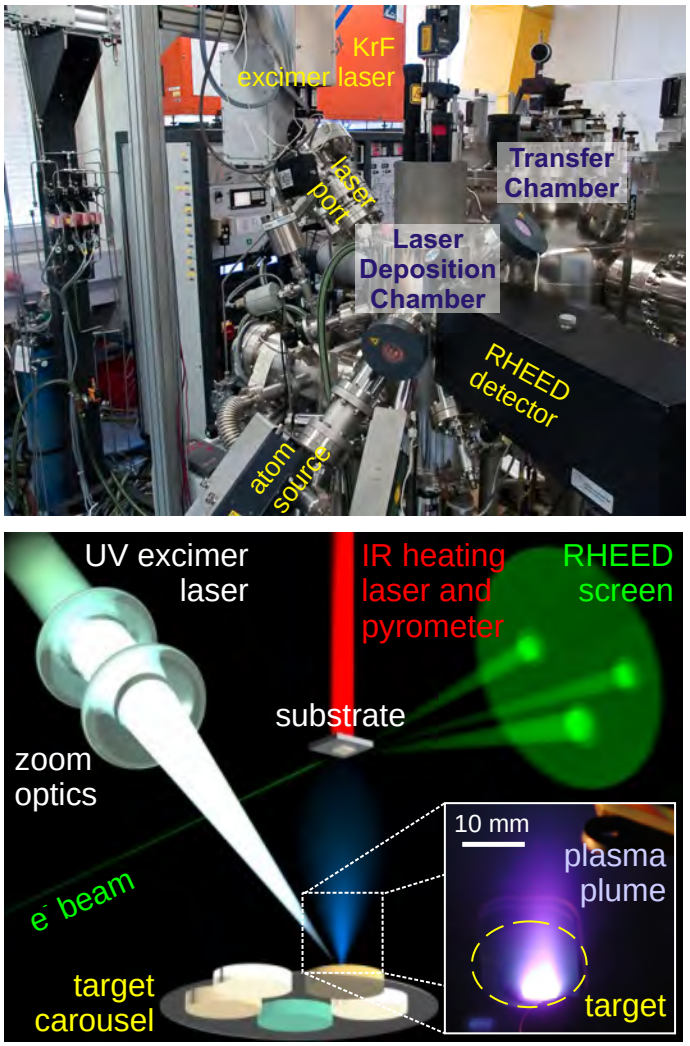

Figure 1: Top: UHV laser-molecular beam epitaxy system. Bottom: principle of the deposition process.

The system is used for the growth of complex oxide heterostructures consisting of superconducting, ferromagnetic, ferroelectric, and semiconducting materials such as high-temperature superconductors, doped manganites, (double) perovskites, magnetite, zinc oxide, rare earth iron garnets, pyrochlore iridates, etc..

The L-MBE systems is now more than 20 years old and will be replaced by a new PLD-MBE-systems early in 2022.

UHV Sputter Deposition System – SUPERBOWLS

The UHV sputter deposition system was set up in 2017 and allows for the fully-automated fabrication of complex multilayers consisting of superconducting and magnetic materials. To avoid cross-contamination of the superconducting and magnetic materials the system consists of two separate deposition chambers (see Fig. 2). One deposition chamber is dedicated for superconducting materials (Non-Ferromagnet Chamber: NFC) and the other for the growth of magnetic materials (All Ferromagnet Chamber: AFC). The loadlock chamber is positioned between the two deposition chambers. It serves for inserting substrates and masks into the deposition chambers and enables the in-situ transfer of samples between the two deposition chambers. The system is designed for a face-down substrate orientation with the sputter source residing at the bottom of the deposition chambers. Both deposition chambers achieve a base pressure below 8×10^{-10} mbar, paving the way for the deposition of high purity materials.

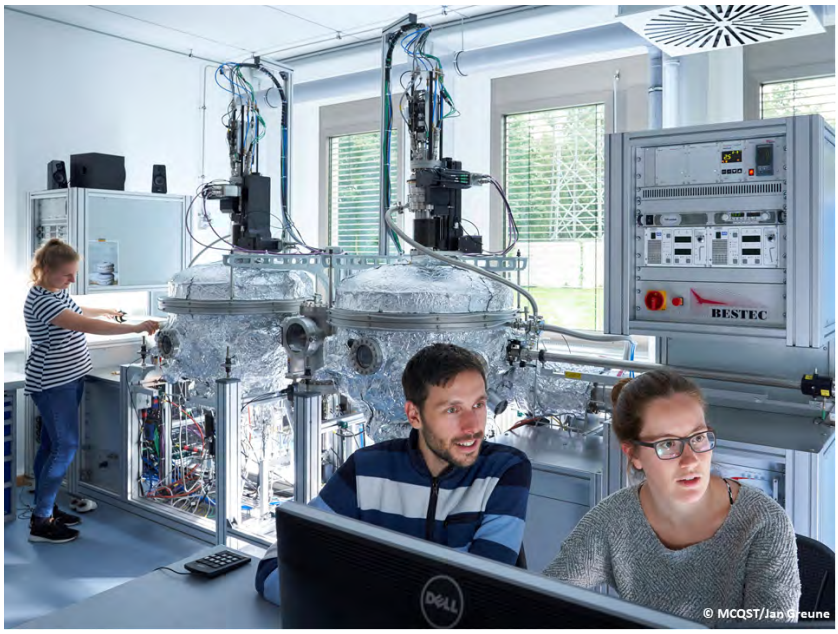

Figure 2: UHV sputter deposition system named «**SUPERBOWLS**». Left chamber is the NFC dedicated to the deposition of superconducting materials, right chamber is the AFC equipped with magnetic materials. Between the two deposition chambers resides the loadlock (LL).

The loadlock chamber is equipped with a substrate and mask storage cassette for up to six substrates. Halogen lamp heaters are installed in the loadlock for thermal precleaning of the substrates. The NFC is currently equipped with two 3 inch magnetrons and one 2 inch magnetron. In the AFC, eight 2 inch tiltable magnetrons are installed. In this chamber the sources can be either oriented into two confocal deposition clusters from 4 sources or 4 sources for face-to-face deposition, providing a large flexibility in the deposition conditions and enabling the fabrication of quaternary alloys from single element targets. All deposition sources are equipped with pneumatically actuated shutters, tilts, and linear translations. This allows for both face-to-face and confocal deposition from all three sources.

Both chambers are equipped with versatile substrate manipulators. They can accommodate substrates with a diameter of up to 2 inch and feature a resistive heater for substrate temperatures up to 800 °C, a motorized substrate shutter for wedge and step-profile deposition, a motorized linear translation for changing the source to substrate position, a main rotation to move the substrate in the chamber to the different deposition positions, a motorized substrate rotation at up to 40 rpm for homogenous deposition, and a quartz crystal microbalance (QCM) for growth rate monitoring. In addition, a Kaufmann source for reactive ion etching is installed in the system for in-situ surface cleaning procedures or even etching processes. Several 1 kW DC power and 600 W RF power supplies are used for the operation of the magnetrons. Mass flow controllers allow to change the composition of the process gas for reactive sputtering processes. More details can be found in the Annual Report 2017.

UHV Sputter Deposition System – ULTRADISC

In 2018, a new UHV sputter deposition system (1600 l/s turbo molecular pump, base pressure: $< 1 \times 10^{-9}$ mbar, automatic up- or down-stream pressure regulation: 8×10^{-4} mbar to 1×10^{-1} mbar) for the fabrication of superconducting thin films on large substrate areas has been installed.[1] The system consists of a main deposition chamber and a load lock, which is equipped with a motorized storage cassette for up to six substrates, a stab-in heater and a linear transfer arm for moving samples into and out of the main deposition chamber.

Figure 3: UHV sputter deposition system named **«ULTRADISC»**. The main chamber contains the deposition sources in the bottom flange and the substrate manipulator on the top flange.

The main deposition chamber has been designed for flexible and homogeneous deposition on substrates with a diameter of up to 100 mm. The substrate holder is electrically isolated to allow for a plasma directly underneath the substrate via applying a DC or RF bias to the substrate holder. A radiative carbide heater is used to homogeneously heat the substrate up to 950 °C. The substrate manipulator has 3 degrees of freedom to move the substrate in the deposition chamber. The main substrate rotation allows to move the substrate over the different deposition clusters. In addition, the distance between substrate and sources can be tuned by 100 mm via a motorized z-shift of the manipulator. For homogeneous deposition, the substrate itself can rotate with up to 30 rpm. An automated substrate shutter allows to protect the substrate from unintentional deposition. Moreover, a motorized wedge shutter enables the fabrication of controlled thickness variations over the area of the substrate.

Flexibility in materials choice is ensured by a total of 11 magnetron sources installed in the chamber. A total of 7 sources can be used for face-to-face deposition on the substrate for high growth rate deposition (several 10 nm/min). In addition, 8 sources can be manually tilted into three separate confocal deposition clusters, which enables simultaneous deposition from up to 3 sources. Automated control of the deposition times is achieved by the motorized shutters attached to each magnetron. The high-purity gas supply is realized via 4 independent mass flow controllers, allowing for flexible gas compositions for reactive sputter deposition of oxide and nitride materials. For more flexibility in reactive sputtering processes and for substrate cleaning purposes the confocal cluster is equipped with a RF discharge ion source (up to 1.0 kV). Two different grids suitable for nitrogen and oxygen or argon are currently available for the system. Two separate mass flow controllers are used to supply the high purity gases to the ion source. The system is fully automated by the supplied computer and software. More details can be found in the Annual Report 2018.

[1] The system is running under the acronym «ULTRADISC »: **U**nlimited **L**egendary **T**ool for **R**eliable **A**chievements in the **D**eposition of **I**ntegrated **S**uperconducting **C**omponents.

PLASSYS MEB 550 S4-I UHV Deposition System for Qubit Fabrication

With increasing complexity of superconducting quantum circuits, a well-controlled fabrication process is mandatory in order to obtain a reasonable fabrication yield. Therefore, a flexible UHV deposition system (model MEB 550 S4-I of PLASSYS Bestek has been set up in 2020 with financial support of the Cluster of Excellence ***MCQST*** . The systems is of key relevance for improving the coherence time of superconducting qubits and their reproducible fabrication with small parameter spread.

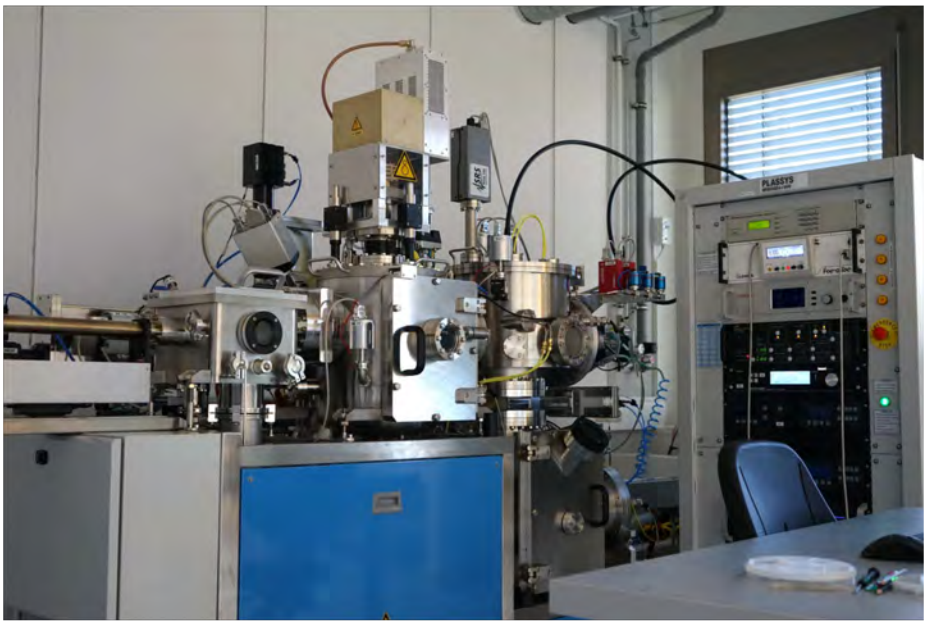

Figure 4: The Plassys UHV deposition system installed at WMI. Left part: load-lock with the sample transfer rod, middle part: sputter deposition chamber, right part: deposition/oxidation and electron beam evaporation chambers. The deposition/oxidation chamber is positioned atop the evaporation chamber separated by a horizontal gate valve. Not shown is the computer system for process control.

The system is fully automated and consists of a load-lock and two further UHV chambers for sputter deposition (e.g. Nb, Ti) and for electron beam deposition (e.g. Al, Ti). The load-lock is equipped with an ion gun for cleaning and etching wafers by neutralized argon or oxygen ions. It also contains an ozone source for removing organic contaminants. In the UHV sputter deposition chamber, there are two 3-inch magnetrons which are compatible with RF and DC power. The magnetrons are oriented in a confocal sputter-up configuration over a spinning 4-inch substrate. The planetary rotation of the substrate holder is compatible with the confocal configuration of the magnetrons. The substrate can be RF polarized for cleaning before deposition or for ion assistance during deposition.

The electron beam evaporator and the motorized substrate holder are placed in two separate chambers – the "oxidation" and "evaporation chamber" – which are positioned on top of each other and can be separated by a horizontal gate valve. The evaporation chamber is equipped with a linear 8×15 ccm electron beam evaporator from Thermionics. In the oxidation chamber, a high-density atomic oxygen plasma can be generated by a 2.45 GHz ECR microwave source. Furthermore, the oxidation chamber is equipped with a residual gas analyser. An ozone treatment can be applied to the wafers both in the load-lock and oxidization chamber. A key part of the oxidation chamber is the fully automated motorized substrate holder, allowing for tilting and spinning substrates with a size up to 4 inch. It provides full flexibility for the two-angle shadow evaporation process. A software controlled oxidation process ensures high reproducibility of oxygen partial pressure and duration of exposure. A rear heating system allows for substrate temperatures up to 750°C.

Single Crystal Growth and Synthesis of Bulk Materials

Transition metal oxides are of great interest due to their various interesting physical properties (e.g. high temperature superconductivity, colossal magnetoresistance, ferroelectricity, nonlinear optical properties etc.) and their high potential for applications. Therefore, the WMI operates a laboratory for the synthesis of bulk materials and single crystals of transition metal oxides. Besides various chamber- and tube furnaces a four-mirror image furnace is used for the crystal growth of various oxide systems. With this furnace crystals of many different compounds of the high temperature superconductors and various other transition metal oxides have been grown as single crystals using the traveling solvent floating zone technique. The furnace consists basically of 4 elliptical mirrors with a common focus on the sample rod and with halogen lamps in their other focus. By irradiation of the focused light the sample rod is locally heated and eventually molten. The molten zone can be moved up and down along the entire sample rod under simultaneous rotation. Due to the anisotropic growth velocity a preferential growth of those grains with the fastest growth velocity along the pulling direction is obtained and the formerly polycrystalline rod is transformed into a single crystal. Single crystal growth can be performed with this furnace at maximum temperatures up to 2200 °C in the pressure range from 1×10^{-5} mbar up to 10 bar and in oxidizing, reducing as well as inert atmosphere.

Figure 5: The four-mirror image furnace installed at the crystal laboratory of the WMI. Crystals can be grown by the floating zone and traveling solvent floating zone techniques at temperatures up to 2200 °C and pressures up to 10 bar.

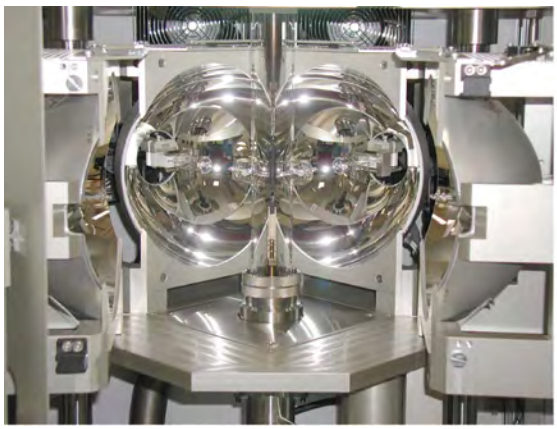

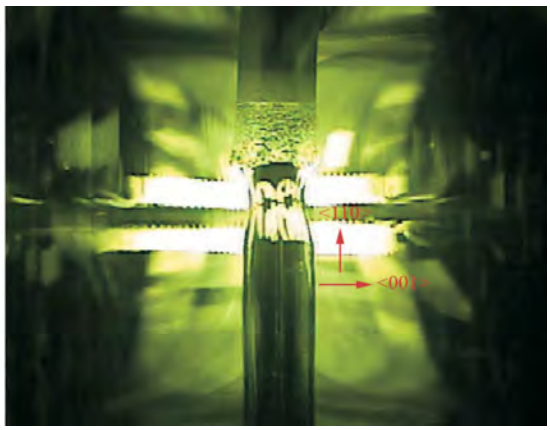

Figure 6: Left: Central part of the image furnace with four elliptical mirrors. In the center one can see the quartz tube with a polycrystalline rod. Right: View on the molten zone of $Pr_{2-x}Ce_xCuO_4$ (melting point: 1280 °C) obtained by a CCD camera.

Structural Characterization: The X-ray Diffraction Systems

For X-ray analysis the WMI operates two X-ray diffractometers (Bruker D8 Advance and D8 Discover). The two-circle system is used for powder diffraction. In this system the samples can be heated in oxygen atmosphere up to 1600 °C. It is equipped with a Göbel mirror and an area detector to save measuring time. The second system is a high resolution four-circle diffractometer that can be used for reciprocal space mappings. It is equipped with a Göbel mirror and an asymmetric two-fold Ge monochromator and allows for the texture analysis of thin film heterostructures, superlattices and single crystalline materials. In both systems measurements can be carried out fully computer controlled.

Beside these two Bruker X-ray systems a Laue camera for single crystal analysis and a Debye-Scherrer camera are available.

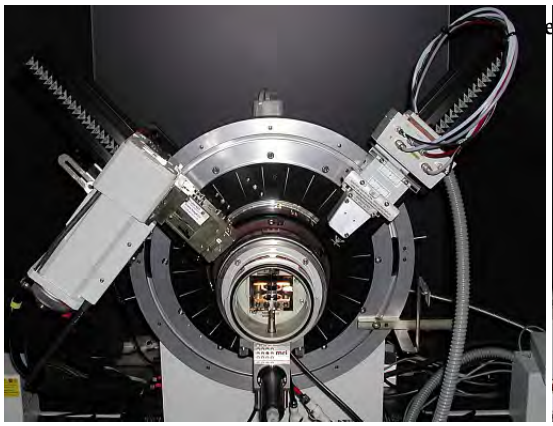

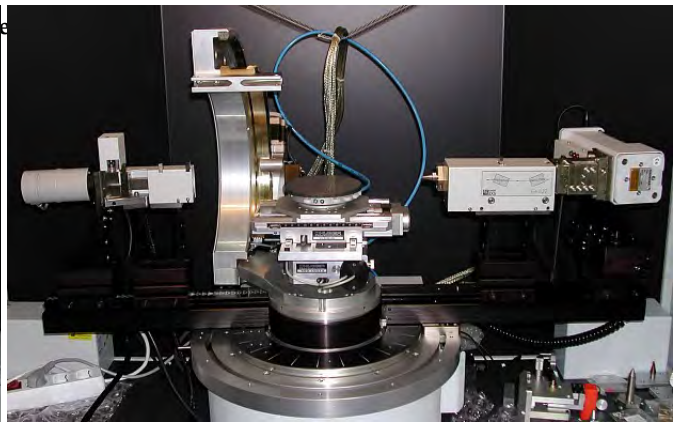

Figure 8: Left: High temperature sample holder of the D8 Advance system. Right: Four-circle high resolution X-ray diffractometer Bruker D8 Discover.

Magnetic Characterization

Figure 9: Quantum Design SQUID magnetometer.

The SQUID Magnetometer

For the analysis of the magnetic properties of materials, a Quantum Design SQUID magnetometer system (Fig. 9) is operated at the WMI. The SQUID magnetometer allows for measurements in the temperature regime from 1.8 to 400 K and provides excellent sensitivity particularly in the low field regime. Due to the excellent sensitivity of the system, thin film samples with a very small sample volume can be analyzed. The SQUID magnetometer is equipped with a superconducting solenoid allowing for a maximum field of 7 T. At present, the magnetometer is used for the characterization of magnetic and superconducting materials (both in bulk and thin film form). Examples are the cuprate high temperature superconductors, the doped manganites, magnetite, the double perovskites, magnetic semiconductors, or multiferroics.

The High Field Laboratory

Transport and thermodynamic properties of samples are often studied as a function of the applied magnetic field. For such measurements several superconducting magnets are available at the WMI. Three of them (8/10 and 15/17 Tesla magnet systems) are located in the high magnetic field laboratory of the WMI. The magnet systems are decoupled from the building to avoid noise due to mechanical vibrations. A variety of sample holders can be mounted allowing for e.g. sample rotation during the measurement. For standard sample holders the accessible temperature regime is $1.5\,\mathrm{K} < T < 300\,\mathrm{K}$. However, also ^{3}He/^{4}He dilution refrigerator inserts ($T > 20\,\mathrm{mK}$) or high temperature units ($T < 700\,\mathrm{K}$) can be mounted. All measurements are fully computer controlled (by the use of the LabView software tool) allowing for remote control and almost continuous measurements.

Figure 10: High field laboratory with Oxford 17 T magnet system.

For experiments which require a flexible change of the field direction, a 3D vector magnet with variable temperature insert, allowing for 2.5 T in-plane and 6 T out-of-plane magnetic fields is available for thermal and electrical transport experiments. This system has been named "Chaos" cryostat (acronym for "Cold, Hot And Other Secret experiments"). It consists of a ^{4}He flow cryostat with a liquid nitrogen shield and includes a vertically oriented 6 T solenoid combined with two horizontally oriented split coil pairs. The magnet system can be operated in two ways:

- in a single axis mode: up to 6(2.5) T are provided in the vertical (horizontal) direction.
- in a arbitrary axis mode: the magnetic field vector can be oriented in arbitrary directions and the magnitude of the magnetic field is limited to 2.5 T.

The magnetic field is controlled by a Mercury IPS superconducting magnet power supply master/slave system. It provides output currents of up to 120 A in bipolar operation for each magnet axis. The control of the system is feasible either directly via touch-screen or remote using a LabView based software.

Figure 11: The 3D vector magnet with control electronics in the "CHAOS" Laboratory.

The Chaos cryostat has a IN100 variable temperature insert (VTI), enabling an operation for temperature setpoints between 1.5 K and 300 K. The temperature control of the sample space inside the VTI can be achieved via an automatic needle valve drive for helium flow control and/or an automatic heater system. The temperature of the VTI is read via a Cernox sensor fitted to the heat exchanger. A remote control of the system is realized by a LabView based software. It provides control of the VTI (heater, needle valve, temperature setpoint) and the IPS (control of the magnetic field setpoints and energizing rates for the three vector components of the field) as well as the display of the actual He and liquid nitrogen levels.

A further 3D vector magnet allowing for 1 T in-plane and 6 T out-of-plane magnetic fields is installed in the WMI Quantum Laboratories as part of a cryogen-free dilution system.

The Clean Room Facility

For the fabrication of nanostructures and quantum circuits including superconducting, spintronic and nanomechanical devices, the WMI operates a class 1000 clean room facility with an area of about 50 m^2. The clean room is subdivided into two parts for optical lithography and electron beam lithography, respectively. The clean room is equipped with the standard tools for optical lithography such as resist coaters, hot plates, wet benches, a Karl Süss MJB3 mask aligner, a direct laser writing system *PicoMaster 200* from 4 PICO, and an optical projection lithography system. The technical infrastructure for the clean room is located in the basement of the WMI directly below the clean room area.

Figure 12: Top: Part of the clean room facility with optical lithography equipment and clean room benches. Bottom: Resist coater and hot plates.

The clean room also is equipped with a reactive ion etching system, Plasmalab 80 Plus with ICP plasma source (Oxford Instruments Plasma Technology).

Electron Beam Lithography

A 100 kV Electron Beam Lithography System nB5 fabricated by NanoBeam Ltd., UK, is installed in the second part of the clean room facility. The nB5 is a round-beam step-and-repeat system oriented towards high-end R&D applications at universities and research institutes. It is designed for nanopatterning and mix-and-match lithography. The innovative design of the electron optics and automation system enhances its throughput and reliability. The electron beam lithography is used for the fabrication of nanostructures required e.g. for the realization of superconducting quantum circuits or the study of quantum effects in mesoscopic samples.

Figure 13: 100 kV Electron Beam Lithography System nB5 of NanoBeam Ltd., UK, inside the WMI cleanroom facility.

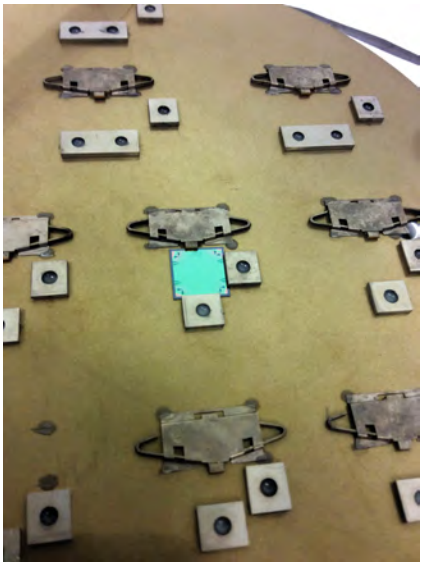

Figure 14: Chuck of the nB5 e-beam lithography system with a mounted $12 \times 12\,\mathrm{mm}^2$ silicon wafer.

The nB5 Electron Beam Lithography System employs low Coulomb-effect electron optics and sophisticated column designs to reduce beam size. The shorter optical column eliminates column bending and reduces system vibration. The modern electronics has low noise and low thermal effects. The perfectly integrated machine structure greatly improves system settling time and total stage move time. The advanced vibration tracking design enables the nB5 system to write on the fly. All these features combined with the fast deflection speed and high data processing rate make the nB5 the highest throughput system available today. Moreover, the nB5 requires undemanding cleanroom conditions, in particular regarding temperature stability, stray field magnitude, and floor vibration level.

The nB5 system is equipped with a thermal field emitter (TFE), an electrostatic lens and magnetic condenser lens, a conjugate beam blanking at $< 5\,\mathrm{ns}$ slew rate and a dual beam deflection. The latter is used to achieve ultra-high deflection speed for beam writing (clock rate: 55 MHz). The total deflection coverage is combined with the mainfield and the subfield and controlled by two independent deflection sub-systems (field size: $1000\,\mu\mathrm{m}$, address resolution: 1 nm). Further characteristic performance parameters are: (i) beam voltage range: 20 kV to 100 kV, (ii) minimum beam current: 0.1 nA, (iii) maximum beam current: 100 nA, (iv) theoretical beam size: 2.3 nm at 100 kV, (v) guaranteed writing beam size: $< 5\,\mathrm{nm}$ at 2 nA, (vi) beam current drift: $< 0.5\%$/hour at 5 nA, (vii) beam position drift: $< 50\,\mathrm{nm}$/hour for 3 nA beam current, including blanking, deflection and stage move.

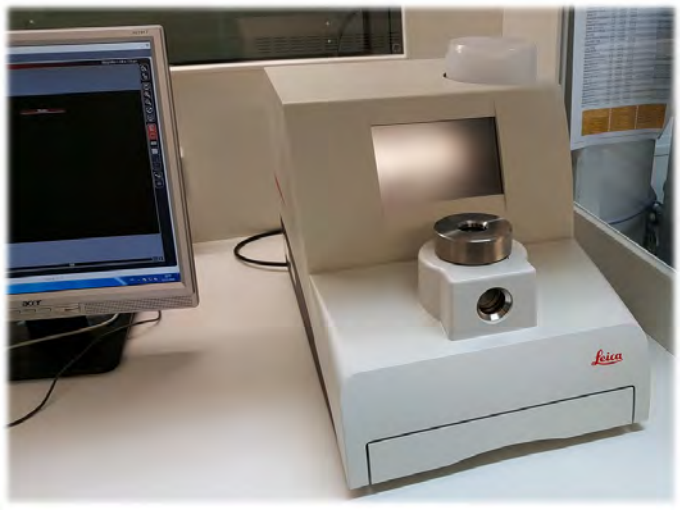

Figure 15: The fully automated Critical Point Dryer Leica EM CPD 300.

The XY-stage allows for a traversal distance of 200 mm with a position measurement resolution of 0.3 nm using laser interferometry. The maximum substrate sizes are $2 - 8$ in for round substrates, $2 - 5$ for square glass masks up to 3 mm thickness. Finally, the nB5 system has airlock operation with automatic loading robotics with a loading cassette for 6 chucks with a maximum diameter of 8 inch.

Automated Critical Point Dryer Leica EM CPD 300

The fabrication of nanomechanical systems requires the removal of solvent used for wet chemical processing by a critical point dryer. At WMI, we use the Critical Point Dryer Leica EM CPD 300, which allows the fully automated drying of biological specimens such as pollen, tissue, plants, insects etc., as well as NEMS (Nano Electro Mechanical Systems).

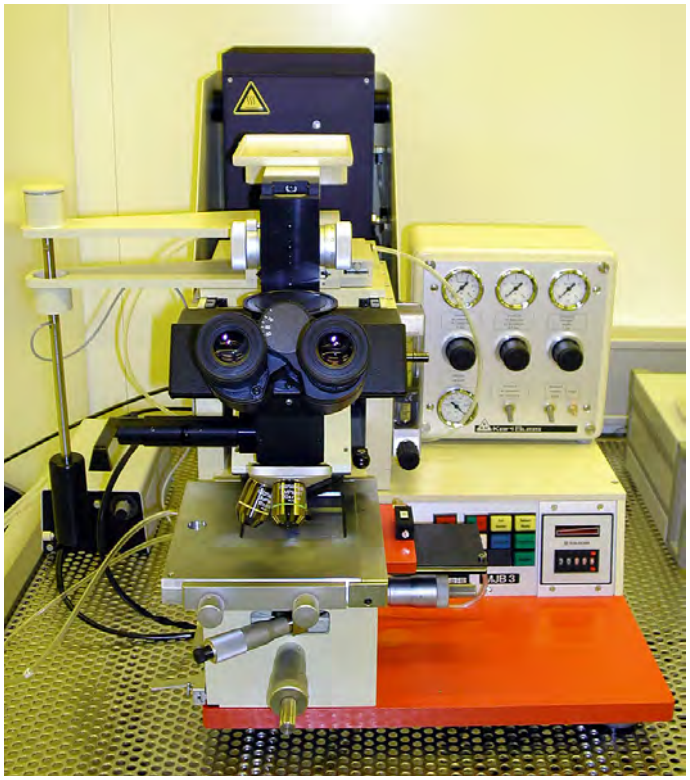

Figure 16: Top: Süss MJB 3 maskaligner for optical lithography. Bottom: Direct laser writing systems *PicoMaster 200*.

Optical Lithography

For optical lithography, a Karl Süss MJB 3 maskaligner or a direct laser writing system are used. The maskaligner operates in the 1 : 1 soft or hard contact mode and uses chromium metal masks.

The direct laser writing system *PicoMaster 200* (PM 200) of the company 4PICO accepts substrate sizes between 5 mm × 5 mm and 200 mm × 200 mm via a turnable chuck. For writing the pattern, it allows for three different spot sizes (300 nm × 600 nm × 900 nm) and a write speed of up to 7.7 mm^2/min. One can choose between two compact writing modules equipped with a 405 nm and a 375 nm laser diode, respectively. The user can easily switch between the two modules within minutes since the full optical path is contained in the modules. Both modules feature automatic focus correction for not too heavily varying resist thickness.

Low and Ultra-Low Temperature Facilities

At the WMI, we have constructed the worldwide first dilution refrigerator with pulse tube pre-cooling for ultra-low temperature experiments in the early 2000s. This type of refrigerator works without cryo-liquids, and thus is a lot more practical, more economical and more reliable than systems with liquid helium pre-cooling. Meanwhile, all major cryo-engineering companies are offering commercial versions of this mK-cooler, and these so-called "dry" refrigerators outsell conventional refrigerators by a wide margin. The general construction concept of most manufacturers is unchanged from our original prototype, where the refrigerator consists of three basic components. The first cooling stage is a commercial pulse tube cryocooler which reaches a base temperature of 2.5 K. The second stage is a Joule-Thomson stage, and the last stage is a dilution refrigeration stage with a base temperature of about 0.01 K (Fig. 17).

Figure 17: The "dry" dilution refrigerator of the WMI.

Figure 18: Low-temperature unit of a WMI dilution refrigerator ready to go into a cryostat.

Figure 19: Two mixing chamber mounting plates with silver sponges. Those are needed to overcome the thermal resistance (Kapitza resistance) between the liquid ^{3,4}He and the mounting plate of the mixing chamber. To fabricate the mounting of the sponge (square pins embedded in the sponge) a spark erosion technique has been employed.

In many low temperature applications a large cooling power is required. Therefore, our design allows for a high circulation rate of ^{3}He and hence cooling power. Presently our "dry" fridge reaches a refrigeration capacity of 700 µW at a temperature of the mixing chamber of 0.1 K and we aim at further improving both the cooling power and base temperature. A smaller version of our cryogen-free fridge has become commercially available later on by *VeriCold Technologies, Ismaning*), which was taken over by *Oxford Instruments* in 2007. It had a refrigeration capacity of 250 µW at a mixing chamber temperature of 0.1 K (Fig. 18).

The WMI also develops and fabricates dilution refrigerator inserts for temperatures down to about 20 mK. The inserts fit into all cryogenic systems (e.g. superconducting magnets) having a two inch bore. They allow fast sample change and rapid cool down cycles of less than five hours. The dilution refrigerator inserts are engineered and fabricated in-house and are also provided to other low temperature laboratories for ultra-low temperature experiments.

Millikelvin Temperatures in Combination with 3D Vector Magnetic-Fields

Figure 20: The dilution refrigerator with the 3D vector magnet located in the Quantum Laboratories.

In the WMI Quantum Laboratories, a cryogen-free dilution refrigerator of Oxford Instruments is installed which is equipped with a 3D vector magnet allowing for 1 T in-plane and 6 T out-of-plane magnetic fields. Additional microwave coaxial lines allow for the microwave spectroscopy up to 18 GHz under these experimental conditions.

Aside from experiments related to circuit quantum electrodynamics, the combination of mK-temperatures and a 3D vector magnet makes the system particularly interesting for the following research directions:

(i) Storage of quantum states in spin systems by transferring quantum information contained in e.g. photons to long-lived spin states and the study the light-matter interaction with long-lived spin systems by integrating them into superconducting quantum circuits.

(ii) Study if the quantum coherent behavior of spin systems in paramagnetic but also in exchange coupled (ferro- or ferri-) magnetic materials. Of particular interest is the magnetization damping as a function of temperature, frequency and magnetic field direction.

(iii) Investigation of circuit electro-mechanical hybrid systems consisting of a nano-mechanical element coupled to a superconducting microwave resonator. Of particular interest are the sideband cooling of the mechanical system into its ground state and pulsed spectroscopy of hybrid systems.

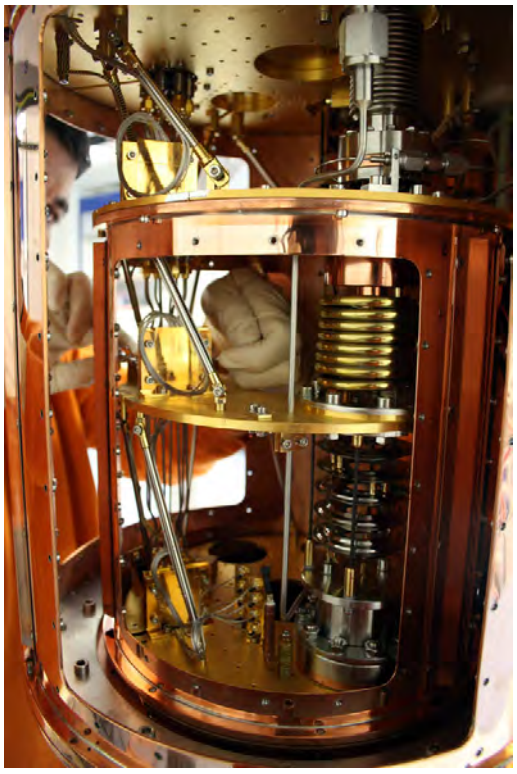

Figure 21: Inside of the dilution system. The windows of the 4 K and the still shield are removed providing access to the low temperature stages.

WMI Millikelvin Facilities for Experiments with Superconducting Quantum Circuits

The research on superconducting quantum circuits at WMI focuses mainly on the study of qubits that can be controlled by an applied flux (e.g. flux qubit, transmon qubit), circuit QED systems where qubits are coupled to transmission line resonators, squeezing physics in flux driven Josephson parametric amplifiers, and propagating quantum microwaves (e.g., quantum state reconstruction methods). In order to further develop our activities on quantum effects in the microwave regime and the study of superconducting quantum circuits, the cryogenic equipment allowing experiments at millikelvin temperatures has been continuously expanded. In addition to sufficient cooling power, the specifications for these mK-systems are mainly dictated by the dimensions the experiments and of bulky microwave components such as circulators or microwave switches.

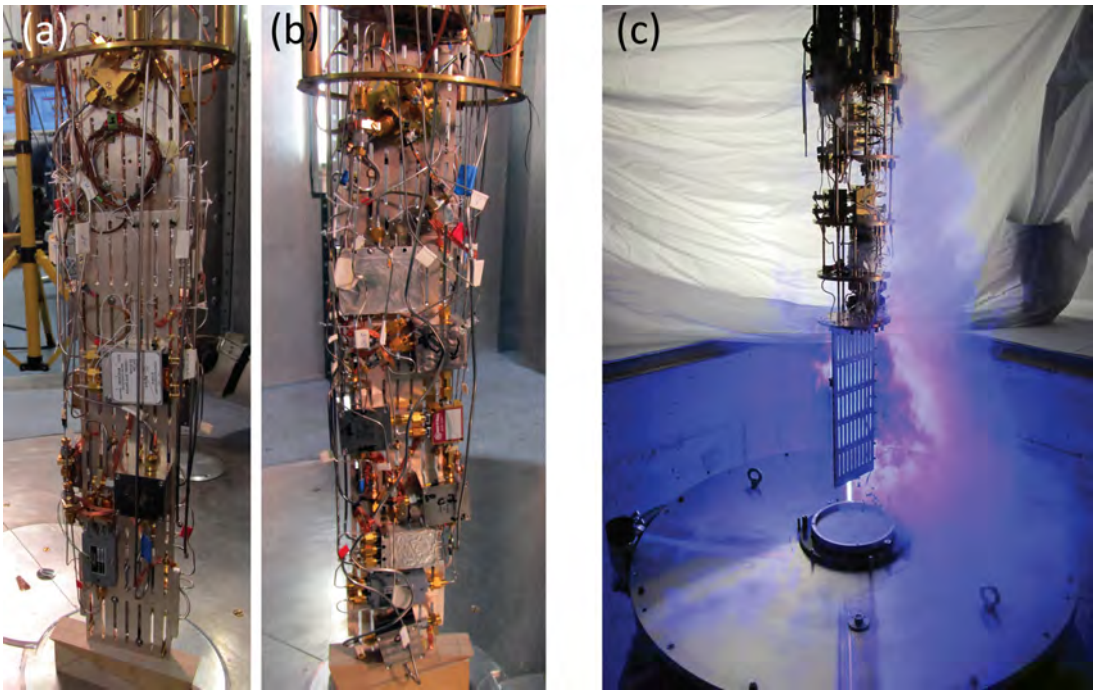

Figure 22: Liquid-helium precooled dilution refrigerators for experiments with superconducting quantum circuits. (a), (b) Back and front sides of the sample stage of the K12-refrigerator equipped with four circuit QED experiments. The height of the silver rod is 50 cm. (c) Sample stage and dewar of the dilution refrigerator in the quantum laboratory K04.

Two liquid-helium precooled dilution refrigerators are available for experiments with superconducting quantum circuits. The dilution refrigerator in laboratory K12 provides a sample space with a cylindrical volume with 11 cm diameter 55 cm height. The refrigerator is equipped with four microwave amplifiers at the 4 K-stage, seven broadband input lines and 80 twisted pair DC lines. This allows for mounting four experiments simultaneously to avoid idle times by interleaved measurements (see Fig. 22(a) and (b)). The base temperature of this refrigerator is 20 mK.

A liquid-helium precooled dilution refrigerator is placed in the quantum laboratory K04. To provide enough sample space we have installed a Cryogenic Ltd. stainless steel dewar with a ^{4}He volume of 89 L. The time between two refills exceeds nine days. The cryostat is equipped with 16 coaxial measurement lines suitable for microwave frequencies down to the mixing chamber stage and low-noise cryogenic HEMT amplifiers. Presently up to four samples can be mounted simultaneously to the sample stage. By expanding the number of input lines in the near future a more complex experiment can be set up. The cooling power of the mixing chamber at 100 mK was determined to about 140 µW.

A cryogen-free dilution refrigerator with a pulse tube refrigerator (PTR) for precooling and with a large sample stage has been designed and built at WMI using the longstanding experience in dry dilution refrigerators. It is set up in room K21 of the WMI Quantum Laboratories. This refrigerator features large diameters (tens of centimeters) of all temperature stages providing sufficient space for advanced quantum experiments. The main components of the refrigerator are the PTR, a 1 K-stage and a dilution unit. The two stages of the PTR cool the incoming ^{4}He and the ^{3}He/^{4}He mixture as well as one radiation shield at each stage. To provide sufficiently high cooling power near 1 K to cool microwave components and cables, this refrigerator has been equipped with a 1 K-stage operating in a closed cycle. A refrigeration capacity of the 1 K-stage of up to 100 mW could be reached. The dilution refrigerator is precooled by a dedicated ^{4}He circuit. The minimum base temperature of the refrigerator is below 11 mK. The cooling power at 100 mK was determined to about 300 µW at the maximum ^{3}He flow rate.

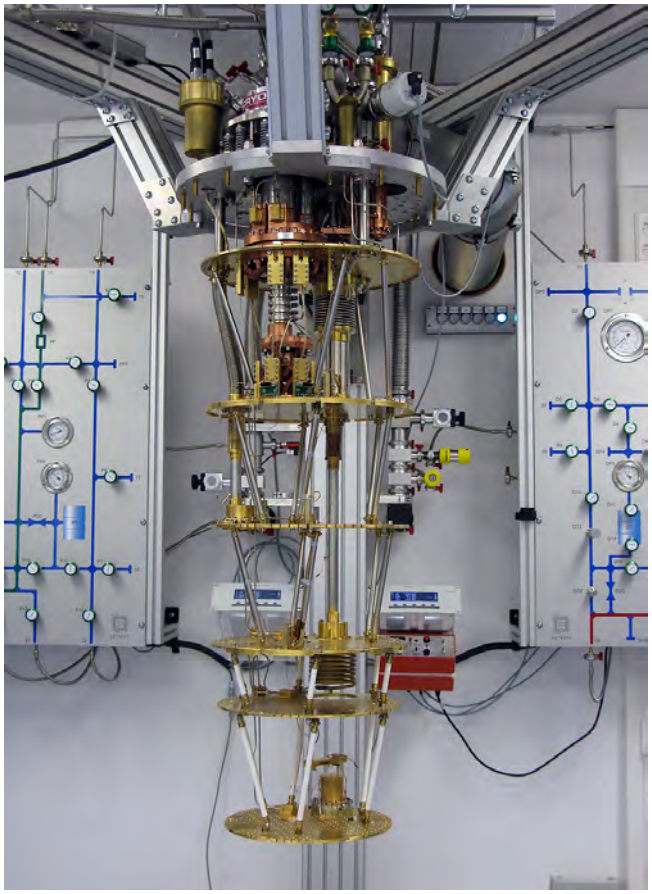

Figure 23: Dry dilution refrigerator with a large sample space.

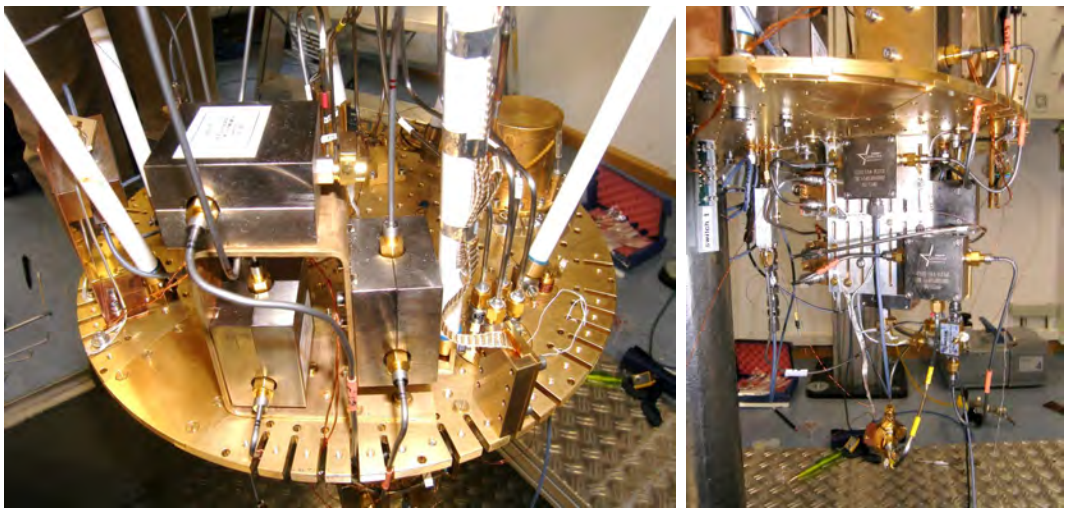

Figure 24: Low temperature platform of K21 dilution refrigerator with experimental setup for circuit QED experiments.

WMI Millikelvin Facilities for Superconducting Quantum Computing

With the increasing interest in superconducting quantum computing, there is a strong need for cryogen-free dilution refrigerators with large cooling power and sample space. This is in particular relevant for experiments circuits and components which are rapidly growing in size

and complexity. Fortunately, the funding for such a dilution refrigerator has been granted by the German Research Foundation via the Excellence Cluster MCQST and a powerful XLD 1000 system of the company Bluefors Oy could be ordered and installed in 2020. The XLD 1000 system can accommodate more than 300 microwave lines and provides a base temperature of about 10 mK. A single push of a button initiates a fully automated cool-down sequence.

Figure 25: New Bluefors XLD 1000 Dry Dilution Refrigerator after installation at WMI. All the compressors and the gas handling systems are located in a technical room underneath the laboratory (photo: MCQST/Jan Greune).

A big advantage of the Bluefors XLD 1000 dry dilution refrigerator is the fact that it features very large experimental space at all temperature stages and an experimental volume with a diameter of 50 cm and a height of 55 cm below the mixing chamber plate. The elegant side loading mechanism allows the straightforward installation of additional microwave lines. In its final development stage this refrigerator can host several experiments at the same time, even if many input and output lines are required for each single experiment. The system reaches a base temperature below 10 mK. The dilution unit is designed for high throughput and provides for a cooling power of more than 1 mW at 100 mK (30 µW at 20 mK).

The XLD 1000 dilution refrigerator is equipped with two pulse tube refrigerators (Cryomech PTR 420 with 2 W cooling power at 4 K each). The cool-down and warm-up of the refrigerator can be handled fully automatic. Oil-free pumps and compressors in the gas handling unit guarantee minimal maintenance requirements with service interval up to 3 years. Moreover, the system is equipped with a unique long-life cold trap that allows for continuous operation of the system for up to three years. The trap is integrated with the system and does not need any cryogenic liquids to operate.

Figure 26: Left: WMI students working on the new Bluefors XLD 1000 cryogen-free dilution refrigerator. Left: Microwave lines connecting to equi-temperature plates (photos: BAdW/ Kai Neunert).

With the start of the Munich Quantum Valley in 2021 and large BMBF projects aiming at the realization of superconducting quantum computers, two additional Bluefors XLD 1000 and LD 400 as well as a bottom loading system for fast sample change have been installed at WMI.

Statistics

Publications

1. **Experimental quantum teleportation of propagating microwaves**
K. G. Fedorov, M. Renger, S. Pogorzalek, R. Di Candia, Q. Chen, Y. Nojiri, K. Inomata, Y. Nakamura, M. Partanen, A. Marx, R. Gross, F. Deppe
Science Advances **7**, eabk0891 (2021).

2. **Temperature-Dependent Spin Transport and Current-Induced Torques in Superconductor-Ferromagnet Heterostructures**
Manuel Müller, Lukas Liensberger, Luis Flacke, Hans Huebl, Akashdeep Kamra, Wolfgang Belzig, Rudolf Gross, Mathias Weiler, Matthias Althammer
Physical Review Letters **126**, 087201 (2021).

3. **Beyond the Standard Quantum Limit for Parametric Amplification of Broadband Signals**
M. Renger, S. Pogorzalek, Q. Chen, Y. Nojiri, K. Inomata, Y. Nakamura, M. Partanen, A. Marx, R. Gross, F. Deppe, K. G. Fedorov
npj Quantum Information **7**, 160 (2021).

4. **High-speed calibration and characterization of superconducting quantum processors without qubit reset**
M. Werninghaus, D. Egger, S. Filipp
Physical Review X Quantum **2**, 020324 (2021).

5. **Characterization and tomography of a hidden qubit**
M. Pechal, G. Salis, M. Ganzhorn, D. J. Egger, M. Werninghaus, S. Filipp
Physical Review X **11**, 041032 (2021).

6. **Integrated tool set for control, calibration, and characterization of quantum devices applied to superconducting qubits**
N. Wittler, F. Roy, K. Pack, M. Werninghaus, A. S. Roy, D. J. Egger, S. Filipp, F. K. Wilhelm, S. Machnes
Physical Review Applied **15**, 034080 (2021).

7. **Leakage reduction in fast superconducting qubit gates via optimal control**
Max Werninghaus and Daniel J Egger and Federico Roy and Shai Machnes and Frank K Wilhelm and Stefan Filipp
npj Quantum Information **7**, 14 (2021).

8. **Zeeman Spin-Orbit Coupling and Magnetic Quantum Oscillations in Antiferromagnetic Conductors**
R. Ramazashvili, P. D. Grigoriev, T. Helm, F. Kollmannsberger, M. Kunz, W. Biberacher, E. Kampert, H. Fujiwara, A. Erb, J. Wosnitza, R. Gross, M. V. Kartsovnik
npj Quantum Materials **6**, 11 (2021).

9. **Superconducting Wireless Power Transfer Beyond 5 kW at High Power Density for Industrial Applications and Fast Battery Charging**
Christoph Utschick, Cem Som, Ján Šouc, Veit Große, Fedor Gömöry, Rudolf Gross
IEEE Transactions on Applied Superconductivity **31**, 5500110 (2021).

10. **In-situ Tunable Nonlinearity and Competing Signal Paths in Coupled Superconducting Resonators**
Michael Fischer, Qi-Ming Chen, Christian Besson, Peter Eder, Jan Goetz, Stefan Pogorzalek, Michael Renger, Edwar Xie, Michael J. Hartmann, Kirill G. Fedorov, Achim Marx, Frank Deppe, Rudolf Gross
Physical Review B **103**, 094515 (2021).

11. **Quantifying the spin mixing conductance of EuO/W heterostructures by spin Hall magnetoresistance experiments**
Paul Rosenberger, Matthias Opel, Stephan Geprägs, Hans Huebl, Rudolf Gross, Martina Müller, Matthias Althammer
Applied Physics Letters **118**, 192401 (2021).

12. **$La_{1-x}Mn_{1-y}O_{1\pm\delta}$ Buffer Layers on Inclined Substrate Deposited Mgo Templates for Coated Conductors**

Oleksiy Troshyn, Christian Hoffmann, Veit Große, Jens Hänisch, Lucas Becker, Rudolf Gross
Superconducting Science and Technology **34**, 035006 (2021).

13. **Growth of Aluminum Nitride on a Silicon Nitride Substrate for Hybrid Photonic Circuits**
G. Terrasanta, M. Müller, T. Sommer, S. Geprägs, R. Gross, M. Althammer, M. Poot
Materials for Quantum Technology **1**, 021002 (2021).

14. **Robust Formation of Nanoscale Magnetic Skyrmions in Easy-Plane Anisotropy Thin Film Multilayers with Low Damping**
Luis Flacke, Valentin Ahrens, Simon Mendisch, Lukas Körber, Tobias Böttcher, Elisabeth Meidinger, Misbah Yaqoob, Manuel Müller, Lukas Liensberger, Attila Kákay, Markus Becherer, Philipp Pirro, Matthias Althammer, Stephan Geprägs, Hans Huebl, Rudolf Gross, Mathias Weiler
Physical Review B **104**, L100417 (2021).

15. **Low Temperature Suppression of the Spin Nernst Angle in Pt**
Tobias Wimmer, Janine Gückelhorn, Sebastian Wimmer, Sergiy Mankovsky, Hubert Ebert, Matthias Opel, Stephan Geprägs, Rudolf Gross, Hans Huebl, Matthias Althammer
Physical Review B **104**, L140404 (2021).

16. **Growth Optimization of TaN for Superconducting Spintronics**
Manuel Müller, Raphael Hoepfl, Lukas Liensberger, Stephan Geprägs, Hans Huebl, Mathias Weiler, Rudolf Gross, Matthias Althammer
Material for Quantum Technology **1**, 045001 (2021).

17. **Tunable Cooperativity in Coupled Spin-Cavity Systems**
Lukas Liensberger, Franz X. Haslbeck, Andreas Bauer, Helmuth Berger, Rudolf Gross, Hans Huebl, Christian Pfleiderer, Mathias Weiler
Physical Review B **104**, L100415 (2021).

18. **RF Antenna Design for 3D Quantum Memories** F. Deppe, Edwar Xie, K.G. Fedorov, G. Andersson, J. Müller, A. Marx, R. Gross
International Applied Computational Electromagnetics Society Symposium (ACES), IEEE Xplore, ISBN:978-1-7335096-2-6 (2021).
Proceedings of ACES 2021.

19. **Magnon Transport in $Y_3Fe_5O_{12}$/Pt Nanostructures with Reduced Effective Magnetization**
J. Gückelhorn, T. Wimmer, M. Müller, S. Geprägs, H. Huebl, R. Gross, M. Althammer
Physical Review B **104**, L180410 (2021).

20. **All-electrical detection of skyrmion lattice state and chiral surface twists**
A. Aqeel, M. Azhar, N. Vlietstra, A. Pozzi, J. Sahliger, H. Huebl, T. T. Palstra, C. H. Back, and M. Mostovoy
Physical Review B **103**, L100410 (2021).

21. **Design of an optomagnonic crystal: Towards optimal magnon-photon mode matching at the microscale**
Jasmin Graf, Sanchar Sharma, Hans Huebl, and Silvia Viola Kusminskiy
Physical Review Research **3**, 013277 (2021).

22. **Spin to charge conversion in Si/Cu/ferromagnet systems investigated by ac inductive measurements**
Ei Shigematsu, Lukas Liensberger, Mathias Weiler, Ryo Ohshima, Yuichiro Ando, Teruya Shinjo, Hans Huebl, and Masashi Shiraishi
Physical Review B **103**, 094430 (2021).

23. **Nonreciprocal Magnetoacoustic Waves in Dipolar-Coupled Ferromagnetic Bilayers**
M. Küß, M. Heigl, L. Flacke, A. Hörner, M. Weiler, A. Wixforth, and M. Albrecht
Physical Review Applied **15**, 034060 (2021).

24. **Sub-50 nm wavelength spin waves excited by low-damping $Co_{25}Fe_{75}$ nanowires**
Hanchen Wang, Luis Flacke, Weiwei Wei, Song Liu, Hao Jia, Jilei Chen, Lutong Sheng, Jianyu Zhang, Mingkun Zhao, Chenyang Guo, Chi Fang, Xiufeng Han, Dapeng Yu, Matthias Althammer, Mathias Weiler, Haiming Yu
Applied Physics Letters 119, 152402 (2021).

25. **Symmetry of the Magnetoelastic Interaction of Rayleigh and Shear Horizontal Magnetoacous-**

tic Waves in Nickel Thin Films on $LiTaO_3$
M. Küß, M. Heigl, L. Flacke, A. Hefele, A. Hörner, M. Weiler, M. Albrecht, and A. Wixforth
Physical Review Applied **15**, 034046 (2021).

26. **All-Electrical Magnon Transport Experiments in Magnetically Ordered Insulators**
Matthias Althammer
Physica Status Solidi (RRL) **15**, 2100130 (2021).

27. **Spin Vortex Crystal Order in Organic Triangular Lattice Compound**
Kira Riedl, Elena Gati, David Zielke, Steffi Hartmann, Oleg M. Vyaselev, Nataliya D. Kushch, Harald O. Jeschke, Michael Lang, Roser Valentí, Mark V. Kartsovnik, Stephen M. Winter
Physical Review Letters **127**, 147204 (2021).

28. **Calculation of an Enhanced A_{1g} Symmetry Mode Induced by Higgs Oscillations in the Raman Spectrum of High-Temperature Cuprate Superconductors**
M. Puviani, A. Baum, S. Ono, Y. Ando, R. Hackl, D. Manske
Physical Review Letters **127**, 197001 (2021).

29. **Phonon Anomalies Associated with Spin Reorientation in the Kagome Ferromagnet Fe_3Sn_2**
Ge He, Leander Peis, Ramona Stumberger, Lilian Prodan, Vladimir Tsurkan, Nico Unglert, Liviu Chioncel, István Kézsmárki, and Rudi Hackl
Phys. Status Solidi B, 2100168 (2021).

30. **Probing charge density wave phases and the Mott transition in 1T-TaS_2 by inelastic light scattering**
S. Djurdjić Mijin, A. Baum, J. Bekaert, A. Solajić,1 J. Pešić, Y. Liu, Ge He, M. V. Milošević, C. Petrovic, Z. V. Popović, R. Hackl, and N. Lazarević
Phys. Rev. B **103**, 245133 (2021).

31. **Spray-Deposited Anisotropic Ferromagnetic Hybrid Polymer Films of PS-b-PMMA and Strontium Hexaferrite Magnetic Nanoplatelets**
Wei Cao, Shanshan Yin, Martina Plank, Andrei Chumakov, Matthias Opel, Wei Chen, Lucas P. Kreuzer, Julian E. Heger, Markus Gallei, Calvin J. Brett, Matthias Schwartzkopf, Artem A. Eliseev, Evgeny O. Anokhin, Lev A. Trusov, Stephan V. Roth, Peter Müller-Buschbaum
ACS Appl. Mater. Interfaces **13**, 1592 (2021).

32. **Controlling Domain-Wall Nucleation in Ta/CoFeB/MgO Nanomagnets via Local Ga^+ Ion Irradiation**
Simon Mendisch, Fabrizio Riente, Valentin Ahrens, Luca Gnoli, Michael Haider, Matthias Opel, Martina Kiechle, Massimo Ruo Roch, Markus Becherer
Physical Review Applied **16**, 014039 (2021).

33. **In Situ Study of FePt Nanoparticles-Induced Morphology Development during Printing of Magnetic Hybrid Diblock Copolymer Films**
Wei Cao, Shanshan Yin, Martin Bitsch, Suzhe Liang, Martina Plank, Matthias Opel, Manuel A. Scheel, Markus Gallei, Oliver Janka, Matthias Schwartzkopf, Stephan V. Roth, Peter Müller-Buschbaum
Advanced Functional Materials, 2107667 (2021).

34. **Twenty-three millisecond electron spin coherence of erbium ions in a natural-abundance crystal**
Marianne Le Dantec, Miloš Rančić, Sen Lin, Eric Billaud, Vishal Ranjan, Daniel Flanigan, Sylvain Bertaina, Thierry Chanelière, Philippe Goldner, Andreas Erb, Ren Bao Liu, Daniel Estève, Denis Vion, Emmanuel Flurin, Patrice Bertet
Science Advances **7**, eabj9786 (2021).

35. **Superconductor-insulator transition in space charge doped one unit cell $Bi_{2.1}Sr_{1.9}CaCu_2O_{8+x}$**
Fang Wang, Johan Biscaras, Andreas Erb, Abhay Shukla
Nature Communications **12**, 2926 (2021).

36. **Moissanite anvil cell single crystal NMR at pressures of up to 4.4 GPa**
Carsten Kattinger, Robin Guehne, Stefan Tsankov, Michael Jurkutat, Andreas Erb, Juergen Haase
Review of Scientific Instruments **92**, 113901 (2021).

37. **Erste Demonstration von Quantenüberlegenheit**

Michael J. Hartmann, Frank Deppe
Physik in unserer Zeit **52**, 12 (2021).

38. **Faszinierende Welt der Quanten**
Rudolf Gross
Akademie Aktuell, Heft 2, Nummer 74 (2021), pp. 14-19 (2021), ISSN 1436 -753X.

39. **Quantencomputer - können wir damit rechnen?**
Stefan Filipp
Akademie Aktuell, Heft 2, Nummer 74 (2021), pp. 20-23 (2021), ISSN 1436 -753X.

40. **Pioniere der Quantenforschung**
Hans Hübl
Akademie Aktuell, Heft 2, Nummer 74 (2021), pp. 32-35 (2021), ISSN 1436 -753X.

41. **Lokales Quantennetzwerk für Alice und Bob**
Frank Deppe, Kirill G. Fedorov, Achim Marx
Akademie Aktuell, Heft 2, Nummer 74 (2021), pp. 36-38 (2021), ISSN 1436 -753X.

42. **Tuning and Amplifying the Interactions in Superconducting Quantum Circuits with Subradiant Qubits**
Qi-Ming Chen, Florian Fesquet, Kedar E. Honasoge, Fabian Kronowetter, Yuki Nojiri, Michael Renger, Kirill G. Fedorov, Achim Marx, Frank Deppe, Rudolf Gross
Physical Review A **105**, 012405 (2022).

43. **Quantum Fourier Transform in Oscillating Modes**
Qi-Ming Chen, Frank Deppe, Re-Bing Wu, Luyan Sun, Yu-xi Liu, Yuki Nojiri, Stefan Pogorzalek, Michael Renger, Matti Partanen, Kirill G. Fedorov, Achim Marx, Rudolf Gross
arXiv:1912.09861, submitted for publication (2019).

44. **Dia- and Adiabatic Dynamics in a Phononic Network**
Daniel Schwienbacher, Thomas Luschmann, Rudolf Gross, Hans Huebl
arXiv:2011.08080, submitted for publication (2020).

45. **Tendencies of enhanced electronic nematicity in the Hubbard model and a comparison with Raman scattering on high-temperature superconductors**
Tianyi Liu, Daniel Jost, Brian Moritz, Edwin W. Huang, Rudi Hackl, Thomas P. Devereaux
arXiv:2101.07486, submitted for publication (2021).

46. **Mechanical frequency control in inductively coupled electromechanical systems**
Thomas Luschmann, Philip Schmidt, Frank Deppe, Achim Marx, Alvaro Sanchez, Rudolf Gross, Hans Huebl
arXiv:2104.10577, submitted for publication (2021).

47. **The scattering coefficients of superconducting microwave resonators: I. Transfer-matrix approach**
Qi-Ming Chen, Meike Pfeiffer, Matti Partanen, Florian Fesquet, Kedar E. Honasoge, Fabian Kronowetter, Yuki Nojiri, Michael Renger, Kirill G. Fedorov, Achim Marx, Frank Deppe, Rudolf Gross
arXiv:2109.07762, submitted for publication (2021).

48. **How pressure enhances the critical temperature for high temperature superconductivity in $YBa_2Cu_3O_{6+y}$**
Michael Jurkutat, Carsten Kattinger, Stefan Tsankov, Richard Reznicek, Andreas Erb, Jürgen Haase
arXiv:2109.10157, submitted for publication (2021).

49. **Aluminum nitride integration on silicon nitride photonic circuits: a new hybrid approach towards on-chip nonlinear optics**
Giulio Terrasanta, Timo Sommer, Manuel Müller, Matthias Althammer, Rudolf Gross, Menno Poot
arXiv:2110.01993, submitted for publication (2021).

50. **Quantum critical fluctuations in an Fe-based superconductor**
D. Jost, L. Peis, G. He, A. Baum, S. Geprägs, J. C. Palmstrom, M. S. Ikeda, I. R. Fisher, T. Wolf, S. Lederer, and R. Hackl

arXiv:2111.07521, submitted for publication (2021).

51. **Direct implementation of a perceptron in superconducting circuit quantum hardware**
Marek Pechal, Federico Roy, Samuel A. Wilkinson, Gian Salis, Max Werninghaus, Michael J. Hartmann, Stefan Filipp
arXiv:2111.12669, submitted for publication (2021).

52. **Influence of low-energy magnons on magnon Hanle experiments in easy-plane antiferromagnets**
Janine Gückelhorn, Akashdeep Kamra, Tobias Wimmer, Matthias Opel, Stephan Geprägs, Rudolf Gross, Hans Huebl, Matthias Althammer
arXiv:2112.03820, submitted for publication (2021).

53. **Magnetic field robust high quality factor NbTiN superconducting microwave resonators**
Manuel Müller, Thomas Luschmann, Andreas Faltermeier, Stefan Weichselbaumer, Leon Koch, Gerhard B. P. Huber, Hans Werner Schumacher, Niels Ubbelohde, David Reifert, Thomas Scheller, Frank Deppe, Achim Marx, Stefan Filipp, Matthias Althammer, Rudolf Gross, Hans Huebl
arXiv:2112.08296, submitted for publication (2021).

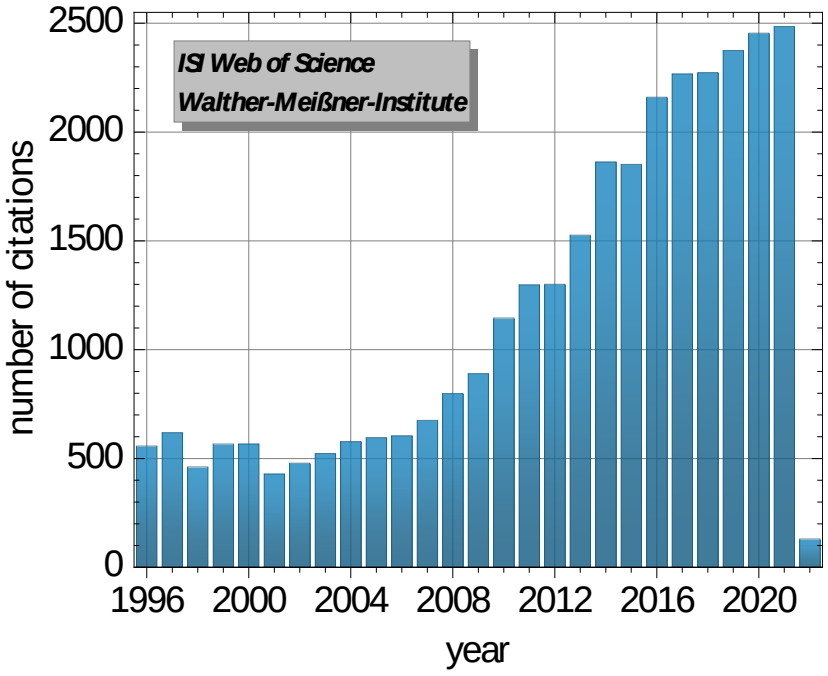

The total number of citations per year of papers published by members of WMI since 1996. This number has about quadrupled within the last twenty years and presently approaches 2 500.

Bachelor, Master, Doctoral, and Habilitation Theses

A. Completed and Ongoing Habilitation Theses

At present, three postdoctoral researchers – Matthias Althammer, Kirill Fedorov and Nadezhda Kukharchyk – pass through the habilitation procedure of the Technical University of Munich. The habilitation serves as the formal assessment tool ascertaining whether or not a candidate is suitable, from an academic and a pedagogical point of view, to be a professor in a particular field at the university level. The WMI strongly supports habilitation candidates, as the fostering of young scholars is one of its key concerns.

In 2021, Matthias Althammer has completed the habilitation procedure. After the very positive reports of the international experts and the final report of his *Fachmentorat* (Rudolf Gross, TU Munich, Martin Brandt, TU Munich, Arunava Gupta, MINT Center, University of Alabama) have been received, the Physics Department of TUM recommended his appointment as a docent in experimental physics. Only the final decision of the TUM Board of Management is still missing and expected early in 2022.

Matthias Althammer was accepted as a *"Habilitand"* in 2016. The research topic of his habilitation project was the *Experimental Study of Spin-dependent Transport Phenomena*. His research work attracts broad international interest. This is particularly true for his seminal work on the discovery and explanation of the Spin Hall Magnetoresistance (SMR). Meanwhile his publications have been cited more than 5 000 times (h-index 30, according to Google Scholar). His annual citation rate is rapidly growing and approaching 800. Regarding teaching, Matthias Althammer regularly offered the lectures on *Magnetism* and *Spin Electronics* and additionally was organizing the seminar on *Spin Currents and Skyrmionics*. We are very happy about the successful completion of the habilitation process of Matthias Althammer and wish him all the best for his future scientific career.

1. Dr. Kirill Fedorov

Kirill Fedorov presently completes his habilitation process and plans to submit his documents early in 2022. He was accepted as a habilitation candidate by the Faculty of Physics of TU Munich in September 2016 and successfully passed the midterm evaluation in 2019. In his case, Rudolf Gross (TU Munich), Jonathan Finley (TU Munich/Walter Schottky Institute) and Enrique Solano (Universidad del País Vasco and Ikerbasque Foundation, Bilbao, Spain) form the *Fachmentorat*. His key research topic is the realization of seminal quantum experiments based on propagating quantum microwaves. With the realization of quantum teleportation using propagating quantum microwaves he added a further important milestone experiment in 2021 (see K.G. Fedorov *et al.*, Science Advances 7, eabk0891 (2021)).

Kirill Fedorov studied physics in Russia (Institute for Physics of Microstructures, Russian Academy of Sciences, Nizhny Novgorod), where he received his

master degree in 2008. He then joined the group of Prof. Alexey Ustinov at the Karlsruhe Institute of Technology as a Ph.D. student. He finished his Ph.D. thesis entitled *Fluxon readout for superconducting flux qubits* in 2013 and then joined Walther-Meißner-Institute as a postdoctoral researcher in December 2013.

2. Dr. Nadezhda Kukharchyk

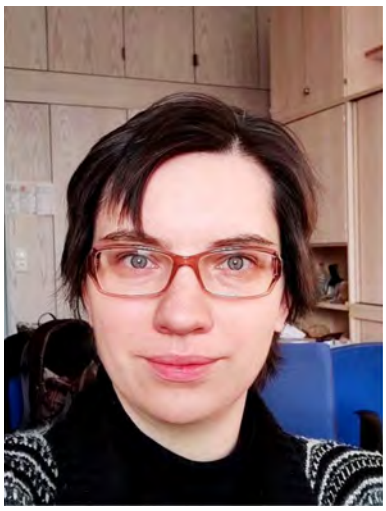

Nadezhda Kukharchyk received one of the prestigious START Fellowships of the Excellence Clusters MCQST in 2020. Supported by this fellowship, she joined WMI in November 2020 and is building up a new research group at WMI focusing on the spectroscopy and application of spin-based quantum systems. On 25th November 2021, she gave a talk on *Rare earth spin ensemble at millikelvin temperatures: development, difficulties and potential* within the Solid-State Colloquium of the TUM Physics Department to present her key research topic to the teaching body of the Faculty of Physics. After this informal step, she submitted the required documents to the dean's office and formally applied for being accepted as a habilitation candidate by the Faculty of Physics of TUM.

Nadezhda Kukharchyk studied physics at the Belarussian State University in Minsk, Belarus, and then joined the University of Bochum (group of Prof. Andreas Wieck) as a Ph.D. student in 2011. She finished her thesis entitled *Focused Ion-Beam Implantation of Rare-Earth Ions for Realisation of Spin-Ensemble Systems* in 2015. She then joined the Saarland University, where she was setting up a newly established experimental laboratory for optical and microwave spectroscopy of rare-earth doped single crystals at mK-temperatures before accepting the MCQST offer. The WMI is very happy to be able to support the scientific career of an ambitious female researcher. Meanwhile, Nadezhda Kukharchyk already acquired a new BMBF-project on the ***Storage of Microwave Quantum Tokens in Electron and Nuclear Spin Ensembles (QuaMToMe)***. She is the coordinator of this new project, which started in November 2021.

B. Completed and Ongoing Ph.D. Theses

Completed Ph.D. Theses:

1. **Untersuchung des Wärmetransports in expandiertem Perlit zur Entwicklung einer Vakuumpulverisolation für Hochtemperatur-Anwendungen bis 800°C**
   Matthias Johannes Rottmann, Technical University of Munich, Januar 2021.
2. **Coupling Phenomena in Nanomechanical Hybrid Systems**
   Daniel Schwienbacher, Technical University of Munich, March 2021.
3. **Magnon Hybrid Dynamics**
   Lukas Liensberger, Technical University of Munich, July 2021.
4. **Superconducting Wireless Power Transfer at High Power Densities for Industrial Applications and Fast Battery Charging**
   Christoph Utschick, Technical University of Munich, August 2021.
5. **Control and Manipulation of Magnonic Spin Currents in Magnetic Insulators**
   Tobias Wimmer, Technical University of Munich, November 2021.

The Ph.D. students of the Walther-Meißner-Institute finishing their Ph.D. theses in 2021. The Ph.D. defense of Peter Eder was planned for December 2021, but had to be postponed at sort notice until January 2022 due to Corona related travel restrictions.

Ongoing Ph.D. Theses:

1. **Propagating Quantum Microwave Photonics: Transmon Qubit in a Broadband On-Chip Environment**
   Peter Eder, Technical University of Munich, December 2021.
2. **In-situ Tunable Nonlinearity and Competing Signal Paths in Coupled Superconducting Resonators**
   Michael Christian Fischer, Technical University of Munich, since January 2015.
3. **ReBCO-Schichten auf ISD biaxial texturierten Substraten für supraleitende Bandleiter der 2. Generation**
   Oleksiy Troshyn, Technical University of Munich, since August 2017.
4. **Spin Wave Transport and Skyrmion Formation in CoFe-Based Thin Film Heterostructures**
   Luis Antonio Flacke, Technical University of Munich, since September 2018.
5. **Correlation Measurements in Coupled Nonlinear Resonators**
   Qiming Chen, Technical University of Munich, since October 2018.
6. **Quantum Microwave Communication**
   Michael Renger, Technical University of Munich, since November 2018.
7. **Pure Spin Currents in Epitaxial All Oxide Heterostructures**
   Janine Gückelhorn, Technical University of Munich, since March 2019.
8. **Hybride Solid State Quantum Systems**
   Thomas Luschmann, Technical University of Munich, since September 2019.
9. **Coherent Adiabatic Quantum Annealer Based on Superconducting Quantum Circuits**
   Yuki Nojiri, Technical University of Munich, since September 2019.
10. **Spin Phenomena in Superconductor/Ferromagnet Heterostructures**
    Manuel Müller, Technical University of Munich, starting from March 2020.
11. **Fabrication and Investigation of Superconducting Quantum Processors with Novel Architectures**
    Leon Koch, Technical University of Munich, since July 2020.
12. **Tailoring the Control of Superconducting Qubits to Efficiently Solve Molecular Chemistry Problems**
    Malay Singh, Technical University of Munich, since October 2020.
13. **Multi-Qubit Gates for the Efficient Exploration of Hilbert Space with Superconducting Circuits**
    Ivan Tsitsilin, Technical University of Munich, since October 2020.
14. **Microwave Photo Detection for a Quantum Radar Receiver**
    Kedar Honasoge, Technical University of Munich, since February 2021.
15. **Receiver for Quantum Microwave Radar**
    Fabian Kronowetter, Technical University of Munich, since February 2021.
16. **Remote Entanglement of Superconducting Qubits with Two-Mode Squeezing**
    Florian Fesquet, Technical University of Munich, since February 2021.
17. **Implementation of Optical Approaches in Microwave Quantum Memory Systems**
    Ana Strinic, Technical University of Munich, since April 2021.
18. **Optimal Control for High-Fidelity Qubit Operations**
    Max Werninghaus, Technical University of Munich, since May 2021 (before at IBM Re-

search - Zurich, since May 2018).

19. **Development of Quantum Devices for Travelling Wave Parametric Amplifiers**
Nicolas Arlt, Technical University of Munich, since July 2021.

20. **Josephon Travelling Wave Parametric Amplifier for Multi-qubit Readout**
Daniil Bazulin, Technical University of Munich, since August 2021.

21. **Hardware-tailored Quantumalgorithms with Superconducting Qubits**
Frederik Pfeiffer, Technical University of Munich, since November 2021.

22. **Scalable Multi-Qubit Architectures Based on Superconducting Qubits**
Niklas Glaser, Technical University of Munich, since December 2021.

23. **Scaling of Superconducting Qubit Systems for Quantum Information Processing**
Florian Wallner, Technical University of Munich, starting in January 2022.

24. **Experimental Realization of Quantum Memory Based on Phosphorous Donors in Silicon Including Storage and Retrieval of Q-Tokens**
Patrizia Oehrl, Technical University of Munich, starting in February 2022.

C. Completed and Ongoing Bachelor and Master Theses

Completed Master Theses:

1. **Disentangling Electrical and Thermal Modulations of Magnon Conductivity in Yttrium Iron Garnet**
   Emir Karadza, Master Thesis, Technical University of Munich, January 2021.
2. **Fabrication of Superconducting Thin-film Resonators and Josephson Junctions**
   Christoph Scheuer, Master Thesis, Technical University of Munich, Februar 2021.
3. **Magnetization Dynamics and Magnetic Skyrmions in Thin Film Multilayer and Hybrid Systems**
   Misbah Yaqoob, Master Thesis, Technical University of Munich, April 2021.
4. **Spin Excitations in Nanostructures**
   Korbinian Rubenbauer, Master Thesis, Technical University of Munich, Juli 2021.
5. **Scanning Tunneling Microscopy and Raman Spectroscopy in 1T-$TaSe_2$**
   Minghao Zhang, Master Thesis, Technical University of Munich, May 2021.
6. **Development of Scalable On-Chip Circuit Quantum Acoustodynamics**
   Christopher Waas, Master Thesis, Technical University of Munich, June 2021.
7. **Investigation of the Amplitude of the Spin Hall Magnetoresistance in Antiferromagnetic FeO**
   Mayank Sharma, Master Thesis, Indian Institute of Technology Madras and Technische Universität München, June 2021.
8. **Charge and Spin Wave Transport in Hybrid Magnetic Multilayers**
   Elisabeth Meidinger, Master Thesis, Technical University of Munich, July 2021.
9. **Optimal Control of Entangling Gates in Superconducting Tunable-Coupler Architectures**
   Niklas Glaser, Master Thesis, Technical University of Munich, November 2021.
10. **Designing superconducting qubit chips and multi-qubit couplers**
    Gerhard Huber, Master Thesis, Technical University of Munich, November 2021.
11. **Development of a Fabrication Process for High-Coherence Niobium Qubits**
    Niklas Bruckmoser, Master Thesis, Technical University of Munich, November 2021.
12. **Vertical Pt/$Y_3Fe_5O_{12}$/Pt Heterostructures for Magnon Mediated Magnetoresistance Measurements**
    Philipp Schwenke, Master Thesis, Technical University of Munich, November 2021.
13. **Magnetism and Geometrical Frustration in Archimedean Lattices**
    Ramona Melinda Stumberger, Master Thesis, Technical University of Munich, December 2021.
14. **Tuning the Amplitude of the Spin Hall Magnetoresistance**
    Monika Scheufele, Master Thesis, Technical University of Munich, December 2021.

Completed Bachelor Theses:

1. **Simulation of Multi-Body Coupler for Lechner-Hauke-Zoller Quantum Annealing Architecture**
   Aristo Kevin Ardyaneira P, Technical University of Munich (2021).
2. **Fabrication of Low-Loss Josephson Junctions for Quantum Devices**

Patrick Missale, Technical University of Munich (2021).

3. **Electro-magnetic Simulation of Transmission Line-Based Designs of RE-doped YSO Crystals for Optimized Spin Ensemble to Microwave Coupling**
   Noah Weinhold, Technical University of Munich (2021).
4. **Qubit Gates and Crosstalk Mitigation Pulses in the Presence of Local Oscillator Phase Instabilities**
   Alexander Orlov, Technical University of Munich (2021).
5. **Control of Qubit-Qubit Coupling Strength by a Microwave Driven Coupler Element**
   Lukas Vetter, Technical University of Munich (2021).
6. **Shaping Microwave Signals for Qubit Control**
   Florian Maier, Technical University of Munich (2021).
7. **Superconducting Spintronics with Magnetic Insulators**
   Vincent Haueise, Technical University of Munich (2021).

Ongoing Master Theses:

1. **Optimization of Aluminum Thin Films and Fabrication of Superconducting Qubit Systems**
   Leonhard Hölscher, Master Thesis, Technical University of Munich, since November 2020.
2. **Towards Single-Shot Microwave Quantum Key Distribution**
   Philipp Krüger, Master Thesis, Technical University of Munich, since March 2021.
3. **Controlling the Environment of Superconducting Qubits**
   Johannes Schirk, Master Thesis, Technical University of Munich, since March 2021.
4. **Controlling Magnon Transport in Antiferromagnetic Insulators**
   Matthias Grammer, Technical University of Munich, since June 2021.
5. **Pulse Optimization for Qutritts and a Function Approximator using Quantum Machine Learning**
   Shawn Storm, Master Thesis, Technical University of Munich, since August 2021.
6. **Entanglement Distribution via a Thermal Microwave Link**
   Wun Kwan Yam, Technical University of Munich, since September 2021.
7. **Fabrication of High-Coherence Superconducting Qubits**
   David Cole Bunch, Master Thesis, Technical University of Munich, since October 2021.
8. **Improving Multiplexed Readout of Superconducting Qubits**
   Michal Cherczynski, Master Thesis, Technical University of Munich, since November 2021.
9. **Scaling and 3D integration of Superconducting Qubit Devices**
   Tammo Sievers, Master Thesis, Technical University of Munich, since December 2021.
10. **Elektrischer Spin-Transport in Supraleiter/Ferromagnetischer Isolator Heterostrukturen / All-electrical spin transport in Superconductor/Ferromagnetic Insulator Heterstructures**
    Yuhao Sun, Technical University of Munich, since December 2021.
11. **Akustische Quantenschaltkreise / Quantum Acoustics in the Giant Atom Limit**
    Alexander Jung, Technical University of Munich, since December 2021.
12. **Clamped and Levitating Superconductors for Nanoelectromechanics**

Lukas Niekamp, Technical University of Munich, starting in January 2022.

13. **Fabrication of GdN Ferromagnetic Thin Films**
Raphael Höpfl, Technical University of Munich, starting in March 2022.

14. **Manipulation von Magnontransport mittels Mikrowellen**
Franz Weidenhiller, Technical University of Munich, starting in April 2022.

Research Projects

A large number of our research projects are benefiting from the collaboration with other research institutions and industry in coordinated research projects, as well as from individual collaborations, exchange programs and visitors. Most collaborations are based on joint projects, which are funded by different funding agencies (see list below). A considerable number of collaborations also exists with universities, other research institutions and industry without direct financial support.

A. German Research Foundation: Excellence Initiative & Strategy

Cluster of Excellence «*Munich Center for Quantum Science and Technology*» *(MCQST)*

The new Cluster of Excellence has been granted in September 2018 within Germany's Excellence Strategy and started in January 2019. Together with Immanuel Bloch of LMU Munich and Ignacio Cirac of Max Planck Institute of Quantum Optics, Rudolf Gross of Walther-Meißner-Institute is one of the three spokespersons of MCQST and coordinator of the Research Unit C on Quantum Computing.

1. Research Unit C: *Quantum Computing*
   Principal Investigators: F. Deppe, S. Filipp, R. Gross
   Contributing Researchers: K. Fedorov, A. Marx, M. Partanen
2. Research Unit D: *Quantum Communication*
   Principal Investigators: F. Deppe, S. Filipp, R. Gross
   Contributing Researchers: K. Fedorov, A. Marx, M. Partanen
3. Research Unit E: *Quantum Sensing*
   Principal Investigators: F. Deppe, H. Hübl, R. Gross
   Contributing Researchers: K. Fedorov, A. Marx
4. Research Unit F: *Quantum Matter*
   Principal Investigators: H. Hübl, R. Gross
   Contributing Researchers: M. Althammer, S. Geprägs, M. Weiler

B. German Research Foundation: Collaborative Research Centers

Transregional Collaborative Research Center TRR 80: ***«From Electronic Correlations to Functionality»***

1. Project A2: *Spatially and Momentum Resolved Raman Studies of Correlated Systems*
   Principal Investigator: R. Hackl

C. German Research Foundation: Priority Programs

1. Spin Dynamics of Hybrid Skyrmion-Magnon Solitons
   within the DFG Priority Program 2137 *Skyrmionics: Topological Spin Phenomena in Real-Space for Applications*
   M. Weiler, R. Gross (Az. WE 5386/5-1)

D. German Research Foundation: Research Projects

1. *Shortcuts to Adiabaticity for Quantum Computation and Simulation (STAQS)*, project within the QuantERA II ERA-NET Cofund in Quantum Technologies.
   F. Deppe, with K. Fedorov, R. Gross, A. Marx (Az. DE 3444/1-1)
2. Project: *Evolution of the Charge Carrier Properties and Electronic Correlations in Layered Organic Metals near the Mott Metal-Insulator Transition*, joint German-Russian project proposal within the RFBR-DFG Cooperation.
   M. Kartsovnik, R. Gross (Az. KA 1652/5-1 and GR 1132/19-1)
3. Project: *Multi-qubit Gates for the Efficient Exploration of Hilbert Space with Superconducting Qubit Systems*
   S. Filipp (Az. FI 2549/1-1)
4. Project: *Fluctuations and Novel Phases in Systems with Spin, Charge and Orbital Correlations*
   R. Hackl (Az. HA 2071/12-1)
5. Project: *Pure Spin Currents in Oxide-Based Epitaxial Heterostructures*
   M. Althammer, R. Gross (Az. AL 2110/12-1)
6. Project: *Direct and Inverse Spin-Orbit Torques*
   M. Weiler (Az. WE 5386/14-1)

E. European Union

1. EU Collaborative Project (call identifier H2020-FETFLAG-2018-2020), project title: *Quantum Microwave Communication and Sensing – QMiCS*
   F. Deppe, K. Fedorov, A. Marx, R. Gross, Grant Agreement No. 820505
   project coordination: Walther-Meißner-Institute, partners: several European Universities, research facilities and companies.
2. EU Collaborative Project (call identifier H2020-FETOPEN-FET H2020-FETOPEN-2018-2020), project title: *Neuromorphic Quantum Computing - Quromorphic*
   S. Filipp, Grant Agreement No. 828826
   partners: several European Universities and research facilities.
3. EU Innovative Training Network (call identifier H2020-MSCA-ITN-2020), project title: *MOlecular Quantum Simulations - MOQS*
   S. Filipp, Grant Agreement No. 955479
   partners: several European Universities and research facilities.
4. EU MSCA Cofund Action (call identifier H2020-MSCA-COFUND-2018), project title: *Quantum Science and Technologies at the European Campus (QUSTEC)*
   S. Filipp, Grant Agreement 847471
   partners: several European Universities and research facilities.
5. EU Collaborative Project (call identifier H2020-FETOPEN-1-2016-2017), project title: *Magnetomechanical Platforms for Quantum Experiments and Quantum Enabled Sensing Technologies – MaQSens*
   H. Huebl, R. Gross, Grant Agreement No. 736943
   partners: several European Universities and research facilities.

F. Bundesminister für Bildung, Wissenschaft, Forschung und Technologie

1. Coordinated Project: *Munich Quantum Valley Quantum Computer Demonstrators - Superconducting Qubits (MUNIQC-SC)*, project number: 13N16188

project part: *Systemoptimierung und -integration*
project coordinator: S. Filipp (WMI)
principal investigators of WMI: R. Gross, H. Hübl, A. Marx
project partners: TUM, Fraunhofer-Gesellschaft, FAU Erlangen-Nürnberg, Infineon Technologies AG, IHP GmbH - Innovations for High Performance Microelectronics/Leibniz-Institut für innovative Mikroelektronik, IQM Germany GmbH, kiutra GmbH, Parity Quantum Computing Germany GmbH, Forschungszentrum Jülich GmbH, Zurich Instruments Germany GmbH.
project period: 01/2022 – 12/2026

2. Coordinated Project: *Storage of Microwave Quantum Tokens in Electron and Nuclear Spin Ensembles (QuaMToMe)*, project number: 16KISQ036
project coordinator: N. Kukharchyk (WMI)
principal investigators of WMI: K. Fedorov, R. Gross, H. Huebl, N. Kukharchyk.
project period: 11/2021 – 10/2024
3. Coordinated Project: *QUAntenRAdarTEam (QUARATE)*, project number: 13N15380,
project part: *Superconducting Circuits and Quantum Microwaves for Quantum Radar*,
project coordinator: Rohde & Schwarz GmbH & Co. KG,
principal investigators of WMI: F. Deppe, K. Fedorov, S. Filipp, R. Gross, A. Marx),
project partners: German Aerospace Center (DLR), Technical University of Munich
project period: 02/2021 – 01/2024
4. Coordinated Project: *German Quantum Computer based on Superconducting Qubits (GeQCoS)*, project number: 13N15680
project part: *Scaling and Demonstrator*,
project coordinator: S. Filipp (WMI)
principal investigators of WMI: F. Deppe, K. Fedorov, R. Gross, A. Marx
project partners: Forschungszentrum Jülich GmbH, Karlsruher Institut für Technologie, Friedrich-Alexander-Universität Erlangen-Nürnberg, Fraunhofer Gesellschaft zur Forderung der angewandten Forschung e.V, Infineon Technologies AG.
project period: 02/2021 – 01/2025

G. Free State of Bavaria

1. Munich Quantum Valley (MQV)
project part: Quantum Technology Park and Entrepreneurship (QTPE)
Principal Investigators at WMI: R. Gross (coordination), S. Filipp, K. Fedorov, R. Gross, A. Marx, H. Hübl
Jointly with research groups at the Technical University of Munich, the LMU Munich, the FAU Erlangen, the Max Planck Institute of Quantum Optics, and the Fraunhofer-Gesellschaft zur Förderung der angewandten Forschung e.V.
project period: 10/2021–09/2026
2. Munich Quantum Valley (MQV)
project part: Superconducting Qubit Quantum Computing (SQQC)
Principal Investigators at WMI: S. Filipp (coordination), K. Fedorov, R. Gross, A. Marx, H. Hübl
Jointly with research groups at the Technical University of Munich, the LMU Munich, the FAU Erlangen, the Max Planck Institute of Quantum Optics, and the Fraunhofer-Gesellschaft zur Förderung der angewandten Forschung e.V.
project period: 10/2021–09/2026
3. International PhD Programme of Excellence *Exploring Quantum Matter (ExQM)* within the Elite Network of Bavaria, Project No. K-NW-2013-231,

R. Gross, A. Marx, F. Deppe, K. Fedorov,
jointly with 12 quantum physics research groups at the TU Munich, the LMU Munich, and the Max Planck Institute of Quantum Optics.
project period: 06/2014–05/2022

H. Max Planck Society

1. International Max Plank Research School for *Quantum Science and Technology (IMPRS-QST)*, spokesperson: Prof. Dr. J. Ignacio Cirac,
R. Gross, A. Marx, F. Deppe, K. Fedorov,
with several partners from the Max Planck Institute of Quantum Optics, the Ludwig-Maximilians-Universität Munich and the Technical University of Munich.
project period: 03/2016– 02/2028

I. German Academic Exchange Service

1. Project-based Personnel Exchange Programme (PPP) with Serbia, project 57449106: *Fluctuations, Magnetic Frustration, and Sub-Dominant Pairing in Fe-Based Compounds*, collaboration with the Institute of Physics, University of Belgrade (Dr. Z. V. Popovic),
R. Hackl
2. Project-based Personnel Exchange Programme (PPP) with India, project 57452943: *Spin Current Transport Across Antiferromagnetic/Metallic Oxide Interfaces*, collaboration with the IIT Madras, Chennai (Prof. Dr. M. S. Ramachandra Rao),
R. Gross

J. Scientific Instrumentation

1. UHV PLD-MBE System, DCA Instruments,
(R. Gross, DFG, Excellence Strategy, EXC-2111-390814868)
2. Tieftemperatur-Mikrowellenmessapparatur für schnellen Probenaustausch
(S. Filipp, DFG-GZ: INST 95/1636-1 FUGG)
3. Heliumverflüssigungsanlage, Vorbuchner VL 100
(R. Gross, DFG-GZ: INST 95/1637-1 LAGG)
4. Cryogen-Free Dilution Refrigerator System with Microwave Measurement Systems, Bluefors Model BF-XLD 400,
(S. Filipp, DFG-GZ: INST 95/1623-1 FUGG)

Conferences, Workshops, Public Engagement

Every year the Walther-Meißner-Institute organizes/co-organizes conferences, workshops, symposia, seminars and other events. It also participates in several public outreach events aiming at making science accessible to the public. For example, Stefan Filipp was organizing the 737th WE-Heraeus-Seminar on *Advances in Scalable Hardware Platforms for Quantum Computing* from 11 – 13 January 2021 at Bad Honnef together with Andreas Fuhrer, IBM Zurich, Frank Willhelm-Mauch, Forschungszentrum Jülich GmbH, and Maud Vinet, CEA-Grenoble. Rudolf Gross was contributing to the Münchener Wissenschaftstage, taking place from 08 – 10 Oktober 2021 at the Deutsches Museum Verkehrszentrum with a public lecture on quantum computing. Matthias Opel was contributing to a public event at the Humboldt-Gymnasium Vaterstetten with a talk and live experiments to mention just a few.

In previous years we were reporting in more depth on events and outreach activities in our Annual Report. However, meanwhile these topics are well covered by our new web pages which went online in 2021. The same is true for press releases on highlight publications and other important developments. Therefore, we are no longer covering these topics here in depth and refer the interested reader to the news section of our web pages: https://www.wmi.badw.de/news.

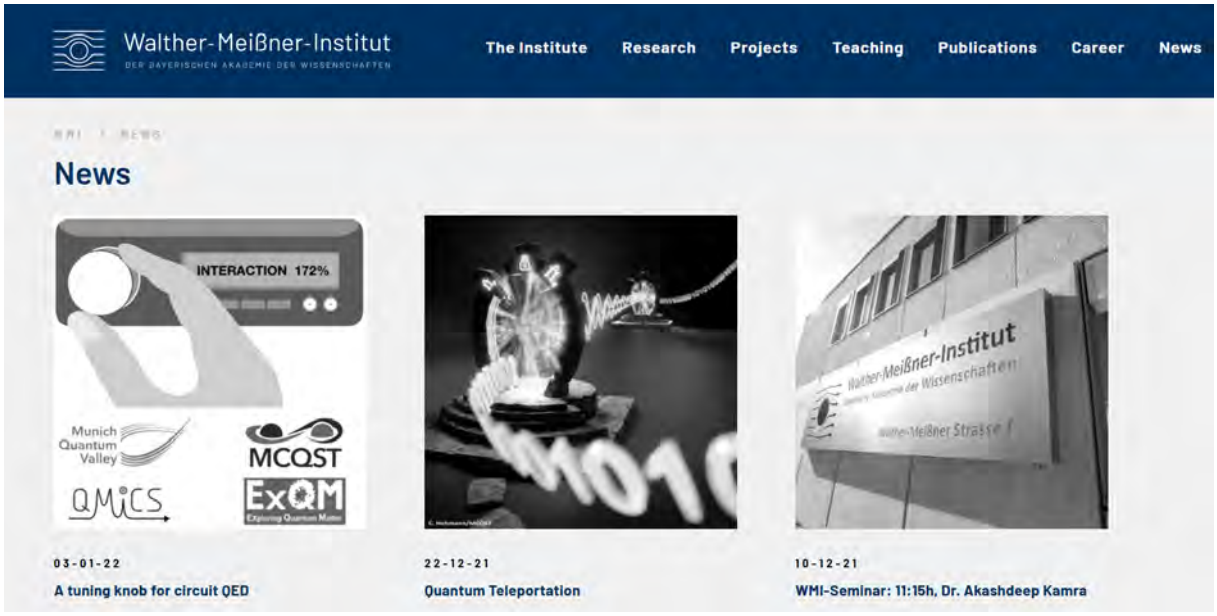

Cooperations

The Walther-Meißner-Institute is involved in many collaborations also without any direct project funding. In the following we list the most relevant collaboration partners:

- IBM Research - Zurich, Zurich, Switzerland (A. Fuhrer, D. Egger, G. Salis)
- Green Innovation Research Laboratories, NEC Corporation, Japan (J.S. Tsai, K. Inomata, T. Yamamoto)
- Forschungszentrum Jülich (P. Bushev, F.K. Wilhelm-Mauch, D. DiVincenzo)
- University of Tokyo, Tokyo, Japan (Y. Nakamura)
- ETH-Zurich, Switzerland (C. Eichler, A. Wallraff, L. Degiorgi, R. Monnier, Dr. M. Lavagnini)
- Chalmers University of Technology Gothenburg, Sweden (J. Bylander, P. Delsing, G. Wendin)
- Stanford University, Stanford, USA (T.P. Devereaux, I. Fisher, B. Moritz, H.N. Ruiz, S.A. Kivelson)
- Universidad del País Vasco and Ikerbasque Foundation, Bilbao, Spain (E. Solano, M. Sanz, L. Lamata)
- Instituto de Física Fundamental, CSIC, Madrid, Spain (J.J. Garcia-Ripoll)
- Instituto de Ciencia de Materials de Barcelona, CSIC, Spain (E. Canadell)
- University of Tohoku, Sendai, Japan (G.E.W. Bauer, E. Saitoh, J. Barker)
- Japan Science and Technology Agency, Sendai, Japan (H. Adachi, S. Maekawa)
- Osaka Prefecture University, Osaka, Japan (H. Fujiwara)
- University of Chinese Academy of Science, Beijing, China (D. Li, P.P. Shen, X.L. Dong, Z.X. Zhao)
- European Synchrotron Radiation Facility (ESRF), Grenoble (H. Müller, F. Wilhelm, K. Ollefs, A. Rogalev)
- Lund University, Lund, Sweden (D. Mannix)
- Materials Science Research Centre, IIT Madras, India (M.S. Ramachandra Rao, J. Mukherjee, T.S. Suraj)
- University of Geneva, Geneva, Switzerland (I. Maggio-Aprile)
- University of Alabama, MINT Center, Tuscaloosa, USA (A. Gupta)
- Helsinki University of Technology, Materials Physics Laboratory, Finland (T. Heikkilä)
- Delft University of Technology, Kavli Institute of NanoScience, Delft, The Netherlands (T.M. Klapwijk, G.E.W. Bauer)
- B. Verkin Institute for Low Temperature Research and Engineering, Kharkov, Ukraine (V.G. Peschansky)
- Landau Institute for Theoretical Physics, Chernogolovka, Russia (P. Grigoriev)
- University of Oxford, Clarendon Laboratory, England (A. Karenowska)
- Institute of Solid State Physics, Chernogolovka, Russia (V. Zverev)
- Russian Academy of Sciences, Chernogolovka, Russia (N. Kushch, E. Yagubskii)
- High Magnetic Field Laboratory, Dresden (E. Kampert, J. Wosnitza, T. Helm)
- High-Magnetic-Field Laboratory, Grenoble, France (I. Sheikin, D. LeBoeuf)
- High Magnetic Field Laboratory, Toulouse, France (C. Proust, D. Vignolles)
- National High Magnetic Field Laboratory, Tallahassee, USA (J. Brooks)

- University of British Columbia, Vancouver, Canada (D. Bonn, A. Damascelli)
- Université de Toulouse, Laboratoire de Physique Théorique, Toulouse, France (R. Ramazashvili)
- Lawrence Berkeley National Laboratory, Berkeley, USA (A. F. Kemper)
- University of Belgrade, Belgrade, Serbia (Z. Popovic, N. Lazarevic, D. U. Ralevic, R. Gajic)
- University of Aveiro, Portugal (N. A. Sobolev)
- Macquarie University, MQ Research Centre for Quantum Science and Technology, Australia (J. Twamley)
- Hungarian Academy of Sciences, Research Institute for Solid State Physics and Optics, Budapest, Hungary (I. Tüttö)
- University of Rome "La Sapienza", Rome, Italy (S. Caprara, C. Di Castro, M. Grilli)
- Budapest University of Technology and Economics, Budapest, Hungary (A. Virosztek, G. Mihály)
- EPFL Lausanne, Switzerland (T. Kippenberg, H. Ronnov)
- University of New South Wales, Sydney, Australia (M. Simmons, A. Morello, J. Pla)
- University of Vienna, Austria (M. Aspelmeyer, S. Rotter)
- University of Innsbruck, Austria (G. Kirchmair)
- National Institute of Standards and Technology, Boulder, USA (H. Nembach, J. Shaw, T.J. Silva, E. Edwards)
- University of Florida, Gainesville, Florida, USA (P.J. Hirschfeld, S. Maiti)
- University of California, Santa Barbara, USA (D.J. Scalapino)
- University of Manitoba, Winnipeg, Canada (C.-M. Hu)
- Kyoto University, Japan (M. Shiraishi)
- IFIMAC and Departamento de Física Teórica de la Materia Condensada, Universidad Autónoma de Madrid, Spain (A. Kamra)
- Universität Erlangen-Nürnberg (M. Hartmann, F. Marquardt)
- Universidad Nacional de Colombia, Colombia (O. Moran)
- University of Birmingham, UK (E.M. Forgan)
- University of Groningen, The Netherlands (T. Palstra, M. Mostovoy, A. Aqeel)
- IFW Dresden, Germany (B. Büchner, J. Fink, S.V. Borisenko, M. Knupfer, A. Thomas)
- Max-Planck-Institut für Festkörperforschung, Stuttgart (B. Keimer, L. Boeri)
- Max-Planck-Institute for the Science of Light, Erlangen (S. Viola-Kusminsky)
- University of Tübingen, Germany (R. Kleiner, D. Kölle)
- University of Würzburg, Germany (W. Hanke, R. Thomale)
- University of Augsburg, Germany (A. Wixforth, A. Kampf, J. Deisenhofer, V. Tsurkan)
- University of Leipzig, Germany (J. Haase)
- Ernst-Moritz-Arndt Universität Greifswald, Germany (M. Münzenberg)
- Martin-Luther-Universität Halle, Germany (G. Woltersdorf, G. Schmidt)
- Universität Bielefeld, Germany (G. Reiss, T. Kuschel M. Meinert)
- Aalto University, Aalto, Finland (R. Di Candia)
- Technical University of Munich, Physics Department, Germany (Ch. Back, P. Böni, Ch. Pfleiderer, M. Poot, F.C. Simmel, P. Müller-Buschbaum)
- Technical University of Munich, Walter Schottky Institute, Germany (M. Stutzmann, J.

Finley, M. Brandt, A. Holleitner)

- Technical University of Munich, Electrical Engineering (M. Becherer, W. Utschick, E. Weig)
- LMU Munich, Physics Department, Germany (J. von Delft, E. Frey, J. Rädler, A. Högele)
- LMU Munich, Chemistry Department, Germany (H. Ebert, D. Ködderitzsch)
- University of Konstanz (A. Leitenstorfer, E. Weig, J. Demsar, A. Pashkin, W. Belzig)
- Jülich Centre for Neutron Science JCNS, Garching, Germany (S. Pütter)
- Goethe University, Frankfurt, Germany (S. Winter, M. Lang)
- Technical University of Braunschweig, Germany (D. Menzel, S. Süllow)
- Technical University of Dresden, Germany (S.T.B. Gönnenwein)
- Fritz Haber Institut Berlin, Germany (T. Seifert, T. Kampfrath)
- Technical University of Dortmund, Germany (M. Müller)
- Johannes-Gutenberg University, Mainz, Germany (C. Cramer, M. Kläui, O. Gomomay)
- Universität Potsdam, Potsdam, Germany (A.v. Reppert, M. Bargheer)
- Infineon AG, Munich, Germany (F. Brandl, S. Luber)
- Rohde & Schwarz GmbH, Munich, Germany (B. Guezelarslan, C. Dille, K. Glas, G. Hechtfischer)
- BMW Group, Munich, Germany (J. Klepsch, A. Luckow, W. Stadlbauer, G. Steinhoff)
- Attocube, Munich, Germany (K. Karrai, D. Andres, E. Hoffmann)
- THEVA Dünnschichttechnik, Ismaning, Germany (W. Prusseit)
- Innovent Technologieentwicklung Jena, Germany (C. Dubs, O. Surzhenko)

Stays abroad

Also in 2021, extended visits of members of the Walther-Meißner-Institute at foreign research laboratories have been significantly reduced due to the Covid-19 pandemic.

1. **Stephan Geprägs**
   European Synchrotron Radiation Facility (ESRF), Grenoble, France
   01. 12. - 06. 12. 2021
2. **Mark Kartsovnik**
   Laboratoire National des Champs Magnétiques Intenses (LNCMI), Grenoble, France
   30. 11. - 15. 12. 2021
3. **Rudi Hackl**
   Institute of Physics, University of Belgrade, Serbia
   03. 11. - 15. 11. 2021

Conference Talks and Seminar Lectures

Matthias Althammer

1. **Observation of Antiferromagnetic Magnon Pseudospin Dynamics and the Magnon Hanle effect**
   Invited Online Talk, Organization of the 736. WE Heraeus Seminar, Bad Honnef, Germany
   06. - 08. 01. 2021
2. **Pure Spin Currents in Antiferromagnetic Insulators: Observation of the Magnon Hanle Effect**
   Invited Online Talk, Special Seminar, Technical University, Dresden, Germany
   26. 03. 2021
3. **Spin Angular Momentum Transport: Spin Waves Pushing New Frontiers**
   Online Talk, Intermag 2021, Lyon, France
   26. - 30. 04. 2021
4. **Temperature-dependent Spin-Transport and Current-Induced Torques in Superconductor/Ferromagnet Heterostructures**
   Online Talk, Nanoengineered Superconductors NES21, University of Vienna, Austria
   10. - 12. 05. 2021
5. **Potentials for NVs Sensing Magnetic Phases, Textures and Excitations**
   Online Talk, Organisation of Symposium at the DPG-Meeting SKM 2021
   27. 09. - 01. 10. 2021

Frank Deppe

1. **Microwave Quantum Teleportation**
   Invited Online Talk, Workshop on Entanglement Assisted Communication Networks, Technical University of Munich
   11. 03. 2021
2. **Towards Quantum Local Area Networks (QLANs) with Microwaves**
   Invited Online Presentation, Webinar, Quantum Internet
   23. 03. 2021
3. **Microwave Quantum Teleportation**
   Invited Online Seminar Talk, University of Glasgow for Quantum Technology
   26. 04. 2021
4. **Towards Quantum Local Area Networks (QLANs) with Microwaves**
   Invited Online Video Presentation, Rohde & Schwarz International Developers Conference 2021
   12. 05. 2021
5. **Progress on Quantum Microwaves for Communication and Sensing (QMICS)**
   Online Presentation, European Quantum Technology Conference 2021
   30. 11. 2021

Kirill Federov

1. **Continuous-Variable Quantum Information Precessing with Superconducting Circuits**
   Invited Online Talk, ICQT Workshop
   19. - 22. 07. 2021

Stefan Filipp

1. **Quantum Science and Technology in Munich**
   Invited Online Talk, Quantum Hackathon – Qiskit Fall Fest
   23. 11. 2021
2. **Munich Quantum Valley**
   Presentation and Panel Discussion, MikroSystemTechnik Kongress 2021, Stuttgart, Germany
   10. 11. 2021
3. **Quantum Computing**
   Online Panel Discussion, Infineon University Evening
   14. 10. 2021

4. **German Roadmap in Quantum Technology**
   Invited Online Talk, Quantum Industry Day in Switzerland
   05. 10. 2021
5. **Getting the Quantum Advantage on the Road**
   Panel Discussion, BMW Reclaim the Future, Munich
   15. 07. 2021
6. **Controlling Superconducting Quantum Circuits for Quantum Computing**
   Invited Online Talk, QUANTUM Seminar, University Mainz
   15. 07. 2021
7. **Quantensprung – Transfer von der Forschung in die Wirtschaft**
   Panel Discussion, Bayerische Akademie der Wissenschaften, Munich
   01. 07. 2021
8. **Munich Quantum Valley**
   Invited Talk, LASER World of Photonics, Munich
   24. 06. 2021
9. **Controlling Superconducting Quantum Circuits for Quantum Computing And Simulation**
   Invited Online Talk, Physics Colloquium Leipzig
   01. 06. 2021
10. **Quantum Computing: Solving computationally hard problems**
    Invited Online Talk, bidt Colloquium
    23.03.2021
11. **Quantencomputing with Superconducting Qubits: Technology and Challenges**
    Invited Online Seminar Talk, Fraunhofer EMFT
    16. 02. 2021
12. **Quantencomputing with Focus on Superconducting Qubits**
    Invited Online Talk, Helmholtz Quantum Workshop
    12. 02. 2021
13. **Quantum Computing Roadmap – Academic Perspective**
    Invited Online Talk, Quantum Industry Group Meeting
    27. 01. 2021

Rudolf Gross

1. **Quantum Technology**
   Invited Talk, Online, Rohde & Schwarz International Developers Conference.
   07. 05. 2021
2. **Quantum Computing**
   R. Gross
   Invited Tutorial, Online, MCQST Summer Student Program.
   14. 07. 2021
3. **Quantum Computing with Superconducting Circuits: Part I**
   Invited Tutorial, Study Week, University of Regensburg.
   30. 08. 2021
4. **Quantum Computing with Superconducting Circuits: Part II**
   Invited Tutorial, Study Week, University of Regensburg.
   31. 08. 2021
5. **Quantum Computing with Superconducting Circuits: Part III**
   Invited Tutorial, Study Week, University of Regensburg.
   02. 09. 2021
6. **Was machen eigentlich Quantencomputer?**
   Invited Talk, FORSCHA Münchener Wissenschaftstage, Deutsches Museum Verkehrszentrum.
   10. 10. 2021

Hans Hübl

1. **Hybrid Systems: Spins, Strings, and Superconducting Circuits**
   Invited Online Talk, Karlsruher Institut für Technologie, Karlsruhe, Germany

17. 03. 2021

2. **Hybrid Quantum Systems based on Superconducting Circuits**
   Invited Online Talk, Universität Konstanz, Konstanz, Germany
   17. 06. 2021
3. **Spin-based hybrid systems**
   Invited Online Talk, Universität Halle-Wittenberg, Germany
   02. 07. 2021
4. **Boosting Coupling Rates in Nano-Electromechanics**
   Invited Online Talk, 722. WE-Heraeus Seminar, Bad Honnef, Germany
   13. - 16. 12. 2021

Mark Kartsovnik

1. **Layered Organic Metals in High Magnetic Fields**
   Invited Talk, University of Lisbon, Lisbon, Portugal
   15. 11. 2021

Thomas Luschmann

1. **Mechanical Frequency Control in Inductively Coupled Electromechanical Systems**
   Invited Talk, Young Investigators Workshop Nanoengineering Superconductors – NES21, University of Vienna, Vienna, Austria
   12. 05. 2021
2. **Inductively Coupled Electromechanics Based on a Mechanically Compliant SQUID**
   Invited Online Talk, Symposium of the CRC 910: Going beyond weak coupling: nonlinear magnetomechnanics
   26. 11. 2021

Manuel Müller

1. **Temperature-dependent Spin-Transport and Current-Induced Torques in Superconductor/Ferromagnet Heterostructures**
   Online Talk, APS March Meeting 2021
   19. 03. 2021
2. **Temperature-Dependent Spin-Transport and Current-Induced Torques in Superconductor/Ferromagnet Heterostructures**
   Online Talk, DPG-Tagung der Sektion Kondensierte Materie (SKM)
   30. 09. 2021

Matthias Opel

1. **Spin Hall Magnetoresistance in Antiferromagnetic Insulators**
   Invited Online Talk, 6th International Conference on Nanoscience and Nanotechnology (ICONN 2021), SRM Institute of Science and Nanotechnolgy, Kattankulathur, India
   01. - 03. 02. 2021
2. **Tiefe Temperaturen, Supraleitung und Spinelektronik**
   Invited Online Talk, MINT-Berufsinformationstag im Rahmen der Humboldt Academy of Science and Engineering, Humboldt-Gymnasium Vaterstetten, Germany
   21. 05. 2021
3. **Magnonic Hanle Effect and Spin-Nernst Effect in Antiferromagnetic α-Fe_2O_3/Pt**
   27th International Workshop on Oxide Electronics, Genoa, Italy
   13. - 15. 10. 2021
4. **Spin Hall Magnetoresistance and Magnon Transport in Antiferromagnetic Oxides**
   Invited Online Talk, Indian Institute of Technology Madras, Chennai, India
   20. - 23. 12. 2021

Frederico Roy

1. **Implementation of a CCPhase-Gate by Refocusing Three-Body Interactions**
   Quantum Control in Quantum Technologies 2021, Obergurgl, Austria
   06. 10. 2021

Max Werninghaus

1. **Optimal Control of Superconducting Qubits**
   Invited Online Talk, Munich Conference on Quantum Science and Technology (MCQST 2021)
   19. 07. 2021

Honors and Awards

A. Best Presentation and Poster Awards

Most of our Ph.D. and master students give several oral and poster presentations at national and international conferences over the year. We are very happy that they are regularly receiving awards for their presentations. In 2021, Philipp Krüger of WMI has been awarded a Best Poster Prize for his excellent poster contribution on *Microwave Quantum Key Distribution in a Noisy Environment* presented at the International Conference on Quantum Science & Technology organized by the Excellence Cluster MCQST.

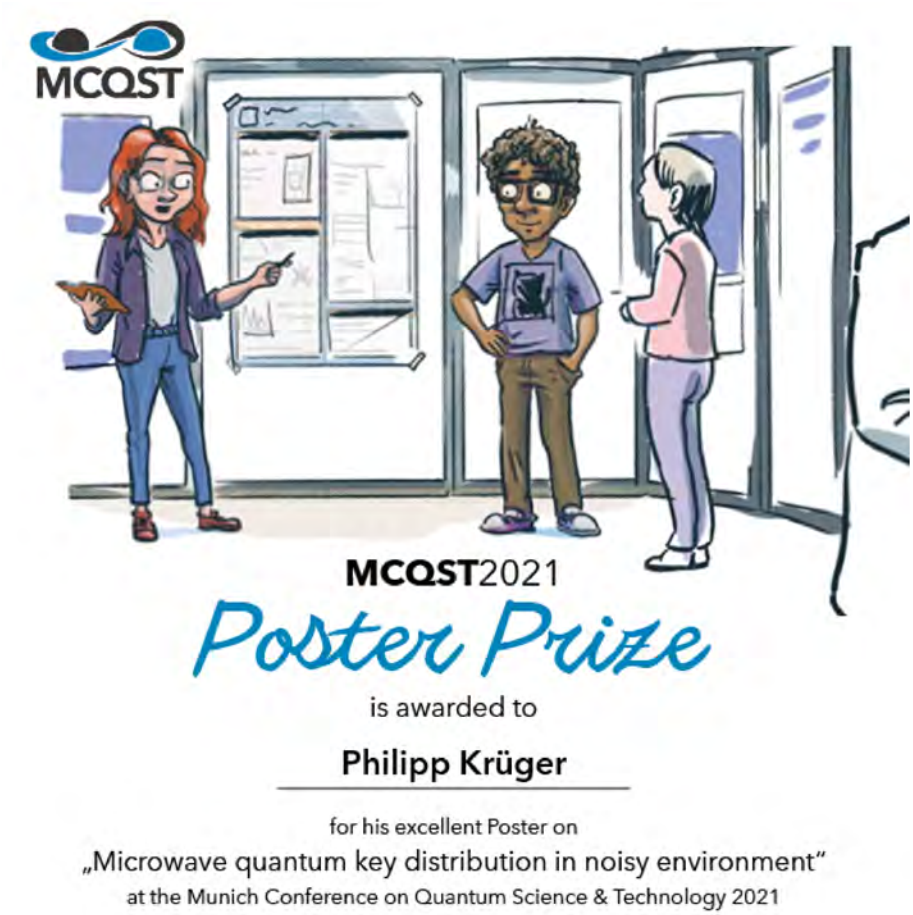

The Best Poster Award has been handed over within the Award Ceremony Session on 23 July 2021 together with a prize money donated by Menlo Systems GmbH.

Membership in Advisory Boards, Committees, etc.

1. **Frank Deppe** is Coordinator of the European Quantum Technology Flagship Project *Quantum Microwaves for Communication and Sensing (QMiCS)*.
2. **Frank Deppe** is member and principal investigator of the Cluster of Excellence *Munich Center for Quantum Science and Technology (MCQST)*.
3. **Andreas Erb** is spokesmen of the *Arbeitskreis Intermetallische und oxydische Systeme mit Spin- und Ladungskorrelationen* of the *Deutsche Gesellschaft für Kristallzüchtung und Kristallwachstum (DGKK)*.
4. **Stefan Filipp** is advisory board member of the *International AIQT Foundation*.
5. **Stefan Filipp** is member of the *BMBF Programmausschuss Quantensysteme*.
6. **Stefan Filipp** is member of the scientific advisory board of the EU FET Open project *AVAQUS - Annealing based Variational Quantum Processors*.
7. **Stefan Filipp** is member of the scientific advisory board of the *Wallenberg Center for Quantum Technology*.
8. **Stefan Filipp** is editorial board member of the IOP multidisciplinary journal *Materials for Quantum Technology*.
9. **Stefan Filipp** is member and principal investigator of the Cluster of Excellence *Munich Center for Quantum Science and Technology (MCQST)*.
10. **Stefan Filipp** is adjoint Member of the Special Research Fund (SFB) *BeyondC* funded by the Austrian Science Fund (FWF).
11. **Stefan Filipp** is member of the *Munich Quantum Center (MQC)*.
12. **Rudolf Gross** is spokesperson (together with Immanuel Bloch and Ignacio Cirac) of the Cluster of Excellence *Munich Center for Quantum Science and Technology (MCQST)* and coordinator of the Research Unit C on *Quantum Computing*.
13. **Rudolf Gross** is initiator and Principal Investigator of the *Munich Quantum Valley (MQV)*.
14. **Rudolf Gross** is member of the *Deutsche Akademie der Technikwissenschaften e.V. (acatech)*.
15. **Rudolf Gross** is member of the Advisory Board of the permanent exhibition on *Matter and Light* of the German Science Museum.
16. **Rudolf Gross** is member of the *Committee for the allocation of Alexander von Humboldt Foundation Research Awards*.
17. **Rudolf Gross** is member of the *Appointment and Tenure Board* of the Technical University of Munich.
18. **Rudolf Gross** is member of the *Munich Quantum Center (MQC)*.
19. **Rudolf Gross** is member of the *Scientific Advisory Board of the Bavarian Research Institute of Experimental Geochemistry and Geophysics (BGI)*, Bayreuth, Germany.
20. **Rudolf Gross** is member of the *Scientific Advisory Board of the Institut de Ciència de Materials de Barcelona*, Spain.

21. **Rudolf Gross** is course leader of the *Ferienakademie of the Universities Munich (TU), Stuttgart and Erlangen-Nürnberg*.

22. **Rudolf Hackl** is member of the *Evaluation Board of the neutron source Heinz Maier-Leibnitz (FRM II)*.

23. **Hans Hübl** is member and principal investigator of the Cluster of Excellence *Munich Center for Quantum Science and Technology (MCQST)*.

24. **Mark Kartsovnik** is member of the *Selection Committee of EMFL* (European Magnetic Field Laboratories).

25. **Mark Kartsovnik** is member of the *International Advisory Committee of the 14^{th} International Symposium on Crystalline Organic Metals Superconductors and Ferromagnets (ISCOM 2021)*.

26. **Matthias Opel** is one of the four elected members of the *Speaker Council* for the scientists of the Bavarian Academy of Sciences and Humanities.

Teaching

Lectures, Courses and other Teaching Activities

Several members of the Walther-Meißner-Institute give lectures and seminars at the Technical University of Munich.

Matthias Althammer

WS 2020/2021
- Seminar: Spin Currents and Skyrmionics (with M. Althammer, M. Opel, S. Geprägs))
- Seminar: Advances in Solid-State Physics (with R. Gross, S. Geprägs, H. Hübl, A. Marx, M. Opel)
- Seminar: Topical Issues in Magneto- and Spin Electronics (with M. S. Brandt, S. Geprägs, H. Hübl, M. Opel)

SS 2021
- Seminar: Spin Currents and Skyrmionics (with M. Althammer, M. Opel, S. Geprägs)
- Seminar: Advances in Solid-State Physics (with R. Gross, S. Geprägs, H. Hübl, A. Marx, M. Opel)
- Seminar: Topical Issues in Magneto- and Spin Electronics (with M. S. Brandt, S. Geprägs, H. Hübl, M. Opel)

WS 2021/2022
- Magnetismus (Magnetism)
- Übungen zu Magnetismus (Magnetism, Problem Sessions)
- Seminar: Spin Currents and Skyrmionics (with M. Althammer, M. Opel, S. Geprägs)
- Seminar: Advances in Solid-State Physics (with R. Gross, S. Geprägs, H. Hübl, A. Marx, M. Opel)
- Seminar: Topical Issues in Magneto- and Spin Electronics (with M. S. Brandt, S. Geprägs, H. Hübl, M. Opel)

Frank Deppe

WS 2020/2021
- Supraleitung und Tieftemperaturphysik I (Superconductivity and Low Temperature Physics I)
- Übungen zu Supraleitung und Tieftemperaturphysik I (Superconductivity and Low Temperature Physics I, Problem Sessions)
- Seminar: Superconducting Quantum Circuits (with K. Fedorov, S. Filipp, R. Gross, A. Marx)

SS 2021
- Supraleitung und Tieftemperaturphysik II (Superconductivity and Low Temperature Physics II)
- Übungen zu Supraleitung und Tieftemperaturphysik I (Superconductivity and Low Temperature Physics I, Problem Sessions)

WS 2021/2022
- Seminar: Superconducting Quantum Circuits (with K. Fedorov, S. Filipp, R. Gross, A. Marx)
- Seminar: Superconducting Quantum Circuits (with K. Fedorov, S. Filipp, R. Gross, A. Marx)

Dietrich Einzel

WS 2020/2021
- Mathematische Methoden der Physik I (Mathematical Methods of Physics I)
- Übungen zu Mathematische Methoden der Physik I (Mathematical Methods of Physics I, Problem Sessions)

SS 2021
- Mathematische Methoden der Physik II (Mathematical Methods of Physics II)

- Übungen zu Mathematische Methoden der Physik II (Mathematical Methods of Physics II, Problem Sessions)

WS 2021/2022
- Mathematische Methoden der Physik I (Mathematical Methods of Physics I)
- Übungen zu Mathematische Methoden der Physik I (Mathematical Methods of Physics I, Problem Sessions)

Kirill Fedorov

WS 2020/2021
- Seminar: Superconducting Quantum Circuits (with F. Deppe, S. Filipp, R. Gross, A. Marx)

SS 2021
- Applied Superconductivity: Josephson Effects, Superconducting Electronics and Superconducting Quantum Circuits
- Applied Superconductivity: Josephson Effects, Superconducting Electronics and Superconducting Quantum Circuits, Problem Sessions
- Seminar: Superconducting Quantum Circuits (with F. Deppe, S. Filipp, R. Gross, A. Marx)

WS 2021/2022
- Applied Superconductivity I: from Josephson Effects to RSFQ Logic
- Seminar: Superconducting Quantum Circuits (with F. Deppe, S. Filipp, R. Gross, A. Marx)

Stefan Filipp

WS 2020/2021
- Quanten-Computing mit supraleitenden Qubits: Architektur und Algorithmen (Quantum Computing with Superconducting Qubits: Architecture and Algorithms)
- Übungen zu Quanten-Computing mit supraleitenden Qubits: Architektur und Algorithmen (Quantum Computing with Superconducting Qubits: Architecture and Algorithms, Problem Sessions)
- Seminar: Superconducting Quantum Circuits (with F. Deppe, R. Gross, A. Marx, K. Fedorov)
- WMI Seminar on Modern Topics of Low Temperature Solid-State Physics (with M. Althammer, F. Deppe, K. Fedorov, S. Geprägs, R. Gross, H. Hübl, A. Marx, M. Opel)
- Seminar: Quantum Entrepreneurship Laboratory (with Ch. Mendl, F. Pollmann)

SS 2021
- Quanten-Computing mit supraleitenden Qubits: Architektur und Algorithmen (Quantum Computing with Superconducting Qubits: Architecture and Algorithms)
- Übungen zu Quanten-Computing mit supraleitenden Qubits: Architektur und Algorithmen (Quantum Computing with Superconducting Qubits: Architecture and Algorithms, Problem Sessions)
- Seminar: Superconducting Quantum Circuits (with F. Deppe, R. Gross, A. Marx, K. Fedorov)
- WMI Seminar on Modern Topics of Low Temperature Solid-State Physics (with M. Althammer, F. Deppe, K. Fedorov, S. Geprägs, R. Gross, H. Hübl, A. Marx, M. Opel)
- Seminar: Quantum Entrepreneurship Laboratory (with Ch. Mendl, F. Pollmann)
- Journal Club on Quantum Systems

WS 2021/2022
- Quanten-Computing mit supraleitenden Qubits: Architektur und Algorithmen (Quantum Computing with Superconducting Qubits: Architecture and Algorithms)

- Übungen zu Quanten-Computing mit supraleitenden Qubits: Architektur und Algorithmen (Quantum Computing with Superconducting Qubits: Architecture and Algorithms, Problem Sessions)
- Seminar: Superconducting Quantum Circuits (with F. Deppe, R. Gross, A. Marx, K. Fedorov)
- WMI Seminar on Modern Topics of Low Temperature Solid-State Physics (with M. Althammer, F. Deppe, K. Fedorov, S. Geprägs, R. Gross, H. Hübl, A. Marx, M. Opel)
- Seminar: Quantum Entrepreneurship Laboratory (with Ch. Mendl, F. Pollmann)
- Journal Club on Quantum Systems

Rudolf Gross

WS 2020/2021

- Physik der Kondensierten Materie I (Condensed Matter Physics I)
- Übungen zu Physik der Kondensierten Materie I (Condensed Matter Physics I, Problem Sessions, with S. Geprägs)
- WMI Seminar on Modern Topics of Low Temperature Solid-State Physics (with M. Althammer, F. Deppe, K. Fedorov, S. Filipp, S. Geprägs, H. Hübl, A. Marx, M. Opel)
- Seminar: Advances in Solid-State Physics (with M. Althammer, S. Geprägs, H. Hübl, A. Marx, M. Opel)
- Seminar: Superconducting Quantum Circuits (with F. Deppe, K. Fedorov, S. Filipp, A. Marx)
- Festkörperkolloquium (Colloquium on Solid-State Physics, with D. Einzel)

SS 2021

- Physik der Kondensierten Materie II (Condensed Matter Physics II)
- Übungen zu Physik der Kondensierten Materie II (Condensed Matter Physics II, Problem Sessions, with S. Geprägs)
- Seminar: Advances in Solid-State Physics (with M. Althammer, S. Geprägs, H. Hübl, A. Marx, M. Opel)
- WMI Seminar on Modern Topics of Low Temperature Solid-State Physics (with M. Althammer, F. Deppe, K. Fedorov, S. Filipp, S. Geprägs, H. Hübl, A. Marx, M. Opel)
- Seminar: Superconducting Quantum Circuits (with F. Deppe, K. Fedorov, S. Filipp, A. Marx)
- Festkörperkolloquium (Colloquium on Solid-State Physics, with D. Einzel)
- Ferienakademie: Course 3 “Physics and Electronics in Everyday Life”

WS 2021/2022

- Supraleitung und Tieftemperaturphysik I (Superconductivity and Low Temperature Physics I)
- Übungen zu Supraleitung und Tieftemperaturphysik I (Superconductivity and Low Temperature Physics I, Problem Sessions)
- WMI Seminar on Modern Topics of Low Temperature Solid-State Physics (with M. Althammer, F. Deppe, K. Fedorov, S. Filipp, S. Geprägs, H. Hübl, A. Marx, M. Opel)
- Seminar: Advances in Solid-State Physics (with M. Althammer, S. Geprägs, H. Hübl, A. Marx, M. Opel)
- Seminar: Superconducting Quantum Circuits (with F. Deppe, K. Fedorov, S. Filipp, A. Marx)
- Festkörperkolloquium (Colloquium on Solid-State Physics, with D. Einzel)

Hans Hübl

WS 2020/2021

- Magnetismus (Magnetism)
- Übungen zu Magnetismus (Magnetism, Problem Sessions)
- Seminar: Spin Currents and Skyrmionics (with M. Althammer, M. Opel, S. Geprägs)

- Seminar: Advances in Solid-State Physics (with M. Althammer, S. Geprägs, R. Gross, A. Marx, M. Opel)
- WMI Seminar on Current Topics of Low Temperature Solid State Physics (with M. Althammer, F. Deppe, K. Fedorov, S. Filipp, R. Gross, S. Geprägs, A. Marx, M. Opel)
- Seminar: Topical Issues in Magneto- and Spin Electronics (with M. S. Brandt, M. Althammer, S. Geprägs, M. Opel)

SS 2021

- Spinelektronik (Spin Electronics)
- Übungen zu Spinelektronik (Spin Electronics, Problem Sessions)
- Seminar: Spin Currents and Skyrmionics (with M. Althammer, M. Opel, S. Geprägs)
- Seminar: Advances in Solid-State Physics (with M. Althammer, S. Geprägs, H. Hübl, A. Marx, M. Opel)
- WMI Seminar on Current Topics of Low Temperature Solid State Physics (with M. Althammer, F. Deppe, K. Fedorov, S. Filipp, S. Geprägs, R. Gross, A. Marx, M. Opel)
- Seminar: Topical Issues in Magneto- and Spin Electronics (with M. S. Brandt, M. Althammer, S. Geprägs, M. Opel)

WS 2021/2022

- Seminar: Spin Currents and Skyrmionics (with M. Althammer, M. Opel, S. Geprägs)
- Seminar: Advances in Solid-State Physics (with M. Althammer, S. Geprägs, H. Hübl, A. Marx, M. Opel)
- WMI Seminar on Current Topics of Low Temperature Solid State Physics (with M. Althammer, F. Deppe, K. Fedorov, S. Filipp, S. Geprägs, R. Gross, A. Marx, M. Opel)
- Seminar: Topical Issues in Magneto- and Spin Electronics (with M. S. Brandt, M. Althammer, S. Geprägs, M. Opel)

Seminars and Colloquia

A. Walther-Meißner-Seminar on Modern Topics in Low Temperature Physics WS 2010/2021, SS 2021 and WS 2021/2022

WS 2020/2021:

1. **Temporal Coherence of the Excitronic Emission in TMDC Heterostructures**
   Fabian Kronowetter, Rohde & Schwarz GmbH, Munich, Germany
   04. 12. 2020

SS 2021:

Due to the Corona pandemic the Walther-Meißner-Seminar did not take place in SS 2021.

WS 2021/2022

2. **Fabrication of Superconducting-Ferromagnetic and Hybrid S-I-F Devices**
   Mihai Gabureac, Laboratorium für Festkörperphysik, ETH Zurich, Switzerland
   22. 10. 2021
3. **Mid-infrared Intersubband Polariton Devices**
   Ngoc Linh Tran, Université Paris-Saclay, Centre de Nanosciences et de Nanotechnologies(C2N), Palaiseau, France
   28. 10. 2021
4. **Optical heterostructures and multilayer stacks down to atomic scale grown by atomic layer deposition**
   Pallabi Paul, Friedrich-Schiller University Jena, Germany
   09. 11. 2021
5. **Investigation of proximity induced superconductivity in Al-based topological Josephson junctions**
   Wilhelm Wittl, Forschungszentrum Jülich and University of Regensburg, Germany
   26. 11. 2021
6. **Quantum Communication at LNT/Quantum Clustering for Nonlinear Noise Mitigation in Fibre Communication Systems/An information-theoretic perspective on quantum repeaters**
   Christian Deppe/Roberto Ferrara/Uzi Pereg, Department of Electrical Engineering, TU Munich, Germany
   03. 12. 2021
7. **Magnonics: unique opportunities for classical and quantum information sciences**
   Akashdeep Kamra, Universidad Autónoma de Madrid, Spain
   10.12.2021

B. Topical Seminar on Advances in Solid State Physics WS 2020/2021, SS 2021 and WS 2021/2022

WS 2020/2021:

1. **Preliminary discussion and assignment of topics**
   R. Gross, Walther-Meißner-Institute (E23), Technical University of Munich and BAdW
   03. 11. 2020 and 10. 11. 2020
2. **Sensitivity optimization for NV-diamond magnetometry**
   Adrian Misselwitz, Technical University of Munich
   24. 11. 2020
3. **Quantum-critical phase from frustrated magnetism in a strongly correlated metal**
   Malte Bieringer, Technical University of Munich
   08. 12. 2020

4. **Violating Bell's inequality with remotely connected superconducting qubits**
   Johannes Arceri, Technical University of Munich
   15. 12. 2020
5. **Nonlinear Planar Hall Effect**
   Safwan Uddin Ahmed, Technical University of Munich
   22. 12. 2020
6. **Qubit Measurement by Multichannel Driving**
   Arthur Butorev, Technical University of Munich
   12. 01. 2021
7. **The Remarkable Underlying Ground States of Cuprate Superconductors**
   Aristo Kevin, Technical University of Munich
   19. 01. 2021
8. **Evidence of high-temperature exciton condensation in two-dimensional atomic double layers**
   Johannes Kowalewicz, Technical University of Munich
   26. 01. 2021
9. **Giant topological Hall effect in correlated oxide thin films**
   Tobias Konrad, Technical University of Munich
   02. 02. 2021
10. **Waveguide quantum electrodynamics with superconducting artificial giant atoms**
    Fanjun Xu, Technical University of Munich
    09. 02. 2021

SS 2021:

11. **Preliminary discussion and assignment of topics**
    R. Gross, Walther-Meißner-Institute (E23), Technical University of Munich and BAdW
    13. 04. 2021 and 20. 04. 2021
12. **Majorana quantization and half-integer thermal quantum Hall effect in a Kitaev spin liquid**
    Melissa Will, Technical University of Munich
    27. 04. 2021
13. **Heterodyne detection of radio-frequency electric fields using point defects in silicon carbide**
    Manuel Knauft, Technical University of Munich
    04. 05. 2021
14. **Photonic quantum metrology**
    Alexander Orlov, Technical University of Munich
    18. 05. 2021
15. **Synthetic spin–orbit interaction for Majorana devices**
    Peter Wild, Technical University of Munich
    01. 06. 2021
16. **Evidence for Dominant Phonon-Electron Scattering in Weyl Semimetal WP_2**
    Daniel Hagspihl, Technical University of Munich
    01. 06. 2021
17. **Spin current from sub-terahertz-generated antiferromagnetic magnons**
    Daria Nuzhina, Technical University of Munich
    08. 06. 2021
18. **A dissipatively stabilized Mott insulator of photons**
    Sebastian Ruffert, Technical University of Munich
    15. 06. 2021
19. **Real-Space Observation of Magnon Interaction with Driven Space-Time Crystals**
    Lukas Vogl, Technical University of Munich
    15. 06. 2021
20. **Waveguide quantum electrodynamics with superconducting artificial giant atoms**
    Christoph Lindenmeir, Technical University of Munich
    22. 06. 2021

21. **Experimental observation of vortex rings in a bulk magnet**
Bianca Seyschab, Technical University of Munich
29. 06. 2021
22. **Reversible hydrogen control of antiferromagnetic anisotropy in α-Fe_2O_3**
Florian Kollmannsberger, Technical University of Munich
29. 06. 2021
23. **Inertial spin dynamics in ferromagnets**
Ziheng Yang, Technical University of Munich
06. 07. 2021

Strong Interfacial Exchange Field in a Heavy Metal/Ferromagnetic Insulator System Determined by Spin Hall Magnetoresistance
Karolina Weber, Technical University of Munich
13. 07. 2021

WS 2021/2022:

24. **Preliminary discussion and assignment of topics**
R. Gross, Walther-Meißner-Institute (E23), Technical University of Munich and BAdW
19. 11. 2021 and 26. 11. 2021
25. **Observation of first and second sound in a BKT superfluid**
Meike Pfeiffer, Technical University of Munich
07. 12. 2021
26. **Cascaded superconducting junction refrigerators: Optimization and performance limits**
Julian Franz, Technical University of Munich
14. 12. 2021
27. **Quantum-enhanced nonlinear microscopy**
Michael Schmidlechner, Technical University of Munich
21. 12. 2021
28. **All-electric magnetization switching and Dzyaloshinskii-Moriya interaction in WTe_2/ferromagnet heterostructures**
Ferdinand Menzel, Technical University of Munich
18. 01. 2022
29. **to be announced**
Ramona Stumberger, Technical University of Munich and WMI
25. 01. 2022

C. Topical Seminar: Spin current and Skyrmionics WS 2020/2021, SS 2021 and WS 2021/2022

WS 2020/2021:

1. **Preliminary discussion and assignment of topics**
M. Althammer, S. Geprägs, H. Hübl, Walther-Meißner-Institute (E23), Technical University of Munich and BAdW
05. 11. 2020 and 12. 11. 2020
2. **Multilayers for topological spin textures**
Misbah Yaqoob, Walther-Meissner-Institute, Technical University of Munich
19. 11. 2020
3. **Microwave control of magnon transport**
Korbinian Rubenbauer, Walther-Meissner-Institute, Technical University of Munich
26. 11. 2020
4. **Spin and charge transport in multilayers with interfacial Dzyaloshinskii Moriya Interaction**
Elisabeth Meidinger, Walther-Meissner-Institute, Technical University of Munich
10. 12. 2020

5. **Propagation Length of Antiferromagnetic Magnons Governed by Domain Configurations**
   Matthias Grammer, Technical University of Munich
   17. 12. 2020
6. **Fast current-driven domain walls and small skyrmions in a compensated ferrimagnet**
   Joris Thiel, Technical University of Munich
   14. 01. 2021
7. **Constrained yttrium iron garnet trilayers**
   Philipp Schwenke, Walther-Meissner-Institute, Technical University of Munich
   21. 01. 2021
8. **Spin Hall Magnetoresistance in antiferromagnets**
   Monika Scheufele, Walther-Meissner-Institute, Technical University of Munich
   28. 01. 2021
9. **Chiral Spin-Wave Velocities Induced by All-Garnet Interfacial Dzyaloshinskii-Moriya Interaction in Ultrathin Yttrium Iron Garnet Films**
   Daryoush Nosraty Alamdary, Technical University of Munich
   11. 02. 2021

SS 2021:

10. **Preliminary discussion and assignment of topics**
    M. Althammer, S. Geprägs, H. Hübl, M. Opel, Walther-Meißner-Institute (E23), Technical University of Munich and BAdW
    15. 04. 2021 and 22. 04. 2021
11. **Spinexcitations in nanostructures**
    Korbinian Rubenbauer, Technical University of Munich and WMI
    06. 05. 2021
12. **CoFe Multilayers spin transport**
    Elisabeth Meidinger, Technical University of Munich and WMI
    20. 05. 2021
13. **Room-temperature stabilization of antiferromagnetic skyrmions in synthetic antiferromagnets**
    Lukas Niekamp, Technical University of Munich
    27. 05. 2021
14. **Electrical transport in nanostructures**
    Matthias Althammer, Technical University of Munich and WMI
    10.06.2021
15. **Magnon-magnon interactions in a room-temperature magnonic Bose-Einstein condensate**
    Yuhao Sun, Technical University of Munich
    17. 06. 2021
16. **Superconductor/Ferromagnet Heterostructures**
    Manuel Müller, Technical University of Munich and WMI
    24. 06. 2021
17. **Growth and characterization of FeO**
    Mayank Sharma, Technical University of Munich and WMI
    01. 07. 2021

WS 2021/2022:

18. **CoFe hybrids for complex magnetic order**
    Luis Flacke, Technical University of Munich and WMI
    11. 11. 2021
19. **Vertical Pt/YIG/Pt heterostructures**
    Phillip Schwenke, Technical University of Munich and WMI
    18. 11. 2021
20. **Magnetic insulator/superconductor thin film heterostructures**

Vincent Haueise, Technical University of Munich
25.11.2021

21. **Ultrafast spin current generated from an antiferromagnet**
Annarita Ricci, Technical University of Munich
09. 12. 2021
22. **Magnon transport in magnetic insulators**
Matthias Grammer, Technical University of Munich and WMI
13. 01. 2022
23. **Manipulating magnon transport in YIG films with different crystalline orientations**
Janine Gückelhorn, Technical University of Munich and WMI
20. 01. 2022
24. **Spin transport effects in yttrium iron garnet films interfaced with a superconductor**
Yunhao Sun, Technical University of Munich
10. 02. 2022

D. Topical Seminar on Superconducting Quantum Circuits WS 2020/2021, SS 2021 and WS 2021/2022

WS 2020/2021:

1. **Preliminary discussion and assignment of topics**
F. Deppe, A. Marx, R. Gross, Walther-Meißner-Institute (E23), Technical University of Munich and BAdW
03. 11. 2020 and 10. 11. 2020
2. **Challenges and results on the way to quantum acoustodynamics**
Christopher Waas, Walther-Meissner-Institute
01. 12. 2020
3. **Teleportation-based collective attacks in Gaussian quantum key distribution**
Daniel Prelipcean, Technical University of Munich
08. 12. 2020
4. **Solid-state qubits integrated with superconducting through-silicon vias**
Yuyang Huang, Technical University of Munich
15. 12. 2020
5. **The superconducting quasicharge qubit**
Jonas Schmitt, Technical University of Munich
12. 01. 2021
6. **Breaking the trade-off between fast control and long lifetime of a superconducting qubit**
Niklas Bruckmoser, Technical University of Munich
19. 01. 2021
7. **A quantum memory at telecom wavelengths**
Patrick Missale, Technical University of Munich
26. 01. 2021
8. **Atomated discovery of superconducting circuits and its application topolocal coupler design**
Nicolas Gosling, Technical University of Munich
02. 02. 2021

SS 2021:

9. **Preliminary discussion and assignment of topics**
F. Deppe, A. Marx, S. Filipp, R. Gross, Walther-Meissner-Institute (E23), Technical University of Munich and BAdW
13. 04. 2021 and 20. 04. 2021
10. **Josephson junctions for superconducting qubits**
Patrick Missale, Technical University of Munich
27.04.2021

11. **Experimental quantum teleportation of propagating microwaves**
Franz von Silva-Tarouca, Technical University of Munich
04. 05. 2021
12. **Demonstration of two-qubit algorithms with a superconducting quantum processor**
Shawn Storm, Technical University of Munich
11. 05. 2021
13. **New material platform for superconducting transmon qubits with coherence times exceeding 0.3 milliseconds**
Christian Mang, Technical University of Munich
18. 05. 2021
14. **Compiling quantum algorithms for architectures with multi-qubit gates**
Kevin Shen, Technical University of Munich
01.06.2021
15. **Simple pulses for elimination of leakage in weakly nonlinear qubits**
Lukas Vetter, Technical University of Munich
08. 06. 2021
16. **Deterministic multi-qubit entanglement in a quantum network**
Oliver Kuijpers, Technical University of Munich
15. 06. 2021
17. **Characterizing and optimizing qubit coherence based on SQUID geometry**
Michal Cherczynski, Technical University of Munich
22. 06. 2021
18. **Two-level systems in superconducting quantum devices due to trapped quasiparticles**
Florian Maier, Technical University of Munich
29. 06. 2021
19. **Multiqubit coupler with superconducting circuits**
Gerhard Huber, Technical University of Munich and WMI
06. 07. 2021
20. **Optimization od superconducting Nb resonators**
Niklas Bruckmoser, Technical University of Munich and WMI
13. 07. 2021
21. **Optimization of Nb/Al interfaces**
Leonhard Hölscher, Technical University of Munich and WMI
20. 07. 2021
22. **Optimization of qubit gates**
Niklas Glaser, Technical University of Munich and WMI
27. 07. 2021

WS 2021/2022:

23. **Preliminary discussion and assignment of topics**
F. Deppe, A. Marx, S. Filipp, R. Gross, Walther-Meissner-Institute (E23), Technical University of Munich and BAdW
19. 10. 2021 and 26. 10. 2021
24. **Improving qubit coherence using closed-loop feedback**
Federico Roy, Technical University of Munich and WMI
09. 11. 2021
25. **Optimal Control of Entangling Gates in Superconducting Tunable-Coupler Architectures**
Niklas Glaser, Technical University of Munich and WMI
16. 11. 2021
26. **Direct observation of deterministic macroscopic entanglement**
Wun Kwan Yam, Technical University of Munich and WMI
23. 11. 2021
27. **Microwave Package Design for Superconducting Quantum Processors**

Johannes Schirk, Technical University of Munich and WMI
30. 11. 2021

28. **Parity Dependent XY Rotations in Qubit Chains**
Maximilian Nägele, Technical University of Munich
07. 12. 2021
29. **Enhancing quantum annealing performance by a degenerate twolevel system**
Yuki Nojiri, Technical University of Munich and WMI
14.12.2021
30. **A reversed Kerr traveling wave parametric amplifier**
Daniil Bazulin, Technical University of Munich and WMI
21. 12. 2021
31. **Superconducting qubit to optical photon transduction**
Nicoló Salerno, Technical University of Munich
11. 01. 2022
32. **Implementation of a canonical phase measurement with quantum feedback**
Thomas Narr, Technical University of Munich
18. 01. 2022
33. **Spin-Resonance Linewidths of Bismuth Donors in Silicon Coupled to Planar Microresonators**
Georg Mair, Technical University of Munich
25.01.2022
34. **Experimental demonstration of entanglement-enabled universal quantum cloning in a circuit**
Lion Frangoulis, Technical University of Munich
35. **Digital-analog quantum computation**
Malay Singh, Technical University of Munich and WMI
08. 02. 2022

E. Solid State Colloquium

The WMI has organized the Solid-State Colloquium of the Faculty of Physics in WS 2020/2021, SS 2021, and WS 2021/2022 The detailed program can be found on the WMI webpage: www.wmi.badw.de/teaching/colloquium-on-solid-state-physics.

Staff

Staff of the Walther-Meißner-Institute

Scientific Directors
Prof. Dr. Stefan Filipp
Prof. Dr. Rudolf Gross (managing director)

Deputy Director
Priv.-Doz. Dr. habil. Hans Hübl

Technical Director
Dr. Achim Marx

The deputy director, the technical director and the elected representative of the scientific staff (Dr. Matthias Opel) are members of the WMI Executive Committee and support the scientific directors in the management of WMI.

Administration/Secretary's Office
Andrea Person
Carola Siegmayer
Emel Dönertas
Martina Meven

Scientific Staff
Dr. Matthias Althammer
Priv.-Doz. Dr. habil. Frank Deppe
Prof. Dr. Andreas Erb
Dr. Kirill Fedorov
Dr. Oscar Gargiulo
Dr. Stephan Geprägs
Prof. Dr. Rudolf Hackl
Dr. Franz Haslbeck
Dr. Mark Kartsovnik
Dr. Gleb Krylov
Dr. Nadezhda Kukharchyk
Dr. Lukas Liensberger
Dr. Matthias Opel
Dr. Christian Schweizer
Dr. Daniel Schwienbacher
Dr. Christopher Trummer
Dr. Tobias Wimmer
M. Sc. Daniil Bazulin
M. Sc. Qiming Chen
M. Sc. Shamil Erkenov
M. Sc. Florian Fesquet
M. Sc. Luis Flacke
M. Sc. Niklas Glaser
M. Sc. Janine Gückelhorn
M. Sc. Kedar Honasoge
M. Sc. Gerhard Huber
M. Sc. Martin Knudsen
M. Sc. Leon Koch
M. Sc. Thomas Luschmann
M. Sc. Manuel Müller
M. Sc. Yuki Nojiri
M. Sc. Frederik Pfeiffer
M. Sc. Michael Renger
M. Sc. Federico Roy
M. Sc. Malay Singh
M. Sc. Ana Strinic
M. Sc. Ivan Tsitsilin
M. Sc. Max Werninghaus

Technical Staff
Peter Binkert
Thomas Brenninger, M.Sc.
Dieter Guratzsch
Astrid Habel
Dipl.-Ing. (FH) Josef Höß
Sebastian Kammerer
Jan Naundorf
Georg Nitschke
Mario Nodes
Christian Reichlmeier
Alexander Rössl
Andreas Russo
Harald Schwaiger

Assistants
Sybilla Plöderl
Maria Botta

Guest Researchers

The Walther-Meißner-Institute welcomes a significant number of guest every year for strengthening international collaborations and intensifying scientific exchange with internationally leading places. Unfortunately, in 2021 the number of guests dropped to a disappointingly small number due to the Covid-19 pandemic.

1. Dr. Werner Biberacher
   permanent guest
2. Prof. Dr. Dietrich Einzel
   permanent guest
3. Dr. Kurt Uhlig
   permanent guest
4. Prof. Dr. Akashdeep Kamra, Universidad Autónoma de Madrid, Spain
   06. 12. - 10. 12. 2021
5. Prof. Dr. Vladimir Zverev, Institute of Solid State Physics, Chernogolovka, Russia
   21. 11. - 19. 12. 2021
6. Mayank Sharma, Indian Institute of Technology (IIT), Madras, Chennai, India
   16. 10. 2020 - 30. 08. 2021
7. Katharina Fritz, Universität Bielefeld, Bielefeld, Germany
   23. 08. - 27. 08. 2021
8. Dr. Roberto Di Candia, Aalto University, Aalto, Finland
   01. 09. 2021 - 28. 02. 2022

Scientific Advisory Board & Executive Committee

Scientific Advisory Board

According to the statutes of the Bavarian Academy of Sciences and Humanities (BAdW) the Scientific Advisory Board evaluates the quality of the scientific work of Walther-Meißner-Institute (WMI) and gives advice to its Executive Committee to provide scientific quality assurance. The Scientific Advisory Board regularly reports to the Research Committee of BAdW.

The members of the Scientific Advisory Board include members of BAdW with appropriate scientific background, representatives of the two Munich universities (TUM and LMU), as well as leading national and international scientists. They are appointed by the Section III "Naturwissenschaften, Mathematik, Technikwissenschaften" of BAdW for five years. The managing director of WMI is a consultive member of the WMI Scientific Advisory Board. The Scientific Advisory Board is headed by a chairperson and deputy chairperson. They are elected by the Section III "Naturwissenschaften, Mathematik, Technikwissenschaften" of BAdW for five years at the suggestion of the members of the WMI Scientific Advisory Board. The chairperson of the Scientific Advisory Board must be a member of BAdW.

The present members of the WMI Scientific Advisory Board are:

- **Vollhardt, Dieter**, chairman (BAdW, University of Augsburg)
- **Bloch, Immanuel**, deputy chairman (BAdW, LMU Munich and Max-Planck-Institute of Quantum Optics)
- **Abstreiter, Gerhard** (BAdW, Technical University of Munich)
- **Bühler-Paschen, Silke** (Technical University of Vienna)
- **Finley, Jonathan** (Technical University of Munich)
- **Gross, Rudolf**, consultive member (BAdW, Technical University of Munich)
- **Hänsch, Theodor** (BAdW, LMU Munich and Max-Planck-Institute of Quantum Optics)
- **Michael Hartmann** (FAU Erlangen-Nuremberg)
- **Laurens Molenkamp** (BAdW and University of Würzburg)
- **Wallraff, Andreas** (ETH Zurich)
- **Weiss, Dieter** (University of Regensburg)

In 2021, the annual meeting of the scientific advisory board was taking place on 12th February 2021 as an online meeting. There has been a brief second online meeting on 10th December 2021.

Executive Committee

The Walther-Meißner-Institute is headed by the board of scientific directors which is responsible for the development and implementation of the research program. The scientific directors hold a full professor position at one of the Munich universities (TUM or LMU). They are appointed in a joint process of the respective university and BAdW. The scientific directors are supported by the deputy director, the technical director and an elected representative of the scientific staff. They are appointed by the Section III "Naturwissenschaften, Mathematik, Technikwissenschaften" of BAdW for five years at the suggestion of the members of the WMI Scientific Advisory Board.

The present members of the WMI Executive Committee are:

- **Filipp, Stefan**, scientific director
- **Gross, Rudolf**, scientific director (managing director)
- **Hübl, Hans**, deputy director
- **Marx, Achim**, technical director
- **Opel, Matthias**, representative of the scientific staff

Rudolf Gross has been the managing director of WMI for more than 20 years starting from July 2000. As the number of scientific directors in the WMI Executive Committee has been increased to presently two, the position of the managing director can now be switched every second year to allocate the workload among the scientific directors. Rudolf Gross will hand over the task of the managing director to Stefan Filipp on 1st January 2022.

Contact:

Walther–Meißner–Institut
Bayerische Akademie der Wissenschaften
Walther–Meißner–Str. 8
D - 85748 Garching
GERMANY

Phone: +49 – (0)89 289 14202
Fax: +49 – (0)89 289 14206
E–mail: Sekretariat@wmi.badw.de

www.wmi.badw.de

Published by:

Walther–Meißner–Institut
Walther–Meißner–Str. 8, D - 85748 Garching
December 2021

Walther-Meißner-Institut
DER BAYERISCHEN AKADEMIE DER WISSENSCHAFTEN